

# Thermophysical Investigation of Asteroid Surfaces II: Factors Influencing Grain Size

Eric M. MacLennan<sup>a,b,\*</sup>, Joshua P. Emery<sup>a,c</sup>

<sup>a</sup>*Earth and Planetary Sciences Department, Planetary Geosciences Institute, The University of Tennessee, Knoxville, TN 37996, USA*

<sup>b</sup>*Department of Physics, P.O. Box 64, 00560 University of Helsinki, Finland*

<sup>c</sup>*Department of Physics and Astronomy, Northern Arizona University, NAU Box 6010, Flagstaff, AZ 86011, USA*

---

## Abstract

Asteroid surfaces are subjected to mechanical weathering processes that result in the development and evolution of regolith. Two proposed mechanisms—impact bombardment and thermal fatigue—have been proposed as viable and dominant weathering processes. Previously, we compiled and estimated thermal inertias of several hundred asteroids (mostly in the main-belt) for which we determined dependencies on temperature, diameter, and rotation period. In this work, we estimate grain sizes of asteroid regoliths from this large thermal inertia dataset using thermal conductivity models. Following our previous work we perform multi-variate linear model fits to the grain size dataset and quantify its dependency on diameter and rotation period. We find that the best-fit model fit indicates that asteroid grain sizes are inversely dependent on object size for <10 km asteroids and exhibits no relationship above this size cutoff. Rotation period and grain size show a positive relationship when the rotation period is greater than  $\sim 5$  hr, and an inverse relationship below this rotation period. We conclude that both impact weathering and thermal fatigue are significant regolith evolution mechanisms. Furthermore, we run post-hoc t-tests between spectral groups to identify compositional differences among our asteroid set. Notably, suspected metal-rich, M-type and E-type asteroids have larger than expected grain sizes, and P-types have distinctly smaller grains than other groups.

**Keywords:** Thermophysical Model, Infrared Photometry, Thermal Inertia, Asteroid Regolith Evolution, Solar System Processes

---

## 1. Introduction

The study and characterization of asteroid regolith—the unconsolidated, heterogeneous, rocky material covering the surface of planetary bodies (Shoemaker et al., 1969)—is an

---

\*corresponding author

*Email addresses:* [eric.maclennan@helsinki.fi](mailto:eric.maclennan@helsinki.fi) (Eric M. MacLennan),  
[mv.helsinki.fi/home/maceric/home.html](http://mv.helsinki.fi/home/maceric/home.html) (Eric M. MacLennan)

important part of understanding the processes and evolution of airless bodies of the Solar System. Generally speaking, asteroid surfaces evolve from poorly-sorted, blocky mixtures to well-sorted fine-grained regolith (Hörz et al., 2020). Thermal inertia,  $\Gamma$ , is a thermophysical property that can be used to make an estimate of asteroid regolith grain sizes, as bare rock surfaces have higher values of  $\Gamma \sim 1500\text{--}2500 \text{ J m}^{-2} \text{ K}^{-1} \text{ s}^{-1/2}$  (Jakosky, 1986; Bandfield et al., 2011). Although some meteorites have relatively low thermal inertia ( $\Gamma \sim 1000 \text{ J m}^{-2} \text{ K}^{-1} \text{ s}^{-1/2}$ ; Opeil et al., 2010; Opeil et al., 2020), smaller values are generally interpreted to indicate smaller particle sizes. The bulk thermal inertia of a surface can be expressed as  $\Gamma = \sqrt{k_{\text{eff}} \rho_{\text{grain}} c_s (1 - \phi)}$  in which  $k_{\text{eff}}$  is the effective thermal conductivity of the regolith,  $\rho_{\text{grain}}$  is the density of a rock with no void spaces,  $c_s$  is the specific heat capacity of the material, and the regolith porosity,  $\phi$ , is explicitly accounted for. Some mechanisms have been suggested as the primary drivers of regolith mechanical weathering on airless bodies: meteoroid impacts and thermal cycling.

Small meteoroid ( $< 1 \text{ m}$ ) impacts can cause breakdown of surface material over time. Some of the energy from an impact is partitioned into fragmenting near-surface material of the target body, albeit the exact fraction of energy that goes into this mechanical work is uncertain (Horz and Cintala, 1997). Some of the energy is partitioned into launching particles off the surface on various trajectories (ejecta), which partly depend on the proximity to the impact site and on the mechanical properties of the impactor and target. Particles that do not reach escape velocity return to the surface as newly-formed regolith. Other factors, such as the target strength and porosity, also play relevant roles in the production of craters and of regolith. For example, Housen and Holsapple (2003) found a clear inverse relationship between the ejecta:impactor mass ratio and porosity of the target. Impacts that excavate into bedrock that has been previously fractured and weakened will generate a more blocky ejecta blanket. Thus, regolith evolution driven by impacts is dependent on the size of the body, strength of the material, among other factors.

Internal stresses caused by differential thermal expansion, as a result of cyclic heating and cooling, lead to regolith breakdown and erosion (Eppes et al., 2015). The efficiency of this thermal cycling process has been simulated under the thermal environments of airless solar system bodies (e.g., Molaro and Byrne, 2012; Molaro et al., 2017), and its feasibility has been experimentally demonstrated on meteorite samples (Delbo’ et al., 2014; Libourel et al., 2020). Increasing the heterogeneity of a rock (by changing the mineral grain boundaries or pores of empty space) can raise the peak stresses by up to a factor of three, compared to a homogeneous rock (Molaro et al., 2015). Thermal fracturing acts on spatial scales spanning many orders of magnitude, and modeling work has shown that the efficiency depends on heliocentric distance, rotation period, and material thermomechanical properties (Ravaji et al., 2019; El Mir et al., 2019). The propagation of the thermal wave within a boulder initiates one or more cracks at the micro-scale throughout the boulder interior and throughout the diurnal cycle (Hazeli et al., 2018). These micro-cracks most likely originate near mineral grain boundaries, preferentially grow perpendicular to the local surface, and ultimately intersect other fractures reaching sizes of several centimeters (Delbo’ et al., 2014; Molaro et al., 2015). Growth of large-scale cracks occurs in the direction of the heat flow throughout the boulder, and are thus able to transverse rocks that are several times larger

than the initial fracture(s). Although rapidly rotating asteroids exhibit small diurnal temperature differences, [Delbo' et al. \(2014\)](#) showed that even a short heating cycle of 2.2 hrs is sufficient to generate and grow cracks. Lastly, [Molaro and Byrne \(2012\)](#) claim that fast-rotators ought to facilitate larger maximum thermal gradients, thus predicting a rotation period dependence of the overall efficiency.

In this work, we perform an investigation of regolith properties derived from thermal analyses in the context of two proposed mechanisms: meteoroid impact degradation and thermal fatigue cycling. These processes have been proposed as relevant for the creation and subsequent evolution of regolith on asteroid surfaces. The relevance of each weathering mechanism can be examined by comparing the relative correlation between regolith grain size and asteroid diameter or rotation period. If regolith development and evolution is highly dependent on meteoroid impacts then a significant correlation with asteroid diameter is expected. On the other hand, if thermal cycling is effective, then we should observe a correlation with the rotation period. These two hypotheses are not exclusive, and we consider the possibility that both processes are active by using a multi-variate linear model in our analysis of the dataset. We do, in fact, expect both mechanisms to be relevant and therefore hypothesize: 1) larger asteroids exhibit evolved regoliths, quantified by smaller grain sizes, and 2) slowly-rotating asteroids have a poorly-developed regolith, characterized by larger average grain size. We also investigate how the regolith properties of asteroids are related to spectral classification.

## 2. Methods

Some studies have investigated the relationship between  $\Gamma$  and grain size, by experimentally observing and/or theoretically modeling  $k_{eff}$  for a granular mixture. For example, a few experiments have been able to observe empirical effects of particle size on  $k_{eff}$  ([Presley and Christensen, 1997](#); [Presley and Craddock, 2006](#)). Since, for planetary regoliths,  $\Gamma$  is primarily, but not exclusively, influenced by changes in  $k_{eff}$  ([Presley, 2010](#); [Presley and Christensen, 2010](#)), an estimate of grain size can be made from  $\Gamma$  by using an appropriate thermal conductivity model for a granular medium. In general, for airless bodies  $k_{eff}$  has a solid-state component that describes heat conduction through grains and across grain contacts, and a radiative component that describes heat radiated across pore spaces (e.g., [Piqueux and Christensen, 2009](#)):

$$k_{eff} = k_{solid} + k_{rad} = k_1 + k_2 T^3. \quad (1)$$

The  $k_1$  and  $k_2$  coefficients in [Eq. 1](#) are dependent on the material properties of the regolith, such as grain size, packing fraction, and amount of contact between the grains ([Watson, 1964](#)). These coefficients are approximated in the works of [Gundlach and Blum \(2013\)](#) and [Sakatani et al. \(2017\)](#), from which measurements of  $\Gamma$  (combined with the compositional information about the asteroid) can be used to estimate a characteristic grain size for an asteroid. We thus employ both these models, with an anisothermality correction from [Ryan et al. \(2020\)](#), to estimate characteristic regolith grain sizes for each asteroid.

The [Gundlach and Blum \(2013\)](#) formulation of  $k_1$  and  $k_2$  are calibrated using laboratory heat-flow measurements of lunar regolith ([Chan and Tien, 1973](#); [Gundlach and Blum, 2012](#)). On the other hand, [Sakatani et al. \(2017\)](#) used mixtures of powdered glass beads of various size and porosity. The surface temperature is required input for these models, from which we use the color temperature reported in Part I ([MacLennan and Emery, 2021](#)). These models also need compositional information about the material, which we infer from the asteroid’s spectral taxonomic type when available. For objects for which there is no spectral information available, we infer the spectral type from the geometric albedo. Many asteroids belong to a dynamical family, in which case we can infer the spectral type and perform a cross-check with the geometric albedo or reflectance spectrum, if available. We assign a meteorite analog to each spectral type, as discussed in [Sec. 2.2](#) and account for uncertainties in the thermal inertia and various material properties by using a Monte Carlo method ([Sec. 2.3](#)) when determining grain sizes.

### 2.1. Thermal Conductivity Modeling

The solid thermal conductivity component,  $k_1$ , is modeled by [Gundlach and Blum \(2013\)](#) via computing the efficiency of heat transfer through the surface contacts within a network of grains:

$$k_1^{G\&B} = k_{grain} \frac{r_c}{r_g} (f_1 \exp([f_2 \psi])) \Xi. \quad (2)$$

$k_{grain}$  is the thermal conductivity of a grains with zero porosity,  $\mu$  is Poisson’s ratio,  $E$  is Young’s Modulus,  $\psi = 1 - \phi$  is the volume filling factor (packing fraction), and  $\gamma(T) = T \cdot 6.67 \times 10^5 \text{ J m}^{-2}$  is the specific surface energy of each grain—a measure for the adhesive bonding strength between grains. The contact radius between grains,  $r_c$ , is calculated by JKR (Johnson-Kendall-Roberts) theory ([Johnson et al., 1971](#)), assuming that adhesive forces are dominant:

$$r_c = \left[ \frac{9\pi}{4} \frac{(1 - \nu^2)}{E} \gamma(T) r_g^2 \right]^{-1/3}. \quad (3)$$

The empirically-derived constants  $f_1 = (5.18 \pm 3.45) \times 10^2$  and  $f_2 = 5.26 \pm 0.94$  encapsulate information about the path of contact chains in the direction of heat flow ([Gundlach and Blum, 2012](#)). The factors contained within brackets in [Eq. 2](#) approximate the adhesive forces between regolith grains, which dominate over gravity on small bodies, to estimate the contact area between them. Thermal conductivity measurements of Apollo 11 & 12 samples are used to estimate  $\Xi = 0.41 \pm 0.02$ , which incorporates and accounts for the irregular shapes of the particles and heterogeneity of regolith on the whole.

In [Sakatani et al. \(2017\)](#), the solid conductivity component is modeled in a similar way to the formula above:

$$k_1^{Sak} = k_{grain} \frac{r_c}{r_g} \frac{4\psi C \xi}{\pi^2} \quad (4)$$

where  $r_c$  is the contact radius, also represented by [Eq. 3](#). The coordination number,

$$C = \frac{2.8112(1 - \phi)^{-1/3}}{f^2(1 + f^2)}, \quad (5)$$

is the average number of particles that are in contact with each other and is a function of the regolith porosity. Here,  $f = 0.07318 + 2.193\phi - 3.357\phi^2 + 3.914\phi^3$ . The factor  $\xi$  is dependent on the shape and smoothness of the particles and is equal to unity for perfectly smooth spheres. We use  $\xi = 0.4$ , which approximates rough, non-spherical particles and is well within the range of experimentally-derived values from [Sakatani et al. \(2017\)](#).

The radiative thermal conductivity ( $k_{rad}$ ) coefficient is calculated by [Gundlach and Blum \(2013\)](#) to be:

$$k_2^{G\&B} = 8\epsilon\sigma_0 e_1 \frac{1 - \psi}{\psi} r_g, \quad (6)$$

with the empirical coefficient  $e_1 = 1.34 \pm 0.01$  ([Dullien, 1979](#); [Gundlach and Blum, 2012](#)). The right-hand-side of [Eq. 6](#) partly depends on the mean free path of a photon between regolith grains, which is directly proportional to the grain size. In [Sakatani et al. \(2017\)](#) the radiative heat transfer coefficient is calculated via:

$$k_2^{Sak} = 8\sigma_0 \zeta \frac{\epsilon}{2 - \epsilon} \left[ \frac{1 - \psi}{\psi} \right]^{1/3} r_g \quad (7)$$

where  $\zeta$  is an enhancement factor for which we use  $\zeta = 1.7$ —an average of the experimentally-derived values in [Sakatani et al. \(2017\)](#). However, we note that  $k_{rad}$  values presented in [Sakatani et al. \(2017\)](#) show a clear inverse dependency on  $r_g$ , which may be related to the effect of short-range (immediately-adjacent) versus long-range (non-adjacent) radiation exchange that is dependent on the particle size ([van Antwerpen et al., 2012](#)).

Thermal gradients that exist within individual regolith particles cause a non-linear relationship between  $r_g$  and  $k_{rad}$  ([Ryan et al., 2020](#)). In this case, the temperature-dependent thermal conductivity will be less than the  $T^3$  theoretical relationship. Building off the work of [van Antwerpen et al. \(2012\)](#), [Ryan et al. \(2020\)](#) use the dimensionless parameter  $\Lambda_s$  in an updated version of the non-isothermal correction factor,  $f_k$ :

$$\Lambda_s = \frac{k_{grain}}{8r_g\sigma_0 T^3} \quad (8)$$

and

$$f_k = a_1 \tan^{-1}(a_2 \Lambda^{-a_3}) + a_4. \quad (9)$$

When  $\Lambda_s > 25$  then  $f_k$  is set to unity, otherwise  $f_k$  can be calculated via [Eq. 9](#) where  $a_1 = -0.568$ ,  $a_2 = 0.912$ ,  $a_3 = 0.765$ , and  $a_4 = 1.035$ . To account for non-isothermality the coefficients calculated in [Eq. 6](#) and [Eq. 7](#) are multiplied by  $f_k$ .

## 2.2. Input Parameters

Some of the required input parameters to the equations listed above are dependent on the composition of the material. Since meteorites are samples of asteroids, we attempt to establish a meteorite analog that is most appropriate for each asteroid in this study. The most direct approach can be made when high quality spectra have been acquired for an object. Various taxonomic systems have been defined based on combining albedo information with photometric colors ([Tholen, 1984](#)), or absorption features with spectral slopes of reflectance

spectra (Bus and Binzel, 2002; DeMeo et al., 2009). The taxa defined in these works relate to different compositions, although connections can be ambiguous in many cases; particularly, for featureless spectra. Visible spectra and color information can be used to broadly distinguish between the S-complex (any spectral taxon beginning with an “S” and Q-types that are the unweathered endmember), K-type, V-type, B-type, C-complex (any taxon beginning with a “C”), and Bus-DeMeo X-complex. For the X-complex we adopt the Tholen (1984) E, M, and P-type system, which are distinguished by their geometric albedos. We use albedo cutoff of  $p_V \gtrsim 0.42$  for E-type objects,  $0.12 < p_V < 0.42$  for M-types, and  $p_V \lesssim 0.12$  for P-types.

Many asteroids in our sample have no color or spectral information available, thus we are left to infer compositional information based only on the albedo. A cutoff of  $p_V = 0.12$  is used to distinguish between high-albedo S-complex and low-albedo C-complex (lower albedo), whereas objects with  $p_V > 0.45$  are assumed to be E-types. All of these criteria are illustrated in Fig. 2. The  $p_V = 0.12$  cutoff value is consistent with DeMeo and Carry (2013), who present average albedos for different asteroid taxa using a larger sample size than ours. This cutoff criterion is also consistent with laboratory-derived geometric albedos of ordinary chondrites and CO, CM, and CI carbonaceous chondrites (Fig 7 of Beck et al., 2021). However, the laboratory-derived values for CK and CV chondrites have significant overlap with unequilibrated (type 3) ordinary chondrites for  $0.12 < p_V < 0.17$ . Thus, with this criteria, meteorite analog associations for 8 objects in our sample with albedos in this range can be considered ambiguous.

It is interesting to note that the overall population (across taxonomic groups) exhibits a positive correlation between  $p_V$  and  $G_V$  (Fig. 2). Within each taxonomic group this correlation is absent or is slightly inverse. Such a scenario is an example of Simpson’s statistical paradox<sup>1</sup> (Simpson, 1951; Yule, 1903). We briefly note this paradox for future works that may investigate the complex relationship between  $p_V$ ,  $G_V$ , and regolith grain-scale size across different spectral/compositional groups.

We assign ordinary chondrite and carbonaceous chondrite material properties to S-complex (including one O-type) and C-complex (excluding Ch-type) asteroids, respectively. We associate the low-density CM chondrites with Ch and B-type, and CI chondrites with P-type asteroids. Our object set contains a few D-types (color or spectral classification) for which we assume a P-type composition that most likely reflects the primitive compositions of these asteroids. Asteroids classified as K-type (and Xk-type) have been shown to be related to CO, CV, and CK meteorites (Burbine et al., 2001; Clark et al., 2009), and can mostly be found among the Eos family (Mothé-Diniz et al., 2008) in our sample. The V-type association to the HEDs, a basaltic a chondrite meteorite class, has been well established. E-type (Tholen) and Xe-type (Bus-DeMeo) asteroids have a well-established connection to Aubrites (enstatite achondrites) because of their high albedos. Enstatite chondrites, which have a distinct thermal conductivity compared to other meteorite groups Fig. 3 can be related to M-types Clark et al. (2004). On the other hand, M-types that have been identified

---

<sup>1</sup>Simpson’s paradox describes a situation in which a dataset exhibits correlations across the entire sample that are statistically distinguishable from sample correlations within groups.



as having a high radar albedo or a high thermal inertia may have a high FeNi metal content. The thermal conductivity ( $k_{\text{grain}}$ ), grain density ( $\rho_{\text{grain}}$ ), heat capacity ( $c_s$ ), Young’s modulus ( $E$ ), and Poisson’s ratio ( $\mu$ ) for all aforementioned groups are shown in [Table 3](#). Below, we describe how these properties were chosen for each spectral group and analyze data from many sources, when appropriate, to account for temperature and porosity effects.

### 2.2.1. Thermal Conductivity

Laboratory measurements of meteorite thermal conductivities reveal dependence on the material porosity and temperature. In their review paper of thermal conductivities, [Flynn et al. \(2017\)](#) show that laboratory measurements of thermal conductivity do not change significantly in the temperature range from 100 and 300 K, but approach zero at 0 K. Additionally, void spaces can significantly impede the net solid-state heat flow within a meteorite sample ([Soini et al., 2020](#)). To account for porosity effects, we estimate the thermal conductivity at zero porosity using data collected at the same temperature.

In order to estimate thermal conductivity at  $\phi = 0$ , lines are fit to meteorite samples with porosities less than 12% from the literature ([Table 1](#)), as shown in [Fig. 3](#). Since the carbonaceous chondrites with measured  $k_{\text{eff}}$  had porosities exceeding this cutoff, we did not use any for our analysis. We found that enstatite chondrites have a larger thermal conductivity than the ordinary chondrite samples (and one Shergottite), likely due to mineralogical differences. The  $y$ -intercept of the best-fit lines give the thermal conductivity at zero porosity of 4.05 and 6.23  $\text{W m}^{-1} \text{K}^{-1}$  for ordinary chondrites and enstatite chondrites, respectively. Because the thermal conductivity for terrestrial enstatite is 90% that of enstatite chondrites at 275 K we scale the function downward by 10% to approximate the aubrite thermal conductivity, which are mostly comprised of enstatite. We used the same line slope to extrapolate a single measurement of thermal conductivity ([Opeil et al., 2010](#)) of the FeNi meteorite Campo del Cielo to estimate the thermal conductivity at  $\phi = 0$  are used in the thermal conductivity model to compute grain size.

Data presented by [Soini et al. \(2020\)](#) shows that the thermal conductivities of ordinary and carbonaceous chondrites are in agreement when the sample porosities are taken into account. Because we account for sample porosities and are using grain densities, we use the same zero-porosity thermal conductivity value for carbonaceous chondrites and ordinary chondrites, with the exception of CM chondrites. Newer thermal conductivity measurements of CM chondrites from [Opeil et al. \(2020\)](#) are also consistent with other carbonaceous chondrites. However, the spacecraft observations of B-type Bennu and Cg-type Ryugu revealed surfaces with weak, low-conductivity boulders that have thermal inertias which are  $\sim 2\text{--}3$  times smaller than stronger, high-conductivity boulders ([Grott et al., 2019](#); [Rozitis et al., 2020](#)). This stronger material may be identical to CM chondrites found on Earth, yet, the weak material is likely less abundant among meteorite collections ([Popova et al., 2011](#)). In order to account for this weak material on B-types, which are related to CM chondrites, We adopt a lower thermal conductivity for both CM chondrite material, which is use as an analog for both Ch and B-type asteroids. Because this weaker material is most likely primitive in origin, we assign the low thermal conductivity to CI chondrites as well.

Our computed thermal conductivity values agree with the [Soini et al. \(2020\)](#) model fits

to essentially the same dataset as ours. We accounted for temperature-dependent thermal conductivity among these samples by bootstrapping our  $k_{grain}$  calculations with the data compiled in Flynn et al. (2017). Essentially, we scale their relationship to our values of  $k_{grain}$  at 200 K. FeNi meteorites show a roughly linear dependence, and enstatite chondrites (and by deduction, the enstatite-dominated aubrites) show an inverse dependence on temperature. These temperature-dependent  $k_{grain}$  functions, which are valid for 200–350 K, are listed in Table 3 and are assigned a 10% uncertainty when used in the thermal conductivity model. Ordinary chondrites, HEDs, and carbonaceous chondrites do not demonstrate a significant dependence on temperature (Opeil et al., 2012).

### 2.2.2. Grain Density

Meteorite specimens, while not regolith, still contain small pores and cracks that lower the bulk density of the sample (e.g., Cadenhead and Stetter, 1975). These micro-porosities,  $\phi$ , range from 4% to 10%, but can be as high as 20% for weathered finds and as low as 2% for iron meteorites. We wish to use the grain density ( $\rho_{grain}$ ), the density of a material with zero porosity, as input to the thermal conductivity models. We primarily use the findings Macke (2010), who measured the porosities of individual meteorites with various compositions and computed  $\rho_{grain}$ . Table 3 lists grain densities for many meteorite analogs related to their respective spectral types. For the S-complex and V-types we use a uniform distribution for  $\rho_{grain}$  that spans the values reported in Macke (2010), instead of a normal distribution.

### 2.2.3. Heat Capacity

The ability of material to store thermal energy per unit mass is quantified by its specific heat capacity,  $c_s$ . Laboratory heat capacity measurements of several meteorites reveal a clear temperature-dependence (Beech et al., 2009; Opeil et al., 2012; Szurgot et al., 2012; Consolmagno et al., 2013; Wach et al., 2013; Macke et al., 2019; Opeil et al., 2020). We account for this dependence by performing an independent meta-analysis—similar to that on the thermal conductivity dataset above—in which we use literature data on meteorite heat capacities measured at various ambient temperatures. While Flynn et al. (2017) perform a similar analysis, they present fits for a temperature range of 75–200 K, which does not cover the full range of asteroid surface temperatures relevant to this work. Our empirical fits to the data are in agreement to the semi-empirical functions of Macke et al. (2019), who used a larger dataset. Our results are very similar to theirs over the same temperature range.

Opeil et al. (2020) present temperature-dependent heat capacities for five CM chondrites, which we compare our results to below. We compute 2nd order polynomial fits to the data shown in Table 2 over a temperature range of 175–300 K and with a  $y$ -intercept fixed at zero (because at low temperatures the heat capacity approaches zero). Among our dataset, we find that two distinct trends emerge, forming two groupings: one with all the iron-nickel meteorites (metallic) and one comprised of all chondritic and achondritic meteorites (non-metallic). The best-fit heat capacity equations (and coefficient uncertainties) for non-metallic and metallic meteorites at different temperatures are given by  $c_s = -0.0033 (\pm 0.0004) \times T^2 + 3.39 (\pm 0.10) \times T$  and  $c_s = -0.0044 (\pm 0.0004) \times T^2 + 2.84 (\pm 0.11) \times T$ , respectively. Results are shown in Fig. 3 and the fits from Macke et al. (2019) and Opeil



et al. (2020) are included for comparison. Because the Opeil et al. (2020) CM chondrite dataset clearly exhibit higher heat capacities than our fits to other non-metallic meteorites, we use the function  $c_s = -0.0036 \times T^2 + 3.84 \times T$  for Ch and B-type asteroids, which is the fit to the non-metallic meteorites scaled 15% larger.

#### 2.2.4. Mechanical Properties

Young’s modulus ( $E$ ) and Poisson’s ratio ( $\nu$ ) are used in the thermal conductivity model to calculate the contact area between grains within a regolith. In particular, these two quantities are used to approximate the deformation both along the axis of an applied force and in the orthogonal dimensions. For M-type asteroids, we use the values of these properties measured for Fe-Ni alloys, which are similar to iron meteorites, by Ledbetter and Reed (1973). Ibrahim (2012) reports Young’s and Bulk Modulus ( $G$ ) for many ordinary and carbonaceous chondrite meteorites. We calculate Poisson’s Ratio using the relationship between the three variables:  $\nu = \frac{E}{2G} - 1$ . This equation assumes isotropic material properties and is also used to propagate the reported  $E$  and  $G$  uncertainties presented in Ibrahim (2012). The values for E-type asteroids are assumed to be the same as used for S-types, as indicated by italics in Table 3.

#### 2.3. Monte Carlo Implementation

We compute a thermal conductivity,  $k_{eff}^{obs}$ , that is empirically-derived from  $\Gamma$  and assumed values of  $c_s$ ,  $\rho_{grain}$ , and a range of porosities. This value is equated to the theoretically-modeled thermal conductivity calculated using the above procedure, in order to obtain an estimated regolith grain size. Most input variables are taken from a distribution that is generated based on the uncertainty of that parameter given in Table 3 and mentioned above. Most parameters have associated  $1\sigma$  uncertainties from which we generate Gaussian probability distributions. Exceptions include the porosity, for which we use a uniform random distribution from 0.276 to 0.876; the lower value is the porosity of close-hexagonal packing scheme and the upper value represents the hypothesized porosity of cometary regolith (i.e., Sunshine et al., 2016, and references therein). For each iteration, a single grain size is produced, ultimately constructing a distributed set of 10,000 grain sizes. For some trials, the combination of input parameters produced model thermal conductivity values that were incompatible with the observed value. These cases were therefore not included in the final distribution.

Output grain sizes are transformed into the logarithmic scale developed by Krumbein and Aberdeen (1937) which eases comparison of sediment sizes across many orders of magnitude. These Krumbein “phi-scale” grain sizes,  $d_{g\phi}$ , are set to zero at 1 mm. The output grain diameters,  $d_g = 2r_g$ , are transformed into this scale with:

$$d_{g\phi} = -2 \log_2(d_g/1 \text{ mm}). \quad (10)$$

Note that smaller and negative values represent larger grain sizes. Output grain size distribution for an object does not necessarily, or even typically, represent a Gaussian distribution. Thus, we report the median of this distribution as the best-fit grain size, and report upper

and lower uncertainties by computing the grain sizes that encompass one standard deviation from the median value. The diurnal thermal skin depth ( $l_s$ ) is also computed and the median and standard deviations from the output distribution are reported. For reference the output  $r_g$  and  $l_s$  distributions for a hypothetical S-type asteroid with  $\Gamma = 150 \pm 50 \text{ J m}^{-2} \text{ K}^{-1} \text{ s}^{-1/2}$ ,  $T_{surf} = 300 \pm 10 \text{ K}$ , and  $P_{rot} = 10 \text{ hrs}$  are shown in [Fig. 4](#).

#### 2.4. Caveats and Model Limitations

Its possible that in our albedo-based classification that M-types and low-albedo V-types could be misclassified as S-types and, similarly, some P-types may be misclassified as C-types. However, we see no obvious reason to re-assign any of these S-types to the M-type group, as their thermal inertias are inconsistent with a high thermal conductivity which would otherwise suggest a metallic-rich surface. On the other hand, some P-types might be misclassified as C-types. The difference in assumed material properties between C and P-types that we use is not large and would not alter the reported grain size by more than a few percent. We do change the classification of (4003) Schumann from C-type to P-type, based on its location in the outer part of the Main Belt ( $\approx 3.4 \text{ au}$ ) where P-types are more abundant over C-types ([DeMeo and Carry, 2013, 2014](#)).

For some asteroids in our sample, the material properties inferred from spectroscopy, color, or albedo data may not be correct. For example, incorrect assignment of an asteroid as a metallic M-type when it is actually comprised of silicate S-type material is a possible case that could cause non-negligible change in the grain size estimate. To understand the potential effects of incorrect classification, we re-ran our thermal conductivity model for the M-type (22) Kalliope with S-type properties, as its low radar albedo may suggest a silicate-rich instead of a metal-dominated surface ([Lupishko and Belskaya, 1989](#); [Ockert-Bell et al., 2010](#); [Hardersen et al., 2011](#)). Assuming Kalliope as an S-type instead of an M-type increased the grain size by  $\sim 8\%$ , which is *far* below the typical  $d_{g\phi}$  uncertainty reported in [Sec. 3](#). From this extreme case, we can reasonably assume that uncertainty in the assumed material properties do not significantly contribute to any significant bias in grain sizes between compositions.

Both of the thermal conductivity models assume homogeneous, monodispersed grain sizes throughout the surface and constant thermophysical properties with depth. This is also true of reported thermal inertia values. Surface processes that sort grain sizes both vertically and spatially are likely present on asteroids ([Richardson et al., 2020](#), and references therein). Thus, this assumption of regolith homogeneity is certainly not the case for *any* asteroid, and many spacecraft missions have revealed surfaces that are heterogeneous ([Fig. 1](#)). Specifically, the Hayabusa mission showed that the surface of Itokawa was consistent with the remotely-determined thermal inertia ( $600\text{--}800 \text{ J m}^{-2} \text{ K}^{-1} \text{ s}^{-1/2}$ ), yet still contained regions dominated by fine-grained regolith—counter to interpretation of a high thermal inertia ([Müller et al., 2014](#); [Yano et al., 2006](#)). Overall, most asteroid regoliths are expected to be heterogeneous, and the assumption of a single grain size and homogeneous regolith is a practical simplification. However, estimates on the spatial heterogeneity of an asteroid surface are limited due to the fact that we are using disk-integrated (spatially-unresolved) observations.

The recent spacecraft visits to two primitive NEAs, Ryugu and Bennu, unexpectedly revealed surfaces that were different from the original interpretation of their respective thermal remote observations (see Fig. 1). The surfaces of these objects exhibited surfaces comprised of a significant fraction of large boulders that were larger than the grain size estimated from thermal inertia (Grott et al., 2019; Rozitis et al., 2020). Because these boulders have a low thermal conductivity that is similar to a coarse-grained regolith, they exhibit thermal properties indistinguishable from a coarse-grained regolith. Ryan et al. (2020) claimed that the underestimated grain size of Bennu from its thermal inertia can be explained by the inherently low thermal conductivity of Bennu’s surface, which resembles CM chondrites and causes non-isothermal effects within the regolith. Grain size estimates are larger when accounting for this non-isothermality, thus can partly explain the large boulders on Bennu and Ryugu.

Since regoliths are assuredly a mixture of particle sizes with an unknown size-frequency relationship our reported grain size estimates should be thought of as a *thermally-characteristic* grain size. In fact, Presley and Craddock (2006) modeled the thermal conductivity of known granular mixtures and deduced that the modeled grain size is most representative of the larger regolith grains—specifically the 85th to 95th percentiles—rather than the mean or modal grain size. On the other hand, Ryan et al. (2020) showed that the particle size from thermal inertia corresponds to within 15% of the mean volumetric particle size for various size-frequency distributions. Since the emitted thermal flux is strongly temperature dependent ( $\propto T^4$ ), the grain sizes are most representative of the warmest portions of the surface, with less contribution from cooler areas. This may mean that smaller, warmer grains, are most represented in the thermal inertia estimate.

As remarked by Ryan et al. (2020), the apparent thermal inertia will be that of solid rock when the effective particle size is approximately larger than the skin depth, which could be the case for fast rotators with low  $k_{\text{grain}}$ . If the size range of particles exceeds the skin depth, then the surface is best modeled as a lateral, checkerboard-like mixture of regolith and bare-rock (boulders) (e.g., Bandfield et al., 2011; Rozitis et al., 2020). Nevertheless, the aim of this work is to investigate the grain size trends among the broad asteroid population and the thermal conductivity model used provides us with a sufficient, efficient approach of interpreting a large dataset of thermal inertias. Despite these uncertainties, the grain size estimates in this work still have utility and can be used to identify trends within the asteroid population.

### 3. Results and Analysis

We report modeled estimates of grain size and thermal skin depth in Table 4, along with the model input parameters (with associated uncertainties) for each object— $\Gamma$ ,  $T_{\text{surf}}$  and spectral type. In some cases, the estimated grain sizes exceed the calculated thermal skin depth. In order to caution readers who may use these grain sizes we mark these grain sizes in Table 4 with a “\*”. We find that the Sakatani et al. (2017) thermal conductivity model is incompatible with some of the thermal inertias. In these cases the model theoretically predicts a higher thermal conductivity relative to the “observed” value. Therefore, only

the grain size from the [Gundlach and Blum \(2013\)](#) model are reported for these instances. Similarly, we find that several C-type asteroids have very low reported thermal inertias that were incompatible with the assumed thermal conductivity. In these cases, we re-ran the model with B-type input parameters, which assume a lower value for the thermal conductivity. We classify these objects as “B\*-type”, and discuss them further in the discussion. Lastly, we have found that the albedos of a few objects in our set that are inconsistent with the spectral type of the reported family. Similar to [Masiero et al. \(2013\)](#), we thus reject the family membership of these objects and indicate this by crossing through the family name in the rightmost column of [Table 4](#).

We now aim to investigate possible explanatory factors and quantify their influence on the regolith grain size for our sub-sample of the asteroid population. We test the hypothesis that grain sizes are negatively correlated with asteroid diameter (indicating impact driven processes) and whether grain size is positively correlated with rotation period (which is caused by thermal fracturing processes). Various multiple linear (hereafter, multi-linear) regression models are fit to the MBAs to identify and characterize the dependencies of these factors ([Sec. 3.1](#)). Although the NEAs in this work offer insight into the regolith of very small asteroids, the chaotic nature of changes in their orbital parameters makes it difficult to hold other factors constant—such as thermal environment and impact flux—potentially complicating the multi-linear analysis. We perform a separate analyses on NEAs in [Sec. 3.3](#). In our trend analyses, we use the grain sizes produced by the [Gundlach and Blum \(2013\)](#) thermal conductivity model because the [Sakatani et al. \(2017\)](#) model was unable to provide an estimate for some objects. In general the [Sakatani et al. \(2017\)](#) grain size estimates are consistently larger than those from the [Gundlach and Blum \(2013\)](#) model, but we claim that the trends we are investigating should still be found among the [Sakatani et al. \(2017\)](#) grain size dataset.

### 3.1. Multi-linear Regression

Multi-linear regression is a method that attempts to model a dependent variable (the grain size,  $d_{g\phi}$ ) as a linear combination of several independent variables—in our case, diameter and rotation period. The fitted slope, or coefficient, of each independent variable and a  $y$ -intercept, along with  $1\sigma$  uncertainties for each of these parameters is reported. We consider several segmented, or piece-wise, multi-linear regression models with different numbers and combinations of break points for both independent variables ( $D_{eff}^b$ , and  $P_{rot}^b$ ), as listed below:

- *M-1*: No break-points
- *M-2*:  $1 \times D_{eff}^b$
- *M-3*:  $1 \times P_{rot}^b$
- *M-4*:  $1 \times D_{eff}^b, 1 \times P_{rot}^b$
- *M-5*:  $2 \times D_{eff}^b$

These segmented models partition the indicated independent variable into intervals for which a different function (slope) is fit to the data. Adding a break-point creates two lines that form a continuous, piece-wise function in lieu of a single linear fit. In addition to slope estimates of the lines, the location of the break-points are estimated.

The diameter and rotation period are transformed by taking the  $\log_{10}$  when used in the multi-linear regression models. This variable transformation is done to best capture the wide variance in these variables which each span more than 2 orders of magnitude. Unlike the thermal inertia multi-linear analysis presented in [MacLennan and Emery \(2021\)](#), we do not consider temperature as an explanatory variable because it is already accounted for in the thermal conductivity model via temperature-dependent heat capacity values ([Sec. 2.2](#)) and radiative heat transport.

We compare the multi-linear model fits to one another by taking the adjusted  $r^2$  ( $r_{adj}^2$ ) statistic and Bayesian Information Criterion ( $BIC$ ). The  $r_{adj}^2$  is a determination of the degree to which the model explains the variance in the dependent variable (i.e., higher values indicate a better fit), while also accounting for the number of predictor parameters in the model. The  $BIC$  is used to indicate which model maximizes the likelihood of matching the data (lower values indicate a higher likelihood), and accounts for the number of model parameters (more parameters increases the score). Both of these statistics are shown in [Table 5](#), along with the number of free model parameters,  $n$ . The number of free parameters is calculated from the *total* number of fitted variables, which increases by 2 when a break-point is added <sup>2</sup>.

When comparing the results amongst all models, we find that  $M-4$  has the largest  $r_{adj}^2$  and lowest  $BIC$ . Statistically speaking, the difference between two model  $BIC$  values,  $\Delta BIC$ , indicate a preference for one over another. [Kass and Raftery \(1995\)](#) state that  $\Delta BIC > 6$  indicates a *strong* preference for the lower  $BIC$ . Since  $M-4$  has a  $\Delta BIC = 34$  between it and the second lowest  $BIC$  value ( $M-2$ ), we use this as an indication that it is the preferred model. We plot the best-fit and preferred  $M-4$  model in [Fig. 5](#). Black symbols are estimated grain sizes for each object and colored symbols are values from the multi-linear models. Solid bars indicate the  $1\sigma$  range of the diameter and rotation period breakpoints, respectively, at the top of each panel. The estimated intercepts, linear coefficients (slopes), and break-point(s) ( $D_{eff}^b$ ,  $P_{rot}^b$ ), along with the associated uncertainties, are listed in [Table 6](#). We remark that the model intercept value represents the predicted  $d_{g\phi}$  for a hypothetical object with  $D_{eff} = 1$  km and  $P_{rot} = 1$  hr, which is just under 1 m for  $M-4$ .

### 3.2. Compositional Effects

Here, we investigate if, and how much, the grain sizes vary by or depend on the surface composition of an asteroid. For this analysis we use spectral group as a proxy for composition. Simply comparing the means of the grain size distributions between the groups is not appropriate, as some of the independent explanatory variables are correlated with grain size: for example, primitive C-complex and P-type bodies are more represented at larger sizes,

---

<sup>2</sup>This is because each new line has a slope and a  $y$ -intercept that is independent from others, although a single model intercept is ultimately reported.

and the E/Xe-types are largely represented in the lower size range<sup>3</sup>. Instead, we perform post-hoc t-tests between the spectral classes by using the model residuals from *M-4*. Since the multi-linear analysis doesn't account for the spectral type, any differences in the group residuals can be used to indicate disparities in regolith grain sizes.

We apply Welch's t-test<sup>4</sup> (Welch, 1947) in a series of trials between each possible combination of spectral class, as well as between each class and the entire sample with that particular class removed. The null hypothesis that is tested is that the means between the groups do not differ. We report the *p*-values of these trials in Table 7: lower *p*-values indicate a higher probability that the null hypothesis is not supported. Table 7 shows the mean and standard deviation of the model residuals and the number of objects for each group. We analyze the S, C, and E-types both with and without the objects in which their spectral type was inferred by their albedo. Similarly, for B-types we analyze both the confirmed B-types and those marked as B\* in Table 3 for which we assign CM meteorite properties based on their low-thermal inertias.

The model residual distributions, grouped by composition, along with the mean model residuals are depicted in Fig. 6. Compared to the mean of the remainder of the sample, there is strong statistical evidence ( $p < .01$ ) that suspected metal-rich asteroids on average exhibit grain sizes that are nearly twice as large as asteroids of the same diameter and rotation period. We interpret this difference as an indication that one of the thermophysical or material properties of FeNi metal is affecting the efficiency of regolith breakdown process. Additionally, the average grain sizes of M-types and E-types are statistically indistinguishable from one another (Table 7), and from the suspected metal-rich objects. On the other hand, P-types show a much smaller mean grain size than the remainder of the sample ( $p < .01$ ). Finally, we note here that S-types and C-types have statistically smaller and larger grain sizes, on average, compared to the rest of the sample. Consistent with this finding, the carbonaceous K-types have coarser-grained regoliths compared to S-types. Potential explanations for these group differences in grain size are discussed in Sec. 4.

### 3.3. Near-Earth Asteroids

Thus far in our analysis we have excluded NEAs and Mars-Crossers (MCs) in order to mitigate the potential influence on regolith evolution caused by widely-varying thermal and impact environments. Because these asteroids exhibit a wide range of orbital parameters (varying in both semimajor axis,  $a$ , and eccentricity,  $e$ ) they are subject to drastically varying external influence, whereas we wish to examine the factors inherent to asteroids themselves. We analyze the grain sizes (Sec. 3) calculated for the NEAs with thermal inertia estimates from other works ( $N = 21$ ) and those estimated in MacLennan and Emery (2021) ( $N = 7$ ). With grain sizes for these 28 asteroids, we seek to identify regolith dependencies on orbital factors.

---

<sup>3</sup>Similar relationships are apparent between spectral classes and heliocentric distance (DeMeo and Carry, 2013).

<sup>4</sup>We use Welch's t-test, as opposed to the Student's t-test, as the latter assumes that the two groups have equal variance or sample size, which is not the case here.



We perform a multi-linear regression model, similar to the one presented in [Sec. 3.1](#), but with different input factors. We do not consider segmented linear fits as the low number of objects in this NEA subset may result in model over-fitting. The independent explanatory variables we include here are the diameter and rotation period transformed into  $\log_{10}$  space. But now we also include the orbital semimajor axis ( $a$ ), perihelion ( $q$ ), and aphelion distance ( $Q$ ) as possible explanatory variables. However, these orbital parameters are *not* transformed into logarithmic space in the multi-linear model and are left as-is.

The best-fit regression model for NEAs indicated that  $Q$  is the only statistically significant variable. Thus, the NEA grain sizes dataset does not appear to show the same trends with the diameter and rotation period that exist among main-belt objects. On further inspection, potential co-linearity between  $D_{eff}$  and  $Q$  could raise some doubt of the significance of this result. However, employing a multi-linear model with only  $Q$  and  $D_{eff}$  did not change the significance of either variable. We thus conclude that  $Q$  is a better predictor of grain size than diameter and rotation period for NEAs. The grain sizes of NEAs as a function of aphelion, perihelion, diameter, and rotation period are shown in [Fig. 7](#). Symbol colors indicate the spectral type of the objects, with unfilled symbols indicating that the classification was used using the albedo as a proxy. It is interesting to note here that the grain sizes of objects with  $0.9 < q < 1.1$  au are somewhat higher (on average) than the asteroids outside this range and that asteroids with largest grain sizes ( $> 10$  cm) are found having perihelia interior to Earth’s orbit.

An important caveat to note here is the fact that NEA and MC asteroid diameters extend to a lower size range compared to MBAs. Because the overlap in NEA and MBA diameters occurs for  $2 \text{ km} < D_{eff} < 40 \text{ km}$ , it is difficult to draw conclusions about the difference between the two populations from these sets of multi-linear models. Grain sizes for NEAs with  $D_{eff} > 2 \text{ km}$  ([Fig. 7](#)) are similar to those of similarly sized MBAs and exhibit the same inverse dependency on asteroid diameter. On the other hand, NEAs smaller than 2 km don’t show any discernible trend between grain size and asteroid diameter. It is possible that MBAs exhibit a similar lack of trend, but the MBAs in our dataset do not extend to this size range.

Additionally we note that, in general, the comparison between rotation period and grain size for NEAs appears to be consistent with MBAs, with a few exceptions. Asteroids with spin rates near the spin barrier ( $P_{rot} \approx 2.12 \text{ hr}$ ) exhibit a range of grain size spanning 3 orders of magnitude, which mimics the grain size span for the entire Main Belt sample. At the low end of the range is 1950 DA, with two other fast-rotating NEAs exhibiting very large grain sizes. The latter two appear to be very consistent with the inverse trend between rotation period and grain size for main-belt objects. Thus, 1950 DA appears to be an outlier in this respect and we further discuss this point below.

## 4. Discussion

The statistical relationship between grain size and size and rotation period can be used to infer regolith processes. The best-fit multi-variate model,  $M-4$ , indicates that a break-point value near  $\sim 10 \text{ km}$  occurs in the relationship between asteroid diameter and regolith

grain size. The slope fit to objects smaller than this size shows a strong inverse relationship between asteroid diameter and regolith grain size. On average, the regolith grain size of 10 km bodies is 0.6 mm, with  $M-4$  predicting a grain size of 25 mm for 2 km objects—an increase in  $d_{g\phi}$  of nearly a factor of fifty, which translates to a power slope of  $\sim 6$ . The  $M-4$  slope fit for asteroids larger than 10 km is statistically indistinguishable from zero, which suggests no dependence of regolith grain size on asteroid diameter. Interestingly, there appears to be an inverse relationship between the upper limit grain size and asteroid diameter among objects larger than  $\sim 80$  km. This potential trend could indicate a different process or an additional, unaccounted for factor that influences regolith development on 100-km-scale asteroids, which are thought to be primordial bodies.

The preferred multi-linear model predicts that objects with  $P_{rot} \approx 5$  hrs have the smallest grain sizes. As the rotation period increases, the model predicts that the grain size increases. Objects rotating faster than  $\sim 5$  hrs show a steep increase in grain size with decreasing rotation period. Interestingly, the model predicts that objects with 2.2 hrs and 300 hrs rotation periods should both have  $d_g \sim 8$  mm. Both of these trends are statistically significant and may indicate one or more rotation period-dependent processes that act on asteroids. We discuss this point further in [Sec. 4.2](#).

#### 4.1. Meteoroid Impact Breakdown

Repeated impacts of smaller asteroids or meteoroids into the surface of an asteroid will create ejecta—some of which is retained at the surface as regolith. The general relationship between the mass of the ejecta ( $M$ ) above a certain velocity ( $u$ ), as a function of impactor mass and velocity ( $m$  &  $U$ ) is:

$$\frac{M}{m} \propto \left(\frac{u}{U}\right)^{-3\tau} \quad (11)$$

where  $\tau$ , an empirically-derived exponent, is taken as 0.41—the value for sand ([Housen and Holsapple, 2011](#)). For reference, the probability distribution of relative velocities between asteroids in the Main Belt, which is roughly Maxwellian, has a mode of  $4.3 \text{ km s}^{-1}$  and a mean value of  $5.3 \text{ km s}^{-1}$  ([Farinella and Davis, 1992](#); [Bottke et al., 1994](#)). The velocities of incoming meteoroids are mostly independent of the size of target body (due to the extremely small gravitational attraction of an asteroid), which leaves the relative size of the impactor to the target asteroid as the dominant factor in [Eq. 11](#).

Additionally, the mechanical and structural properties of the impacted asteroid play a small but non-negligible role in determining the outcome ([Housen and Holsapple, 2003](#)). For example, in targets with low porosity, the ejecta velocities are larger than that of an otherwise identical impact into a porous target ([Nakamura and Fujiwara, 1991](#); [Nakamura et al., 1994](#)). Energy from the impact is concentrated near the impact site and worked into crushing the surface material, instead of ejecting it at high velocities. [Holsapple et al. \(2002\)](#) points out that if the porosity of the target region is greater than 50%, only 10% of the crater mass is ejected, as most of the energy is partitioned into compacting the material. Additionally, material strength of the target plays a vital role in the ejecta outcome. In general, stronger asteroids produce more ejecta, which can escape the gravitational well of the body more easily than an asteroid comprised of weaker material. A high strength (or

low porosity) may partly explain the larger average grain sizes among M-types, which are all  $> 10$  km in our sample. If internal strength and/or porosity properly explain this difference in M-type grain size, then we expect that asteroids that are not M-type but have similar internal properties will have similar regolith properties. Future efforts in mass determination for many asteroids can be used to investigate a potential relationship between the macro-porosity of asteroids and regolith development. For example, a multi-linear model that incorporates macro-porosity, in addition to object size and rotation period, may be able to identify such a relationship. Our expectation is that the  $\sim 100$  km objects that exhibit larger regolith grains could be stronger and/or less porous than those with smaller regolith grains.

Using the measured meteorite flux at 1 au, [Basilevsky et al. \(2013\)](#) calculated characteristic lunar boulder survival lifetimes from boulder size-frequency statistics on rims of lunar craters with known ages. They calculated that it takes 25–50 Myr to destroy 50% of a typical 1 m-sized boulder, and after 190–300 Myr, more than 99 % of boulders should be completely destroyed. [Basilevsky et al. \(2015\)](#) extrapolated the lunar timescale to Ceres and Vesta assuming that boulders are broken down exclusively via impact weathering. On these large MBAs the boulder weathering timescale is 3% of the lunar value (i.e., 0.75–1.5 Myr), which is mainly a consequence of the meteorite flux being  $\sim 2$  orders of magnitude greater in the Main Belt than at 1 au. In all cases, the remaining fraction of boulders exponentially decreases with time.

This theoretical timescale is significantly shorter than the ages of most asteroid families, although a few young ( $< 1$  Myr) families have been identified (e.g., Table 1 in [Nesvorný et al., 2015](#)) in the Main Belt. In principle, asteroids in these young families could theoretically be used to investigate regolith properties of asteroid surfaces that have been reset from an impact. One consideration that must be made is the fact that the small asteroids that exist in these recently-formed families are less likely to retain fine-grain regolith particles because of their low surface gravity. Statistically-speaking, a 1 km asteroid is expected to experience an average of 5 catastrophic breakups every 1 Myr ([Holsapple et al., 2002](#)), or once every  $\sim 200$  kyr. This timescale is shorter than the estimated boulder survival timescale (0.75–1.5 Myr) of [Basilevsky et al. \(2015\)](#), so we expect that an MBA of this size would not survive long enough to have much of a developed regolith. On the other hand, a 10 km MBA will survive, on average, 16 Myr ( $\sim 80$  times longer than a 1 km body). The implication that 10 km asteroids exist long enough to develop a regolith through impact degradation is consistent with our grain size results.

Our results show that the differences in grain size for NEAs and MCs are most likely dependent on their orbital parameters. This relationship could be explained by the drastic change in collisional probability and velocities of NEAs with MBAs in the Main-Belt ([Bottke et al., 1993](#)). Because an NEA that enter the Main-Belt is traveling relatively slower, the velocity difference between it and a typical MBA will be larger compared to two MBAs with similar orbits. This would theoretically result in more efficient impact weathering rate for NEAs with  $Q \gtrsim 2.2$  au, compared to MBAs of a similar size. However, there is no obvious difference in grain sizes for NEAs and MBAs of similar object sizes. Thus, we suppose that another process is the reason for the grain size dependency on orbital parameters.

Evidence from meteorite impact breccias—fragmented samples of an asteroid collision (Burbine and Binzel, 2002)—offers insight into the state of asteroid regolith. These meteorites are formed from the lithification of near-surface material from the heat and pressure of an impact and classified by their texture and presence/absence of clasts (Bischoff et al., 2006). A direct connection to asteroid regolith can be made if they are rich in solar-wind gases that are identified isotopically (McKay et al., 1989). Clasts ranging in size from several hundred microns up to many centimeters have been found in HEDs, carbonaceous, ordinary, and enstatite chondrites, and other stony meteorite regolith breccias (Bischoff et al., 2006, and references within). Interestingly, Bischoff et al. (2006) point out that some aubrites are known to contain large enstatite clasts up to 10 cm in size, as well as metal grains up to 1 cm in size. If the aubrite parent body is matched by an E-type spectrum, then these systematically-larger clasts and grains are well-matched to the finding that E-types have larger regolith grains than other spectral types.

#### 4.2. Thermal Fatigue Breakdown

The cyclic heating and cooling experienced by asteroid surfaces, as a consequence of time-varying insolation, can result in large spatial temperature gradients within the material. These gradients create heterogeneous thermal stress fields (expansion and contraction) across mineral grain boundaries of a rock (Molaro et al., 2015). This thermal fatigue process involves the structural weakening of the material from thermal gradients and ultimately results in the breakdown of asteroid regolith. Delbo’ et al. (2014) experimentally demonstrated the effectiveness of this process on a chip of the Murchison (CM2 carbonaceous chondrite) and Sahara 97210 (L/LL 3.2 ordinary chondrite) meteorites, and it has been debated whether or not thermal fracturing is a relatively significant weathering mechanism for terrestrial rocks (e.g., Molaro and McKay, 2010, and references within). Convincing evidence from the Moon and Mars (Ruesch et al., 2020; Eppes et al., 2015) indicates that thermal breakdown is efficient on other solar system bodies. Both Molaro et al. (2017) and Ravaji et al. (2019) posit that the efficiency of thermal fracturing is controlled by the maximum thermal stress experienced by the rock, as opposed to the average, so we focus on maximum stress in this discussion.

The surfaces of airless bodies are likely highly susceptible to thermal fatigue, as their lack of a thermally-insulating atmosphere exposes them to extreme insolation variation. Molaro and Byrne (2012) numerically simulated the amount of internal stress experienced by a rock on Vesta, Mercury, and the Moon’s surface. In particular, they estimated the amount of temperature change, per unit time ( $\Delta T/\Delta t$ ) and compared to the temperature gradient  $\nabla T$  within rocks having orientations at different latitudes on the surface. They found that while a rock on Vesta experienced the largest temporal temperature change, it also had the lowest  $\nabla T$ —leading to a smaller stress field. This case is opposite to that of the Moon and Mercury, in which  $\nabla T$  and  $\Delta T/\Delta t$  were highly correlated. The modeling efforts of Molaro and Byrne (2012) demonstrated that greater thermal stresses were experienced for rocks experiencing faster sunrises (i.e., shorter rotation periods). The stresses were more pronounced for airless solar system bodies farther from the Sun and on rock surfaces that faced the rising sun. Daytime shadowing, especially when occurring just after local sunrise or before local sunset,

was also a major contributor to increasing the temperature gradients. The authors also predict that pre-existing cracks would contribute even more to the crack growth rate and shorten weathering timescales.

Our asteroid grain size modeling results indicate that objects with  $P_{rot} = 5$  hrs are most likely to exhibit the fine-grained regoliths. This result coincides with the findings of [Molaro and Byrne \(2012\)](#), as they predicted less-efficient thermal fatigue for objects with slower sunrise times. Coarse-grained regoliths ( $d_g \gtrsim 1$  cm) are found among the asteroids with  $P_{rot} > 100$  hrs. The rotation period breakpoint in the multilinear fit at  $\sim 5$  hrs indicates a local grain size minimum which could indicate an optimal rotation rate that maximizes thermal fracturing for asteroid surfaces. The rotation periods of these objects are slightly less than the prediction of [El Mir et al. \(2019\)](#) and [Ravaji et al. \(2019\)](#) who found that breakdown timescales for a 10 cm rock are minimized for rotation periods in the range 10 – 15 hrs. It is not immediately obvious why these two works predict a slower optimal rotation rate for thermal breakdown and more work may be needed to reconcile the models with our empirical finding. However, both of these works predict longer breakdown timescales for rotation periods outside of this range, which is consistent with the multi-variate model results.

[Molaro et al. \(2015\)](#) studied the sensitivity of their micro-stress model to changes in the material properties of the rock and found the thermal expansion coefficient and Young’s modulus (which describes tensile elasticity) to be the most influential properties, and that thermal conductivity, perhaps counter-intuitively, does not significantly affect the rate of crack growth. The thermal parameter,

$$\Theta = \frac{\Gamma}{\varepsilon \sigma_0 T_{eq}^3} \sqrt{\frac{2\pi}{P_{rot}}} \quad (12)$$

may intuitively at first seem to be useful in predicting the effectiveness of thermal fatigue on asteroid surfaces, as it can be used as a proxy for the amplitude of the diurnal temperature range. However, its formulation doesn’t capture the essential information regarding the heating and cooling *rates* of a boulder/rock at the surface. For example, regolith on very slow rotators will experience slow sunrises that result in relatively slow rate of temperature change. This behavior may seem paradoxical if one were only to examine the thermal parameter for a hypothetical slow-rotator: as  $P_{rot}$  increases,  $\Theta$  becomes smaller and the diurnal temperature range is maximized. However, the rate of temperature change is relatively small for a point on the surface of a slow-rotator, and the insolation change during long sunrises and sunsets does not result in spatial temperature gradients large enough to .

The grain size of suspected metal-rich (Met) asteroids are, on average,  $\sim 2$  times higher than asteroids of the same diameter and rotation period ([Fig. 5](#)), suggesting that either regolith is not efficiently broken down or that smaller regolith grains are preferentially lost via one of the mechanisms discussed in [Sec. 4.3](#). High values of Young’s modulus were shown by [Molaro et al. \(2015\)](#) to significantly increase the efficiency of the thermal fatigue process, because stiffer materials are less able to accommodate the thermal expansion of grains. Iron-nickel meteorites, which are compositionally homogeneous could serve as an analog for M-type asteroids. Mesosiderites, a silicate-metal mixture, are a more heterogeneous alternative

analog that would be more susceptible to thermal stress buildup surrounding silicate grains. Assuming that thermal cycling is the dominant weathering process, and given the high Young’s modulus of metals, it would stand to reason that asteroids that are composed of metal-silicate mixtures should have fine-grained surfaces and more homogeneous pure metal surfaces should not have fine-grained regoliths. Regoliths of these metal-rich bodies could be subject to a process or processes that remove the fine-grained portion of regolith. Impact ejection seems the most likely, as discussed in the following subsection, because metal targets have a much higher strength compared to silicate or carbonaceous meteorites. This larger strength would lead to an increase in the overall velocities (Nakamura et al., 1994) of ejecta particles relative to S-complex and C-complex asteroids.

In the absence of other processes, thermal fatigue may become less efficient for a given object’s regolith through time. As smaller grains are broken down through time they form an insulating layer. In this regard, thermal fracturing may be a self-limiting process, and may lead to regolith stratification of a surface through time in the absence of other processes. In actuality, impact processes disrupt asteroid surfaces over time and mix the material (Hörz and Schaal, 1977, i.e., impact gardening;). However, depending on the impact gardening timescale relative to thermal breakdown, asteroid regolith may become stratified at mm or sub-mm length scales with smaller grains at the top.

#### 4.3. Regolith Retention & Loss

Once formed and throughout its evolution, the regolith layer of an asteroid is subject to processes that may remove material from the object. The discovery of and categorization of active asteroids—those which are observed to exhibit mass-loss—has been a recent focus of study. Several potential mechanisms can conceivably remove regolith from the surface of asteroids. Jewitt (2012) reviews such mechanisms, which include impact, centrifugal (inertial), and electrostatic ejection. Depending on the physical properties of an asteroid and its orbital location, each of these processes may or may not be effective. Additionally, the effects that each has on altering the grain size distribution of a regolith may be different. Observations of active asteroids provide important knowledge about the nature of ejection mechanisms.

In addition to mechanically weathering regolith, the process of multiple meteoroid impacts may also *remove* regolith grains from an asteroid surface. Energy from a meteoroid impact upon an asteroid surface is partly transferred to individual regolith grains, resulting in a velocity distribution that depends on the size of the grains. Ejecta grains traveling at a velocity that exceeds the escape velocity of the object are permanently ejected from the surface. The other factors, impactor mass and target mass, thus can be varied in order to predict the mass fraction of ejecta that is retained as a function of velocity (Eq. 11). In any case, smaller regolith particles are more likely than larger particles/boulders to be removed through impact ejection.

Our grain size dataset shows that, on average, asteroids larger than  $\sim 10$  km have regoliths that are similar to the largest bodies, with M-types having a notable exception. On the other hand, grain size increases with decreasing asteroid size for smaller asteroids.



This 10 – km size threshold could be indicative of an abrupt change in the process of regolith breakdown, or alternatively, may be the result of regolith loss from smaller asteroids of smaller grains that have reached speeds above the escape velocity. Using crater scaling laws, [Housen et al. \(1979\)](#) predict that asteroids in the 1–10 km range should not harbor a significant regolith ( $\ll 1$  mm thick) due to a decrease in *both* the strength and gravitational field of bodies of this size.

For fast-rotators, the outward centripetal acceleration near their equators is comparable to the downward gravitational acceleration. Regolith grains in these locations therefore exist in a precarious state, and a small perturbation can transfer enough energy to cause the ejection of equatorial material where the effective gravity is near-zero ([Guibout and Scheeres, 2003](#)). It is difficult to theoretically predict whether this kind of mass-loss occurs incrementally, on a grain-by-grain basis, or catastrophically, with large portions ejected at a time ([Scheeres, 2015](#)).

Among small asteroids, the cohesive (e.g., van der Waals) forces between regolith grains smaller than  $\sim 1$  cm have theoretically ([Scheeres et al., 2010](#)) and experimentally ([Murdoch et al., 2015](#)) been shown to dominate over gravitational, inertial, and electrostatic forces in some cases. Evidence for cohesive forces acting on an asteroid surface was found for the 1.3 km NEA (29075) 1950 DA ([Rozitis et al., 2014](#); [Gundlach and Blum, 2015](#)). [Rozitis et al. \(2014\)](#) calculated the amount of cohesion to be at least  $64^{+12}_{-20}$  Pa. Cohesive forces are inversely dependent on the surface area of the regolith grains ([Scheeres et al., 2010](#)) which indicates that a regolith comprised of smaller grains may be stronger than one comprised of larger grains. The cohesive forces within a regolith alters the effectiveness and behavior of potential loss mechanisms. Individual regolith grains (or larger rocks) lacking cohesion could incrementally be lost at an incremental rate, but inter-particle forces causes the regolith to be more susceptible to large-scale structural failure—since planes of weakness will preferentially form around massive clumps of grains ([Sánchez and Scheeres, 2020](#)). As these grain structures are held in a higher energy state, even a small perturbing force that exceeds the yield stress could trigger a landslide, potentially resulting in a catastrophic loss of regolith ([Scheeres et al., 2010](#)).

The best-fit multilinear model predicts that faster rotators (with  $P_{rot} < 5$  hrs) have larger regolith grains. Generally speaking, this finding is consistent with thermal breakdown of regolith and with centrifugal ejection of small grains. Interestingly, two fast rotators in our sample, 1950 DA ( $D_{eff} \approx 1.3$  km,  $P_{rot} \approx 2.12$ ) and Amun ( $D_{eff} \approx 2.7$  km,  $P_{rot} \approx 2.53$  hrs), posses regolith characteristics at the extremes of the sample: Amun has a high thermal inertia, suggesting it may be completely devoid of fine-grained regolith in contrast to 1950 DA. Amun may have always been completely void of regolith or it could had been similar to 1950 DA in the past. In the latter case, it was a rubble pile held together by cohesive forces, and was subsequently and periodically spun-up such that a catastrophic resurfacing (or even disruption of a once-larger body) occurred. In this scenario, we might expect 1950 DA to lose a portion of its regolith as its rotation rate incrementally increases and structural failure occurs. More thermal inertia estimates of rapid rotators ( $P_{rot} < 3$  hrs) may provide greater detail into the efficiency and probability of centrifugal ejection and the cohesive strength of regolith ([Rozitis et al., 2014](#)).

Regolith grains can carry a positive static charge when exposed to ionized solar wind particles that are primarily comprised of protons (Lee, 1996). At the same time, the photoelectrons are released from the surface and a negatively-charged sheath builds up on the sunlit side of an asteroid. The electrostatic forces that regolith grains experience in this field can *potentially* reach or exceed the cohesive and gravitational forces. For small grains, cohesive forces are dominant and are not likely to be lofted via electrostatic forces. The largest grains, on the other hand, are held onto asteroid surfaces by gravity. Because of these two effects, there is an optimal size—proportional to  $g_a^{1/4}$ —for which electrostatic forces are sufficiently strong to directly launch grains from the surface (Hartzell and Scheeres, 2011). The optimal grain size is estimated by Hartzell and Scheeres (2011) to be around 2–4 cm for an Eros-sized object ( $g_a \sim 5 \times 10^{-3} \text{ m s}^{-2}$ ) and 10–30 cm for an Itokawa-sized object ( $g_a \sim 8 \times 10^{-5} \text{ m s}^{-2}$ ).

If electrostatic forces dominate over cohesive forces, we would then expect a *positive* correlation between asteroid size and regolith grain size as opposed to an inverse relationship. Although the entire NEA grainsize dataset doesn’t show any correlation with asteroid size, the sub-km NEAs in our dataset do exhibit a positive correlation between effective asteroid diameter and grain size that is consistent with this expectation. We suspect that regolith processes in this size range become confounded by multiple competing forces and future modeling could show which process(es) dominate on different bodies.

## 5. Conclusions and Future Work

In this work we have presented regolith grain size estimates for 452 asteroids (Sec. 3) and performed a few multi-linear models fits to the dataset and *post-hoc* tests between compositional groups and asteroid families. From our results we conclude the following:

- 1) Regolith grain size across our sample of main-belt asteroids is inversely dependent on object size when the effective diameter is below  $\sim 10 \text{ km}$  (Sec. 3.1). We suspect that this relationship is most likely due to the removal of smaller regolith particles via impact processes due to the lower surface gravity of smaller objects. For MBAs larger than  $\sim 10 \text{ km}$ , regolith grain size does not exhibit any dependence on asteroid size. Additionally, grain size shows a positive dependence on rotation period for  $P_{rot} > 5 \text{ hrs}$  and an inverse relationship below this value. Nearly all the asteroids with rotation periods above 100 hrs are coarse-grained with grain sizes  $> 1 \text{ cm}$ .
- 2) We show that metal-rich asteroids have consistently larger regolith grains than objects belonging to other spectral types of similar size and rotation period Sec. 3.2. We find that M-types and E-types have coarser-grained regoliths, which may be related to their enstatite content. Finally, the compositionally-primitive P-types exhibit lower-than-average regolith grain sizes (more fine-grained) than any other spectral type.
- 3) The regolith grain sizes of NEAs, which represent asteroid diameters smaller than the MBAs in our sample, are inversely dependent on aphelion (Sec. 3.3)

but not diameter or rotation period. Additionally, the grain sizes of NEAs with aphelia in the Main-Belt are consistent with MBAs with similar aphelia, and the grain sizes of  $> 2$  km NEAs are consistent with that of MBAs at the same sizes. Thus, it is not possible to say if NEAs have different regoliths than MBAs, or if aphelion, rather than size, is a controlling factor of NEA grain sizes.

- 4) Finally, we infer from our analyses that evidence for both impact weathering and thermal fatigue/fracture exists in the asteroid population. In future work, processes that remove regolith (Sec. 4.3), which may preferentially act on smallest regolith particles or largest boulders, should be accounted for when modeling asteroid regolith evolution.

Future work will focus on increasing the number of objects in categories for which there are a relatively low number of thermal inertia estimates. In particular, NEAs, MBAs smaller than  $\approx 3$  km, super slow rotators ( $P_{rot} > 100$  hrs), and members of very young asteroid families ( $< 10$  Myr). In addition, thermophysical investigation of the regoliths of object groups not studied in this work (e.g., contact binary asteroids, asteroids with satellites, objects with close planetary encounters, low perihelion asteroids, etc.) would further elucidate regolith breakdown mechanisms and evolution processes as well as the timescales over which they operate.

## References

- Alí-Lagoa, V., Müller, T., Kiss, C., Szakáts, R., Marton, G., Farkas-Takács, A., Bartczak, P., Butkiewicz-Bak, M., Dudziński, G., Marciniak, A., Podlowska-Gaca, E., Duffard, R., Santos-Sanz, P., and Ortiz, J. (2020). Thermal properties of large main-belt asteroids observed by herchel pacs. *A&A*, 638:A84.
- Bandfield, J. L., Ghent, R. R., Vasavada, A. R., Paige, D. A., Lawrence, S. J., and Robinson, M. S. (2011). Lunar surface rock abundance and regolith fines temperatures derived from LRO Diviner Radiometer data. *Journal of Geophysical Research*, 116:E00H02.
- Basilevsky, A. T., Head, J. W., and Horz, F. (2013). Survival times of meter-sized boulders on the surface of the Moon. *Planetary and Space Science*, 89:118–126.
- Basilevsky, A. T., Head, J. W., Horz, F., and Ramsley, K. (2015). Survival times of meter-sized rock boulders on the surface of airless bodies. *Planetary and Space Science*, 117:312–328.
- Beck, P., Schmitt, B., Potin, S., Pommerol, A., and Brissaud, O. (2021). Low-phase spectral reflectance and equivalent “geometric albedo” of meteorites powders. *Icarus*, 354:114066.
- Beech, M., Coulson, I. M., Nie, W., and McCausland, P. (2009). The thermal and physical characteristics of the Gao-Guenie (H5) meteorite. *Planetary and Space Science*, 57:764–770.
- Bischoff, A., Scott, E. R. D., Metzler, K., and Goodrich, C. A. (2006). Nature and origins of meteoritic breccias. In Lauretta, D. S. and McSween, H. Y., editors, *Meteorites and the Early Solar System II*, pages 679–712.
- Bottke, W. F., Jr., Nolan, M. C., and Greenberg, R. (1993). Collision Lifetimes and Impact Statistics of Near-Earth Asteroids. In *Lunar and Planetary Science Conference*, Lunar and Planetary Science Conference, page 159.
- Bottke, Jr., W. F., Nolan, M. C., Greenberg, R., and Kolvoord, R. A. (1994). Velocity Distributions Among Colliding Asteroids. *Icarus*, 107:255–268.
- Burbine, T. H. and Binzel, R. P. (2002). Small Main-Belt Asteroid Spectroscopic Survey in the Near-Infrared. *Icarus*, 159:468–499.

- Burbine, T. H., Binzel, R. P., Bus, S. J., and Clark, B. E. (2001). K asteroids and co3/cv3 chondrites. *Meteoritics & Planetary Science*, 36(2):245–253.
- Bus, S. J. and Binzel, R. P. (2002). Phase II of the Small Main-Belt Asteroid Spectroscopic Survey: A Feature-Based Taxonomy. *Icarus*, 158:146–177.
- Cadenhead, D. A. and Stetter, J. R. (1975). Specific gravities of lunar materials using helium pycnometry. In *Lunar and Planetary Science Conference Proceedings*, volume 6 of *Lunar and Planetary Science Conference Proceedings*, pages 3199–3206.
- Capria, M. T., Tosi, F., Sanctis, M. C. D., Capaccioni, F., Ammannito, E., Frigeri, A., Zambon, F., Fonte, S., Palomba, E., Turrini, D., Titus, T. N., Schröder, S. E., Toplis, M., Li, J.-Y., Combe, J.-P., Raymond, C. A., and Russell, C. T. (2014). Vesta surface thermal properties map. *Geophysical Research Letters*, 41:1438–1443.
- Chan, C. K. and Tien, C. L. (1973). Conductance of packed spheres in vacuum. *Journal of Heat Transfer*, 95:302–308.
- Chapman, C. R. and Gaffey, M. J. (1979). Reflectance spectra for 277 asteroids. In Gehrels, T. and Matthews, M. S., editors, *Asteroids*, pages 655–687.
- Clark, B. E., Bus, S. J., Rivkin, A. S., McConnochie, T., Sanders, J., Shah, S., Hiroi, T., and Shepard, M. (2004). E-type asteroid spectroscopy and compositional modeling. *Journal of Geophysical Research*, 109:E02001.
- Clark, B. E., Ockert-Bell, M. E., Cloutis, E. A., Nesvorny, D., Mothé-Diniz, T., and Bus, S. J. (2009). Spectroscopy of K-complex asteroids: Parent bodies of carbonaceous meteorites? *Icarus*, 202:119–133.
- Consolmagno, G. J., Britt, D. T., and Macke, R. J. (2008). The Significance of Meteorite Density and Porosity. *Chemie der Erde*, 68:1–29.
- Consolmagno, G. J., Schaefer, M. W., Schaefer, B. E., Britt, D. T., Macke, R. J., Nolan, M. C., and Howell, E. S. (2013). The measurement of meteorite heat capacity at low temperatures using liquid nitrogen vaporization. *Planetary and Space Science*, 87(146–156):146–156.
- Delbo’, M., Libourel, G., Wilkerson, J., Murdoch, N., Michel, P., Ramesh, K. T., Ganino, C., Verati, C., and Marchi, S. (2014). Thermal fatigue as the origin of regolith on small asteroids. *Nature*, 508(7495):233–236.
- Delbo’, M., Mueller, M., Emery, J. P., Rozitis, B., and Capria, M. T. (2015). Asteroid Thermophysical Modeling. In Michel, P., DeMeo, F. E., and Bottke Jr., W. F., editors, *Asteroids IV*, pages 107–128. University of Arizona Press.
- DeMeo, F. E., Binzel, R. P., Slivan, S. M., and Bus, S. J. (2009). An extension of the Bus asteroid taxonomy into the near-infrared. *Icarus*, 202:160–180.
- DeMeo, F. E. and Carry, B. (2013). The taxonomic distribution of asteroids from multi-filter all-sky photometric surveys. *Icarus*, 226(1):723–741.
- DeMeo, F. E. and Carry, B. (2014). Solar System evolution from compositional mapping of the asteroid belt. *Nature*, 505:629–634.
- Devogèle, M., MacLennan, E., Gustafsson, A., Moskovitz, N., Chatelain, J., Borisov, G., Abe, S., Arai, T., Fedorets, G., Ferrais, M., Granvik, M., Jehin, E., Siltala, L., Pöntinen, M., Mommert, M., Polishook, D., Skiff, B., Tanga, P., and Yoshida, F. (2020). New Evidence for a Physical Link between Asteroids (155140) 2005 UD and (3200) Phaethon. *The Planetary Science Journal*, 1(1):15.
- Dullien, F. A. L. (1979). *Porous Media*. Academic Press.
- El Mir, C., Ramesh, K. T., and Delbo, M. (2019). The efficiency of thermal fatigue in regolith generation on small airless bodies. *Icarus*, 333:356–370.
- Eppes, M.-C., Willis, A., Molaro, J., Abernathy, S., and Zhou, B. (2015). Cracks in Martian boulders exhibit preferred orientations that point to solar-induced thermal stress. *Nature Communications*, 6(6712).
- Farinella, P. and Davis, D. R. (1992). Collision Rates and Impact Velocities in the Main Asteroid Belt. *Icarus*, 97:111–123.
- Fieber-Beyer, S. (2015). Fieber-Beyer IRTF Mainbelt Asteroid Spectra. NASA Planetary Data System. V3.0. EAR-A-I0046-3-FBIRTFSPEC-V3.0.
- Flynn, G. J., Consolmagno, G. J., Brown, P., and Macke, R. J. (2017). Physical properties of the stone meteorites: Implications for the properties of their parent bodies. *Chemie der Erde - Geochemistry*.

- Gietzen, K. and Lacy, C. (2007). Visible and Near Infrared Spectra of Main Belt and Near Earth Asteroids. In *Lunar and Planetary Science Conference*, Lunar and Planetary Science Conference, page 1104.
- Grott, M., Knollenberg, J., Hamm, M., Ogawa, K., Jaumann, R., Otto, K. A., Delbo, M., Michel, P., Biele, J., Neumann, W., Knapmeyer, M., Kührt, E., Senshu, H., Okada, T., Helbert, J., Maturilli, A., Müller, N., Hagermann, A., Sakatani, N., Tanaka, S., Arai, T., Mottola, S., Tachibana, S., Pelivan, I., Drube, L., Vincent, J. B., Yano, H., Pilorget, C., Matz, K. D., Schmitz, N., Koncz, A., Schröder, S. E., Trauthan, F., Schlotterer, M., Krause, C., Ho, T. M., and Moussi-Soffys, A. (2019). Low thermal conductivity boulder with high porosity identified on c-type asteroid (162173) ryugu. *Nature Astronomy*, 3(11):971–976.
- Guibout, V. and Scheeres, D. J. (2003). Stability of surface motion on a rotating ellipsoid. *Celestial Mechanics and Dynamical Astronomy*, 87(3):263–290.
- Gundlach, B. and Blum, J. (2012). Outgassing of icy bodies in the Solar System – II. Heat transport in dry, porous surface dust layers. *Icarus*, 219:618–629.
- Gundlach, B. and Blum, J. (2013). A New Method to Determine the Grain Size of Planetary Regolith. *Icarus*, 223:479–492.
- Gundlach, B. and Blum, J. (2015). Regolith grain size and cohesive strength of near-Earth Asteroid (29075) 1950 DA. *Icarus*, 257:126–129.
- Hanuš, J., Delbó, M., Durech, J., and Alí-Lagoa, V. (2015). Thermophysical Modeling of Asteroids from WISE Thermal Infrared Data – Significance of the Shape Model and the Pole Orientation Uncertainties. *Icarus*, 256:101–116.
- Hanuš, J., Delbo’, M., Ďurech, J., and Alí-Lagoa, V. (2018). Thermophysical Modeling of Main-Belt Asteroids from WISE Thermal Data. *Icarus*, 309:297–337.
- Hanuš, J., Delbo’, M., Vokrouhlický, D., Pravec, P., Emery, J. P., Alí-Lagoa, V., Bolin, B., Devogèle, M., Dyvig, R., Galád, A., Jedicke, R., Kornoš, L., Kušnirák, P., Licandro, J., Reddy, V., Rivet, J. P., Világi, J., and Warner, B. D. (2016). Near-Earth asteroid (3200) Phaethon: Characterization of its orbit, spin state, and thermophysical parameters. *A&A*, 592:A34.
- Hardersen, P. S., Cloutis, E. A., Reddy, V., Mothe-Diniz, T., and Emery, J. P. (2011). The m-/x-asteroid menagerie: Results of an nir spectral survey of 45 main-belt asteroids. *Meteoritics & Planetary Science*, 46(12):1910–1938.
- Hartzell, C. M. and Scheeres, D. J. (2011). The role of cohesive forces in particle launching on the Moon and asteroids. *Planet. Space Sci.*, 59(14):1758–1768.
- Hazeli, K., El Mir, C., Papanikolaou, S., Delbo, M., and Ramesh, K. T. (2018). The origins of Asteroidal rock disaggregation: Interplay of thermal fatigue and microstructure. *Icarus*, 304:172–182.
- Holsapple, K., Giblin, I., Housen, K., Nakamura, A., and Ryan, E. (2002). Asteroid Impacts: Laboratory Experiments and Scaling Laws. In Bottke, Jr., W. F., Cellino, A., Paolicchi, P., and Binzel, R. P., editors, *Asteroids III*, pages 443–462. University of Arizona Press.
- Hörz, F., Basilevsky, A. T., Head, J. W., and Cintala, M. J. (2020). Erosion of lunar surface rocks by impact processes: A synthesis. *Planet. Space Sci.*, 194:105105.
- Horz, F. and Cintala, M. (1997). Impact experiments related to the evolution of planetary regoliths. *Meteoritics and Planetary Science*, 32:179–209.
- Hörz, F. and Schaal, R. B. (1977). Impact cratering and regolith dynamics. *Physics and Chemistry of the Earth*, 10:3–15.
- Housen, K. R. and Holsapple, K. A. (2003). Impact cratering on porous asteroids. *Icarus*, 163:102–119.
- Housen, K. R. and Holsapple, K. A. (2011). Ejecta from impact craters. *Icarus*, 211:856–875.
- Housen, K. R., Wilkening, L. L., Chapman, C. R., and Greenberg, R. (1979). Asteroidal Regoliths. *Icarus*, 39:317–351.
- Ibrahim, E.-M. I. (2012). The Elastic Properties of Carbonaceous Chondrites. Master’s thesis, University of Calgary.
- Jakosky, B. M. (1986). On the Thermal Properties of Martian Fines. *Icarus*, 66:117–124.
- Jewitt, D. (2012). The Active Asteroids. *Astronomical Journal*, 143(3):66.
- Jewitt, D. and Hsieh, H. (2006). Physical observations of 2005 ud: A mini-phaethon. *The Astronomical journal.*, 132(4).

- Jiang, H., Ji, J., and Yu, L. (2020). Determination of Size, Albedo, and Thermal Inertia of 10 Vesta Family Asteroids with WISE/NEOWISE Observations. *AJ*, 159(6):264.
- Johnson, K. L., Kendall, K., and Roberts, A. D. (1971). Surface Energy and the Contact of Elastic Solids. *Proceedings of the Royal Society of London Series A*, 324(1558):301–313.
- Kass, R. E. and Raftery, A. E. (1995). Bayes Factors. *Journal of the American Statistical Association*, 90(430):773–795.
- Keihm, S., Tosi, F., Kamp, L., Capaccioni, F., Gulkis, S., Grassi, D., Hofstadter, M., Filacchione, G., Lee, S., Giuppi, S., Janssen, M., and Capria, M. (2012). Interpretation of combined infrared, submillimeter, and millimeter thermal flux data obtained during the Rosetta fly-by of Asteroid (21) Lutetia. *Icarus*, 221(1):395–404.
- Krumbein, W. C. and Aberdeen, E. J. (1937). The sediments of barataria bay [louisiana]. *Journal of Sedimentary Research*, 7:3–17.
- Lazzaro, D., Angeli, C. A., Carvano, J. M., Mothé-Diniz, T., Duffard, R., and Florczak, M. (2004). S3OS2: the visible spectroscopic survey of 820 asteroids. *Icarus*, 172:179–220.
- Ledbetter, H. M. and Reed, R. P. (1973). Elastic Properties of Metals and Alloys, I. Iron, Nickel, and Iron-Nickel Alloys. *Journal of Physical and Chemical Reference Data*, 2(3):531–618.
- Lee, P. (1996). Dust Levitation on Asteroids. *Icarus*, 124:181–194.
- Leyrat, C., Coradini, A., Erard, S., Capaccioni, F., Capria, M. T., Drossart, P., de Sanctis, M. C., Tosi, F., and Virtis Team (2011). Thermal properties of the asteroid (2867) Steins as observed by VIRTIS/Rosetta. *A&A*, 531:A168.
- Libourel, G., Ganino, C., Delbo, M., Niezgoda, M., Remy, B., Aranda, L., and Michel, P. (2020). Network of thermal cracks in meteorites due to temperature variations: new experimental evidence and implications for asteroid surfaces. *Monthly Notices of the Royal Astronomical Society*, 500(2):1905–1920.
- Lupishko, D. and Belskaya, I. (1989). On the surface composition of the m-type asteroids. *Icarus*, 78(2):395 – 401.
- Macke, R. J. (2010). *Survey Of Meteorite Physical Properties Density, Porosity And Magnetic Susceptibility*. PhD thesis, University of Central Florida.
- Macke, R. J., Britt, D. T., and Consolmagno, G. J. (2011). Density, porosity, and magnetic susceptibility of achondritic meteorites. *Meteoritics & Planetary Science*, 46(2):311–326.
- Macke, R. J., Consolmagno, G. J., and Britt, D. T. (2011). Density, porosity, and magnetic susceptibility of carbonaceous chondrites. *Meteoritics & Planetary Science*, 46(12):1842–1862.
- Macke, R. J., Consolmagno, G. J., Britt, D. T., and Hutson, M. L. (2010). Enstatite chondrite density, magnetic susceptibility, and porosity. *Meteoritics & Planetary Science*, 45(9):1513–1526.
- Macke, R. J., Opeil, C., and Consolmagno, G. J. (2019). Heat capacities of ordinary chondrite falls below 300 k. *Meteoritics & Planetary Science*, 54(11):2729–2743.
- MacLennan, E. M. and Emery, J. P. (2019). Thermophysical modeling of asteroid surfaces using ellipsoid shape models. *The Astronomical Journal*, 157(1):2.
- MacLennan, E. M. and Emery, J. P. (2021). Thermophysical investigation of asteroid regolith i: Thermal inertia characterization. *Icarus*.
- Marciniak, A., Alí-Lagoa, V., Müller, T. G., Szakáts, R., Molnár, L., Pál, A., Podlowska-Gaca, E., Parley, N., Antonini, P., Barbotin, E., Behrend, R., Bernasconi, L., Butkiewicz-Bak, M., Crippa, R., Duffard, R., Dittéon, R., Feuerbach, M., Fauvaud, S., Garlitz, J., Geier, S., Goncalves, R., Grice, J., Grześkowiak, I., Hirsch, R., Horbowicz, J., Kamiński, K., Kamińska, M. K., Kim, D. H., Kim, M. J., Konstanciak, I., Kudak, V., Kulczak, P., Maestre, J. L., Manzini, F., Marks, S., Monteiro, F., Ogłóza, W., Oszkiewicz, D., Pilcher, F., Perig, V., Polakis, T., Polińska, M., Roy, R., Sanabria, J. J., Santana-Ros, T., Skiff, B., Skrzypek, J., Sobkowiak, K., Sonbas, E., Thizy, O., Trela, P., Urakawa, S., Żejmo, M., and Żukowski, K. (2019). Thermal properties of slowly rotating asteroids: results from a targeted survey. *A&A*, 625:A139.
- Marciniak, A., Bartczak, P., Müller, T., Sanabria, J. J., Alí-Lagoa, V., Antonini, P., Behrend, R., Bernasconi, L., Bronikowska, M., Butkiewicz-Bak, M., Cikota, A., Crippa, R., Dittéon, R., Dudziński, G., Duffard, R., Dziadura, K., Fauvaud, S., Geier, S., Hirsch, R., Horbowicz, J., Hren, M., Jerosimic, L., Kamiński, K., Kankiewicz, P., Konstanciak, I., Korlevic, P., Kosturkiewicz, E., Kudak, V., Manzini, F., Morales,



- N., Murawiecka, M., Ogloza, W., Oszkiewicz, D., Pilcher, F., Polakis, T., Poncy, R., Santana-Ros, T., Siwak, M., Skiff, B., Sobkowiak, K., Stoss, R., Zejmo, M., and Zukowski, K. (2018). Photometric survey, modelling, and scaling of long-period and low-amplitude asteroids. *A&A*, 610:A7.
- Marsset, M., Carry, B., Dumas, C., Hanus, J., Viikinkoski, M., Vernazza, P., Müller, T. G., Delbo, M., Jehin, E., Gillon, M., Grice, J., Yang, B., Fusco, T., Berthier, J., Sonnett, S., Kugel, F., Caron, J., and Behrend, R. (2017). 3d shape of asteroid (6) hebe from vlt/sphere imaging: Implications for the origin of ordinary h chondrites. *A&A*, 604:A64.
- Masiero, J. R., Mainzer, A. K., Bauer, J. M., Grav, T., Nugent, C. R., and Stevenson, R. (2013). Asteroid Family Identification Using the Hierarchical Clustering Method and WISE/NEOWISE Physical Properties. *ApJ*, 770(1):7.
- Matter, A., Delbó, M., Carry, B., and Ligorì, S. (2013). Evidence of a metal-rich surface for the asteroid (16) Psyche from interferometric observations in the thermal infrared. *Icarus*, 226:419–427.
- McKay, D. S., Swindle, T. D., and Greenberg, R. (1989). Asteroidal regoliths - what we do not know. In Binzel, R. P., Gehrels, T., and Matthews, M. S., editors, *Asteroids II*, pages 617–642. University of Arizona Press.
- Milani, A., Spoto, F., Knezevic, Z., Novakovic, B., and Tsirvoulis, G. (2015). Families classification including multiopposition asteroids. *Proceedings of the International Astronomical Union*, 10(S318):28–45.
- Molaro, J. and Byrne, S. (2012). Rates of temperature change of airless landscapes and implications for thermal stress weathering. *Journal of Geophysical Research*, 117:E10011.
- Molaro, J., Byrne, S., and Le, J.-L. (2017). Thermally induced stresses in boulders on airless body surfaces, and implications for rock breakdown. *Icarus*, 294:247–261.
- Molaro, J. L., Byrne, S., and Langer, S. A. (2015). Grain-scale thermoelastic stresses and spatiotemporal temperature gradients on airless bodies, implications for rock breakdown. *Journal of Geophysical Research: Planets*, 120:255–277.
- Molaro, J. L. and McKay, C. P. (2010). Processes controlling rapid temperature variations on rock surfaces. *Earth Surface Processes Landforms*, 35:501–507.
- Mothé-Diniz, T., Carvano, J., Bus, S., Duffard, R., and Burbine, T. (2008). Mineralogical analysis of the Eos family from near-infrared spectra. *Icarus*, 195(1):277–294.
- Müller, T. G. and Blommaert, J. A. D. L. (2004).  $\lambda$ ASTROBJ65 Cybele/ $\lambda$ ASTROBJ $\lambda$  in the thermal infrared: Multiple observations and thermophysical analysis. *A&A*, 418:347–356.
- Müller, T. G., Hasegawa, S., and Usui, F. (2014). (25143) Itokawa: The Power of Radiometric Techniques for the Interpretation of Remote Thermal Observations in the Light of the Hayabusa Rendezvous Results. *Publications of the Astronomical Society of Japan*, 66:52.
- Müller, T. G., Sterzik, M. F., Schütz, O., Pravec, P., and Siebenmorgen, R. (2004). Thermal infrared observations of near-earth asteroid 2002 ny40\*. *A&A*, 424(3):1075–1080.
- Murdoch, N., Sánchez, P., Schwartz, S. R., and Miyamoto, H. (2015). Asteroid Surface Geophysics. In Michel, P., DeMeo, F. E., and Bottke Jr., W. F., editors, *Asteroids IV*, pages 767–792. University of Arizona Press.
- Nakamura, A. and Fujiwara, A. (1991). Velocity Distribution of Fragments Formed in a Simulated Collisional Disruption. *Icarus*, 92:132–146.
- Nakamura, A. M., Fujiwara, A., and Kadono, T. (1994). Velocity of finer fragments from impact. *Planetary and Space Science*, 42(13):1043–1052.
- Nesvorný, D., Brož, M., and Carruba, V. (2015). Identification and Dynamical Properties of Asteroid Families. In Michel, P., DeMeo, F. E., and Bottke Jr., W. F., editors, *Asteroids IV*, pages 297–321. University of Arizona Press.
- Ockert-Bell, M., Clark, B., Shepard, M., Isaacs, R., Cloutis, E., Fornasier, S., and Bus, S. (2010). The composition of m-type asteroids: Synthesis of spectroscopic and radar observations. *Icarus*, 210(2):674 – 692.
- Opeil, C. P., Britt, D. T., Macke, R. J., and Consolmagno, G. J. (2020). The surprising thermal properties of CM carbonaceous chondrites. *Meteoritics and Planetary Science*, 55(8):E1–E20.
- Opeil, C. P., Consolmagno, G. J., and Britt, D. T. (2010). The Thermal Conductivity of Meteorites: New

- Measurements and Analysis. *Icarus*, 208:449–454.
- Opeil, C. P., Consolmagno, G. J., Safarik, D. J., and Britt, D. T. (2012). Stony meteorite thermal properties and their relationship with meteorite chemical and physical states. *Meteoritics & Planetary Science*, 47(3):319–329.
- Piqueux, S. and Christensen, P. R. (2009). A model of thermal conductivity for planetary soils: 1. theory for unconsolidated soils. *Journal of Geophysical Research: Planets*, 114:E9.
- Popova, O., Borovika, J., Hartmann, W. K., Spurna, P., Gnos, E., Nemtchinov, I., and Trigo-Rodriguez, J. M. (2011). Very low strengths of interplanetary meteoroids and small asteroids. *Meteoritics & Planetary Science*, 46(10):1525–1550.
- Pravec, P., Fatka, P., Vokrouhlický, D., Scheirich, P., Ďurech, J., Scheeres, D. J., Kušnirák, P., Hornoch, K., Galád, A., Pray, D. P., Krugly, Y. N., Burkhanov, O., Ehgamberdiev, S. A., Pollock, J., Moskovitz, N., Thirouin, A., Ortiz, J. L., Morales, N., Husárik, M., Inasaridze, R. Y., Oey, J., Polishook, D., Hanuš, J., Kučáková, H., Vrátil, J., Világi, J., Gajdoš, Š., Kornoš, L., Vereš, P., Gaftonyuk, N. M., Hromakina, T., Sergeyev, A. V., Slyusarev, I. G., Ayvazian, V. R., Cooney, W. R., Gross, J., Terrell, D., Colas, F., Vachier, F., Slivan, S., Skiff, B., Marchis, F., Ergashev, K. E., Kim, D. H., Aznar, A., Serra-Ricart, M., Behrend, R., Roy, R., Manzini, F., and Molotov, I. E. (2019). Asteroid pairs: A complex picture. *Icarus*, 333:429–463.
- Presley, M. A. (2010). Thermal conductivity measurements of particulate materials: 4. effect of bulk density for granular particles. *Journal of Geophysical Research*, 115:E07003.
- Presley, M. A. and Christensen, P. R. (1997). Thermal conductivity measurements of particulate materials: 2. results. *Journal of Geophysical Research*, 102(E3):6551–6566.
- Presley, M. A. and Christensen, P. R. (2010). Thermal conductivity measurements of particulate materials: 5. effect of bulk density and particle shape. *Journal of Geophysical Research*, 115:E07004.
- Presley, M. A. and Craddock, R. A. (2006). Thermal conductivity measurements of particulate materials: 3. natural samples and mixtures of particle sizes. *Journal of Geophysical Research*, 111:E09013.
- Ravaji, B., Alí-Lagoa, V., Delbo, M., and Wilkerson, J. W. (2019). Unraveling the Mechanics of Thermal Stress Weathering: Rate-Effects, Size-Effects, and Scaling Laws. *Journal of Geophysical Research (Planets)*, 124(12):3304–3328.
- Reddy, V., Le Corre, L., Hicks, M., Lawrence, K., Buratti, B. J., Abell, P. A., Gaffey, M. J., and Hardersen, P. S. (2012). Composition of near-Earth Asteroid 2008 EV5: Potential target for robotic and human exploration. *Icarus*, 221(2):678–681.
- Richardson, J. E., Steckloff, J. K., and Minton, D. A. (2020). Impact-produced seismic shaking and regolith growth on asteroids 433 Eros, 2867 Šteins, and 25143 Itokawa. *Icarus*, 347:113811.
- Rozitis, B., Duddy, S. R., Green, S. F., and Lowry, S. C. (2013). A Thermophysical Analysis of the (1862) Apollo Yarkovsky and YORP Effects. *Astronomy and Astrophysics*, 555:A20.
- Rozitis, B., Green, S. F., MacLennan, E., and Emery, J. P. (2018). Observing the Variation of Asteroid Thermal Inertia with Heliocentric Distance. *Monthly Notices of the Royal Astronomical Society*, 477(2):1782–1802.
- Rozitis, B., MacLennan, E. M., and Emery, J. P. (2014). Cohesive forces prevent the rotational breakup of rubble-pile asteroid (29075) 1950 DA. *Nature*, 512:174.
- Rozitis, B., Ryan, A. J., Emery, J. P., Christensen, P. R., Hamilton, V. E., Simon, A. A., Reuter, D. C., Al Asad, M., Ballouz, R.-L., Bandfield, J. L., Barnouin, O. S., Bennett, C. A., Bernacki, M., Burke, K. N., Cambioni, S., Clark, B. E., Daly, M. G., Delbo, M., DellaGiustina, D. N., Elder, C. M., Hanna, R. D., Haberle, C. W., Howell, E. S., Golish, D. R., Jawin, E. R., Kaplan, H. H., Lim, L. F., Molaro, J. L., Munoz, D. P., Nolan, M. C., Rizk, B., Siegler, M. A., Susorney, H. C. M., Walsh, K. J., and Lauretta, D. S. (2020). Asteroid (101955) bennu’s weak boulders and thermally anomalous equator. *Science Advances*, 6(41).
- Ruesch, O., Sefton-Nash, E., Vago, J. L., Küppers, M., Pasckert, J. H., Krohn, K., and Otto, K. (2020). In situ fragmentation of lunar blocks and implications for impacts and solar-induced thermal stresses. *Icarus*, 336:113431.
- Ryan, A. J., Pino Muñoz, D., Bernacki, M., and Delbo, M. (2020). Full-Field Modeling of Heat Transfer in

- Asteroid Regolith: Radiative Thermal Conductivity of Polydisperse Particulates. *Journal of Geophysical Research (Planets)*, 125(2):e06100.
- Sakatani, N., Ogawa, K., Iijima, Y., Arakawa, M., Honda, R., and Tanaka, S. (2017). Thermal conductivity model for powdered materials under vacuum based on experimental studies. *AIP Advances*, 7(1):015310.
- Scheeres, D. (2015). Landslides and mass shedding on spinning spheroidal asteroids. *Icarus*, 247:1–17.
- Scheeres, D. J., Hartzell, C. M., Sánchez, P., and Swift, M. (2010). Scaling forces to asteroid surfaces: the role of cohesion. *Icarus*, 210:968–984.
- Shepard, M. K., Margot, J.-L., Magri, C., Nolan, M. C., Schlieder, J., Estes, B., Bus, S. J., Volquardsen, E. L., Rivkin, A. S., Benner, L. A. M., Giorgini, J. D., Ostro, S. J., and Busch, M. W. (2006). Radar and infrared observations of binary near-Earth Asteroid 2002 CE26. *Icarus*, 184(1):198–210.
- Shoemaker, E. M., Batson, R. M., Holt, H. E., Morris, E. C., Rennilson, J. J., and Whitaker, E. A. (1969). Observations of the lunar regolith and the earth from the television camera on Surveyor 7. *J. Geophys. Res.*, 74(25):6081–6119.
- Simpson, E. H. (1951). The Interpretation of Interaction in Contingency Tables. *Journal of the Royal Statistical Society, Series B*, 13:238–241.
- Soini, A. J., Kukkonen, I. T., Kohout, T., and Luttinen, A. (2020). Thermal and porosity properties of meteorites: A compilation of published data and new measurements. *Meteoritics and Planetary Science*, 55(2):402–425.
- Sunshine, J. M., Thomas, N., El-Maarry, M. R., and Farnham, T. L. (2016). Evidence for geologic processes on comets. *Journal of Geophysical Research: Planets*, 121(11):2194–2210.
- Szurgot, M., Wach, R. A., and Przylibski, T. A. (2012). Thermophysical Properties of the Soltmany Meteorite. *Meteorites*, 2(1-2):53–65.
- Sánchez, P. and Scheeres, D. J. (2020). Cohesive regolith on fast rotating asteroids. *Icarus*, 338:113443.
- Tholen, D. J. (1984). *Asteroid taxonomy from cluster analysis of photometry*. PhD thesis, University of Arizona.
- van Antwerpen, W., Rousseau, P., and du Toit, C. (2012). Multi-sphere unit cell model to calculate the effective thermal conductivity in packed pebble beds of mono-sized spheres. *Nuclear Engineering and Design*, 247:183–201.
- Vilas, F., Smith, B. A., McFadden, L. A., Gaffey, M. J., Larson, S. M., Hatch, E. C., and Jarvis, K. S. (1998). Vilas Asteroid Spectra V1.1. NASA Planetary Data System. EAR-A-3-RDR-VILAS-ASTEROID-SPECTRA-V1.1.
- Wach, R. A., Adamus, A., and Szurgot, M. (2013). Specific heat capacity of soltmany and nwa 4560 meteorites. *Meteorit. Planet Sci.*, 48:5017.
- Watson, K. (1964). *I. The thermal conductivity measurements of selected silicate powders in vacuum from 150o - 350oK, II. An interpretation of the moon's eclipse and lunation cooling as observed through Earth's atmosphere from 8-14 microns*. PhD thesis, California Institute of Technology.
- Welch, B. L. (1947). The Generalization of 'Student's' Problem When Several Different Population Variances are Involved. *Biometrika*, 34(1-2):28–35.
- Yano, H., Kubota, T., Miyamoto, H., Okada, T., Scheeres, D., Takagi, Y., Yoshida, K., Abe, M., Abe, S., Barnouin-Jha, O., Fujiwara, A., Hasegawa, S., Hashimoto, T., Ishiguro, M., Kato, M., Kawaguchi, J., Mukai, T., Saito, J., Sasaki, S., and Yoshikawa, M. (2006). Touchdown of the Hayabusa Spacecraft at the Muses Sea on Itokawa. *Science*, 312(5778):1350–1353.
- Yomogida, K. and Matsui, T. (1983). Physical Properties of Ordinary Chondrites. *Journal of Geophysical Research*, 88, B11:9513–9533.
- Yu, L. L., Yang, B., Ji, J., and Ip, W.-H. (2017). Thermophysical characteristics of the large main-belt asteroid (349) Dembowska. *MNRAS*, 472(2):2388–2397.
- Yule, G. U. (1903). Notes on the Theory of Association of Attributes in Statistics. *Biometrika*, 2(2):121–134.

Table 1: Meteorite Thermal Conductivity Measurements at 200 K

Sample	Group	$\phi^a$	$k_{eff}^b$	Source
ALH 77288	H6	2.0	3.53	Yomogida and Matsui (1983)
Arapahoe	L5	2.5	2.31	Yomogida and Matsui (1983)
Bath Furnace 1	L6	4.3	2.26	Opeil et al. (2012)
Bath Furnace 2	L6	4.3	2.72	Opeil et al. (2012)
Bath Furnace 3	L6	4.3	3.15	Opeil et al. (2012)
Bruderheim	L6	8.0	1.03	Yomogida and Matsui (1983)
Farmington	L5	5.5	2.14	Yomogida and Matsui (1983)
Gilgoin Station	H5	5.0	3.60	Yomogida and Matsui (1983)
Gladstone	H5	5.0	2.16	Yomogida and Matsui (1983)
Holbrook 1	L6	10.4	0.45	Opeil et al. (2012)
Holbrook 2	L6	10.4	1.15	Opeil et al. (2012)
Kunashak	L6	5.2	1.86	Yomogida and Matsui (1983)
Leedey,A	L6	10.4	0.40	Yomogida and Matsui (1983)
Leedey,B	L6	10.6	0.47	Yomogida and Matsui (1983)
Los Angeles	Sher*	8.1	0.77	Opeil et al. (2012)
MET 78003	L6	7.8	1.54	Yomogida and Matsui (1983)
Monroe	H4	5.9	2.35	Yomogida and Matsui (1983)
New Concord	L6	9.2	0.78	Yomogida and Matsui (1983)
Pultusk	H5	7.5	1.25	Opeil et al. (2012)
Wellman	H5	6.1	3.85	Yomogida and Matsui (1983)
Y-74156	H4	9.2	1.54	Yomogida and Matsui (1983)
Y-74191	L3	10.3	1.24	Yomogida and Matsui (1983)
Y-74647	H4.5	9.1	1.15	Yomogida and Matsui (1983)
Y-75097	L4	10.3	0.97	Yomogida and Matsui (1983)
Abee	EH4	3.0	5.33	Opeil et al. (2010)
Pillistfer	EL6	2.4	5.51	Opeil et al. (2012)
Campo del Cielo	IAB	1.2	22.4	Opeil et al. (2010)

**Notes.** \*Shergottite meteorite group (Martian origin).

<sup>a</sup>Sample porosity (%).

<sup>b</sup>Effective thermal conductivity ( $\text{W m}^{-1} \text{K}^{-1}$ ).

Table 2: Meteorite Heat Capacity Measurements at Different Ambient Temperatures

Sample	Type	$T_{\text{lab}}$ (K)	$c_s$ (J kg <sup>-1</sup> K <sup>-1</sup> )	Source
Abee	EH4	200	500 ± 10	Yomogida and Matsui (1983)
Allende	CV	180	501 ± 21	Consolmagno et al. (2013)
Bilanga	Di.	180	509 ± 26	Consolmagno et al. (2013)
Bori	L6	180	495 ± 8	Consolmagno et al. (2013)
Cronstad	H5	200	550 ± 10	Yomogida and Matsui (1983)
Cold Bokkeveld	CM2	200	500 ± 100	Yomogida and Matsui (1983)
Cumberland	Aub. <sup>†</sup>	180	513 ± 14	Consolmagno et al. (2013)
Gao-Guenie	H5	296	732 ± 8	Beech et al. (2009)
Hedjaz	L3.7-6	180	488 ± 12	Consolmagno et al. (2013)
Holbrook	L6	180	486 ± 9	Consolmagno et al. (2013)
Los Angeles	Sher.*	185	550 ± 10	Opeil et al. (2012)
Los Angeles	Sher.*	300	780 ± 10	Opeil et al. (2012)
Los Angeles	Sher.*	235	600 ± 10	Opeil et al. (2012)
Los Angeles	Sher.*	265	680 ± 10	Opeil et al. (2012)
Lumpkin	L6	200	570 ± 10	Yomogida and Matsui (1983)
Ness Country	L6	180	517 ± 6	Consolmagno et al. (2013)
NWA 2086	CV	180	519 ± 28	Consolmagno et al. (2013)
NWA 4293	H6	180	498 ± 7	Consolmagno et al. (2013)
NWA 4560	LL3.2	223	566 ± 10	Wach et al. (2013)
NWA 4560	LL3.2	300	682 ± 10	Wach et al. (2013)
NWA 5515	CK4	200	500 ± 10	Yomogida and Matsui (1983)
Ornans	CO	180	497 ± 7	Consolmagno et al. (2013)
Pipe Creek	H6	180	489 ± 10	Consolmagno et al. (2013)
Pultusk	H5	180	496 ± 8	Consolmagno et al. (2013)
Renazzo	CR	180	535 ± 12	Consolmagno et al. (2013)
Soltmany	L6	200	549 ± 30	Szurgot et al. (2012)
Soltmany	L6	300	728 ± 35	Szurgot et al. (2012)
Soltmany	L6	223	575 ± 10	Wach et al. (2013)
Soltmany	L6	300	671 ± 10	Wach et al. (2013)
Thuathe	H4-5	180	487 ± 9	Consolmagno et al. (2013)
Warrenton	CO	180	503 ± 16	Consolmagno et al. (2013)
Augustinovka	IIIAB	180	375 ± 13	Consolmagno et al. (2013)
Campo del Cielo	IAB	200	375 ± 10	Opeil et al. (2010)
Campo del Cielo	IAB	300	450 ± 10	Opeil et al. (2010)
Estherville	Meso <sup>‡</sup>	180	383 ± 6	Consolmagno et al. (2013)
Pirapora	IIIAB	180	342 ± 27	Consolmagno et al. (2013)
Sikhote-Alin	Fe IIAB	350	458 ± 11	Beech et al. (2009)

**Notes.** \*Shergottite meteorite (Martian origin).

<sup>†</sup>Aubrite

<sup>‡</sup>Mesosiderite

Table 3: Material Properties of Meteorite Groups

Spectral Group	Meteorite Analog	$k_{grain}$ (W m <sup>-1</sup> K <sup>-1</sup> )	$\rho_{grain}$ (kg m <sup>-3</sup> )	$c_s^a$ (J kg <sup>-1</sup> K <sup>-1</sup> )	$\epsilon_g$	$E$ (GPa)	$\nu^b$
S-complex	ordinary chondrites	$4.05 \pm 0.35$	3180–3710 <sup>h</sup>	$-0.0033 \times T^2 + 3.39 \times T$	0.9	$28.8 \pm 2.4^i$	$0.23 \pm 0.04^d$
V-type	HEDs	$4.05 \pm 0.35$	3180–3440 <sup>e</sup>	$-0.0033 \times T^2 + 3.39 \times T$	0.9	$28.8 \pm 2.4^i$	$0.23 \pm 0.04^d$
E-type	aubrites	$4.28 + {}^{258}/T$ ( $\pm 10\%$ )	$3150 \pm 20^e$	$-0.0033 \times T^2 + 3.39 \times T$	0.9	$28.8 \pm 2.4$	$0.23 \pm 0.04$
M-type	E chondrites	$4.76 + {}^{287}/T$ ( $\pm 10\%$ )	$3635 \pm 35^g$	$-0.0033 \times T^2 + 3.39 \times T$	0.9	$28.8 \pm 2.4$	$0.23 \pm 0.04$
Met (high- $\Gamma$ M-type)	FeNi metal	$12.4 + 0.05 \times T$ ( $\pm 10\%$ )	$7500 \pm 200^c$	$-0.0042 \times T^2 + 2.77 \times T$	0.66	169–209 <sup>j</sup>	0.27–0.37 <sup>j</sup>
P-type	CI chondrites	$1.5 \pm 0.5$	$2420 \pm 40^f$	$-0.0033 \times T^2 + 3.39 \times T$	0.9	$18.9 \pm 3.7^i$	$0.14 \pm 0.06^d$
C-complex	carb. chondrites	$4.05 \pm 0.35$	$3520 \pm 130^f$	$-0.0033 \times T^2 + 3.39 \times T$	0.9	$18.9 \pm 3.7^i$	$0.14 \pm 0.06^d$
Ch/B-type	CM chondrites	$1.5 \pm 0.5$	$2940 \pm 40^f$	$-0.0036 \times T^2 + 3.84 \times T$	0.9	$18.9 \pm 3.7^i$	$0.14 \pm 0.06^d$
K-type	CK/CO/CV chondrites	$4.05 \pm 0.35$	$3520 \pm 60^f$	$-0.0033 \times T^2 + 3.39 \times T$	0.9	$18.9 \pm 3.7^i$	$0.14 \pm 0.06^d$

**Notes.** *Italicized* values are taken from S-complex values.

<sup>a</sup>All calculated specific heat capacities are assigned a 10% uncertainty.

<sup>b</sup>Poisson’s ratio.

<sup>c</sup>Average using data from: Consolmagno et al. (2008); Opeil et al. (2010); Szurgot et al. (2012).

<sup>d</sup>Calculated from  $E$  and  $G$  values presented in Ibrahim (2012).

<sup>e</sup>Macke et al. (2011)

<sup>f</sup>Macke et al. (2011)

<sup>g</sup>Macke et al. (2010)

<sup>h</sup>Macke (2010)

<sup>i</sup>Ibrahim (2012)

<sup>j</sup>Ledbetter and Reed (1973)



Table 4: Grain Size Model Inputs and Results

Object	$D_{eff}$	$p_V$	$\Gamma^a$	Source	Tax/Color	$P_{rot}$	$T_{surf}$ (K)	Model Comp.	$d_{g\phi}^{G\&B}$	$d_{g\phi}^{Sak}$	$l_s$ (mm)	Family
(1) Ceres	$951 \pm 8$	$0.100^{+0.004}_{-0.006}$	$25^{+15}_{-10}$	[T1]	C <sup>2</sup>	9.0742	$238 \pm 15$	C <sup>S</sup>	$0.91^{+2.10}_{-2.47}$	$1.31^{+0.67}_{-0.77}$	$8.5 \pm 2.3$	
(2) Pallas	$536 \pm 5$	$0.142^{+0.006}_{-0.005}$	$30^{+15}_{-15}$	[T1]	B <sup>2</sup>	$7.8132^\dagger$	$234 \pm 15$	B <sup>S</sup>	$0.74^{+1.70}_{-1.92}$	$1.24^{+0.60}_{-0.73}$	$9.3 \pm 2.6$	
(3) Juno	$254 \pm 4$	$0.209^{+0.020}_{-0.019}$	$70^{+30}_{-40}$	[T1]	Sk <sup>2</sup>	7.2095	$245 \pm 15$	S <sup>S</sup>	$0.11^{+1.47}_{-1.17}$	$-0.19^{+1.13}_{-1.43}$	$11.3 \pm 3.3$	
(4) Vesta	$530 \pm 24$	$0.394^{+0.011}_{-0.024}$	$30^{+10}_{-10}$	[T2]	V <sup>2</sup>	5.3421	$230 \pm 10$	V <sup>S</sup>	$2.14^{+1.07}_{-1.40}$	$1.84^{+0.40}_{-0.63}$	$7.1 \pm 1.6$	
(6) Hebe	$198 \pm 3$	$0.240^{+0.010}_{-0.015}$	$50^{+40}_{-35}$	[T3]	S <sup>2</sup>	$7.2744^\dagger$	$205 \pm 15$	S <sup>S</sup>	$-1.39^{+2.10}_{-2.63}$	$-1.49^{+1.00}_{-1.20}$	$11.5 \pm 4.1$	
(8) Flora	$142 \pm 2$	$0.252^{+0.015}_{-0.014}$	$50^{+35}_{-30}$	[T1]	S <sup>2</sup>	12.865	$244 \pm 15$	S <sup>S</sup>	$-0.06^{+2.10}_{-2.57}$	$-0.22^{+1.20}_{-1.43}$	$13.9 \pm 4.5$	Flora
(10) Hygeia	$441 \pm 6$	$0.064^{+0.003}_{-0.002}$	$50^{+20}_{-25}$	[T1]	C <sup>2</sup>	27.63	$210 \pm 15$	C <sup>S</sup>	$-0.29^{+2.07}_{-2.53}$	$0.14^{+0.83}_{-1.00}$	$20.5 \pm 5.5$	Hygeia
(16) Psyche	$243 \pm 25$	$0.138^{+0.015}_{-0.015}$	$120^{+40}_{-40}$	[T4]	X <sup>2</sup>	$4.1959^\dagger$	$212 \pm 10$	Met <sup>S;A</sup>	$-1.96^{+1.13}_{-0.97}$	—	$9.4 \pm 2.1$	
(18) Melpomene	$135 \pm 3$	$0.234^{+0.019}_{-0.017}$	$50^{+15}_{-44}$	[T1]	S <sup>2</sup>	11.57	$236 \pm 15$	S <sup>S</sup>	$1.28^{+1.30}_{-1.13}$	$1.14^{+0.70}_{-0.77}$	$10.8 \pm 3.7$	
(19) Fortuna	$219 \pm 3$	$0.047^{+0.002}_{-0.002}$	$40^{+30}_{-15}$	[T1]	Ch <sup>2</sup>	7.4432	$232 \pm 15$	Ch <sup>S</sup>	$0.11^{+2.10}_{-2.50}$	$-0.22^{+1.43}_{-1.60}$	$11.9 \pm 3.3$	
(20) Massalia	$147 \pm 2$	$0.217^{+0.013}_{-0.012}$	$35^{+25}_{-10}$	[T1]	S <sup>2</sup>	8.098	$234 \pm 15$	S <sup>S</sup>	$1.04^{+1.27}_{-1.27}$	$0.58^{+0.90}_{-1.03}$	$10.4 \pm 2.7$	Massalia
(21) Lutetia	$96 \pm 4$	$0.221^{+0.011}_{-0.015}$	$20^{+10}_{-12}$	[T5][T1]	X <sup>2</sup>	$8.1655^\dagger$	$215 \pm 15$	M <sup>S;A</sup>	$0.54^{+1.97}_{-2.37}$	—	$5.1 \pm 1.6$	
(22) Kalliope	$167 \pm 17$	$0.152^{+0.006}_{-0.012}$	$125^{+125}_{-120}$	[T6]	X <sup>2</sup>	4.1482	$241 \pm 10$	Met <sup>S;A</sup>	$-2.69^{+1.73}_{-1.40}$	$-3.06^{+1.57}_{-1.63}$	$9.4 \pm 3.9$	
(29) Amphitrite	$202 \pm 3$	$0.198^{+0.012}_{-0.011}$	$25^{+10}_{-13}$	[T1]	S <sup>2</sup>	5.3921	$227 \pm 15$	S <sup>S</sup>	$2.31^{+1.23}_{-1.73}$	$1.48^{+0.80}_{-0.83}$	$6.1 \pm 1.7$	
(32) Pomona	$85 \pm 1$	$0.240^{+0.007}_{-0.011}$	$112^{+8}_{-92}$	[T6]	S <sup>2</sup>	$9.4477^\dagger$	$215 \pm 10$	S <sup>S</sup>	$-0.92^{+1.80}_{-2.70}$	$-1.16^{+1.07}_{-1.27}$	$13.9 \pm 4.4$	
(41) Daphne	$189 \pm 1$	$0.065^{+0.002}_{-0.002}$	$< 50^U$	[T6]	Ch <sup>2</sup>	5.988	$263 \pm 10$	Ch <sup>S</sup>	$2.01^{+2.13}_{-2.47}$	$2.88^{+0.73}_{-0.90}$	$7.0 \pm 2.2$	
(44) Nysa	$81 \pm 1$	$0.429^{+0.012}_{-0.041}$	$115^{+45}_{-35}$	[T6]	Xc <sup>2</sup>	$6.4214^\dagger$	$212 \pm 10$	E <sup>S;A</sup>	$-2.22^{+1.97}_{-2.50}$	$-2.62^{+1.37}_{-1.53}$	$16.5 \pm 3.7$	Nysa-Polana
(45) Eugenia	$198 \pm 20$	$0.048^{+0.002}_{-0.003}$	$45^{+40}_{-40}$	[T6]	C <sup>2</sup>	$5.6991^\dagger$	$236 \pm 10$	B <sup>S</sup>	$-0.12^{+2.13}_{-2.50}$	$-0.79^{+1.27}_{-1.57}$	$9.9 \pm 3.9$	
(52) Europa	$317 \pm 4$	$0.057^{+0.002}_{-0.002}$	$10^{+25}_{-10}$	[T1]	C <sup>2</sup>	5.6304	$209 \pm 15$	B <sup>S</sup>	$0.54^{+2.13}_{-2.57}$	$0.41^{+1.50}_{-1.73}$	$6.9 \pm 3.2$	Hygeia
(54) Alexandra	$153 \pm 2$	$0.063^{+0.004}_{-0.004}$	$10^{+22}_{-10}$	[T1]	C <sup>2</sup>	7.024	$225 \pm 15$	C <sup>S</sup>	$0.78^{+2.20}_{-2.43}$	$0.94^{+0.70}_{-0.97}$	$6.5 \pm 2.7$	
(63) Ausonia	$94.6 \pm 2.4$	$0.189^{+0.010}_{-0.009}$	$50^{+12}_{-24}$	[T7]	Sa <sup>2</sup>	9.282	$303 \pm 50$	S <sup>S;A</sup>	$2.48^{+1.37}_{-1.43}$	$0.64^{+1.17}_{-1.53}$	$9.5 \pm 2.5$	Vesta
(65) Cybele	$275 \pm 4$	$0.044^{+0.002}_{-0.003}$	$25^{+15}_{-20}$	[T8]	C <sup>2</sup>	6.0814	$215 \pm 15$	C <sup>S;A</sup>	$0.58^{+2.13}_{-2.43}$	$1.31^{+0.50}_{-1.13}$	$6.8 \pm 2.2$	Cybele
(73) Klytia	$44.8 \pm 1.7$	$0.189^{+0.019}_{-0.019}$	$14^{+15}_{-13}$	[T9]	S <sup>2</sup>	$8.2831^\dagger$	$224 \pm 5$	S <sup>S</sup>	$2.14^{+1.33}_{-1.87}$	$1.58^{+0.43}_{-0.47}$	$6.3 \pm 2.6$	
(82) Alkmene	$58.2 \pm 1.3$	$0.256^{+0.026}_{-0.026}$	$30^{+14}_{-16}$	[T9]	Sq <sup>2</sup>	$13.0008^\dagger$	$207 \pm 2$	S <sup>S</sup>	$1.28^{+1.37}_{-1.13}$	$1.18^{+0.53}_{-0.63}$	$11.2 \pm 3.2$	
(87) Sylvia	$300 \pm 30$	$0.035^{+0.001}_{-0.002}$	$70^{+60}_{-60}$	[T6]	X <sup>2</sup>	$5.1836^\dagger$	$233 \pm 10$	P <sup>S</sup>	$-1.26^{+1.90}_{-1.47}$	$-1.82^{+1.87}_{-1.73}$	$12.6 \pm 4.9$	Sylvia
(88) Thisbe	$221 \pm 2$	$0.051^{+0.002}_{-0.002}$	$60^{+15}_{-25}$	[T1]	B <sup>2</sup>	6.042	$211 \pm 15$	B <sup>S</sup>	$-0.12^{+1.97}_{-2.47}$	$-0.59^{+1.37}_{-1.53}$	$11.6 \pm 2.7$	
(91) Aegina	$101.4 \pm 13.8$	$0.052^{+0.007}_{-0.007}$	$19^{+31}_{-19}$	[T10]	Ch <sup>2</sup>	6.025	$250 \pm 16$	Ch <sup>S;A;O</sup>	$0.94^{+2.17}_{-2.53}$	$0.54^{+1.40}_{-1.60}$	$8.1 \pm 3.2$	Astrea
(93) Minerva	$167 \pm 3$	$0.047^{+0.003}_{-0.003}$	$25^{+30}_{-10}$	[T1]	C <sup>2</sup>	5.982	$210 \pm 15$	C <sup>S</sup>	$-0.19^{+2.13}_{-2.53}$	$-0.22^{+1.07}_{-1.17}$	$8.6 \pm 2.8$	Gefion/Minerva
(99) Dike	$66.5 \pm 0.9$	$0.072^{+0.027}_{-0.027}$	$35^{+19}_{-19}$	[T9]	Xk <sup>2</sup>	$18.1191^\dagger$	$216 \pm 3$	P <sup>S</sup>	$0.74^{+1.47}_{-1.13}$	$0.24^{+1.40}_{-1.60}$	$17.1 \pm 5.0$	Mitidika
(100) Hekate	$87 \pm 5$	$0.220^{+0.030}_{-0.030}$	$4^{+66}_{-2}$	[T11]	S <sup>2</sup>	$27.0703^\dagger$	$239 \pm 7$	S <sup>S;A;O</sup>	$-0.02^{+1.97}_{-1.53}$	$-1.19^{+1.50}_{-1.67}$	$19.2 \pm 8.9$	Hygeia
(107) Camilla	$245 \pm 25$	$0.046^{+0.002}_{-0.002}$	$25^{+10}_{-10}$	[T6]	X <sup>2</sup>	$4.8439^\dagger$	$213 \pm 10$	P <sup>S;A</sup>	$1.94^{+1.20}_{-1.03}$	$1.84^{+1.00}_{-1.20}$	$7.6 \pm 1.8$	
(109) Felicitas	$85 \pm 6$	$0.065^{+0.008}_{-0.010}$	$40^{+100}_{-105}$	[T11]	Ch <sup>2</sup>	$13.1906^\dagger$	$222 \pm 5$	Ch <sup>S</sup>	$-1.96^{+2.37}_{-2.60}$	$-2.62^{+1.93}_{-1.80}$	$21.3 \pm 8.9$	
(110) Lydia	$93.5 \pm 3.5$	$0.153^{+0.007}_{-0.012}$	$95^{+105}_{-25}$	[T6]	X <sup>2</sup>	$10.9258^\dagger$	$217 \pm 10$	Met <sup>S;A;O</sup>	$-2.72^{+1.93}_{-1.33}$	$-3.02^{+1.50}_{-1.67}$	$16.8 \pm 4.9$	Padua
(115) Thyra	$92 \pm 2$	$0.191^{+0.003}_{-0.013}$	$75^{+25}_{-50}$	[T6]	S <sup>2</sup>	$7.2400^\dagger$	$231 \pm 10$	S <sup>S</sup>	$-0.19^{+1.43}_{-1.03}$	$-0.36^{+1.07}_{-1.33}$	$11.3 \pm 3.4$	
(121) Hermione	$220 \pm 22$	$0.047^{+0.002}_{-0.002}$	$35^{+25}_{-30}$	[T6]	Ch <sup>2</sup>	$5.5509^\dagger$	$224 \pm 10$	Ch <sup>S</sup>	$0.44^{+2.07}_{-2.60}$	$0.08^{+1.33}_{-1.57}$	$8.9 \pm 3.0$	
(125) Liberatrix	$50.7 \pm 1.7$	$0.184^{+0.021}_{-0.021}$	$71^{+24}_{-26}$	[T9]	X <sup>2</sup>	3.9682	$206 \pm 2$	Met <sup>S;A;O</sup>	$-0.59^{+1.07}_{-1.03}$	$-0.09^{+0.57}_{-0.60}$	$7.0 \pm 1.6$	Nemesis
(130) Elektra	$197 \pm 20$	$0.066^{+0.003}_{-0.006}$	$35^{+30}_{-30}$	[T6]	Ch <sup>2</sup>	$5.2246^\dagger$	$223 \pm 10$	Ch <sup>S</sup>	$0.14^{+2.13}_{-2.57}$	$-0.29^{+1.43}_{-1.60}$	$9.0 \pm 3.1$	
(155) Scylla	$38.3 \pm 0.6$	$0.053^{+0.004}_{-0.004}$	$20^{+10}_{-10}$	[T9][T10]	XFC <sup>4b</sup>	$7.9588^\dagger$	$220 \pm 12$	C <sup>S</sup>	$0.58^{+2.10}_{-2.47}$	$1.11^{+1.60}_{-0.80}$	$8.1 \pm 2.6$	
(159) Aemilia	$137 \pm 8$	$0.054^{+0.015}_{-0.015}$	$50^{+50}_{-50}$	[T12]	Ch <sup>2</sup>	24.486	$200 \pm 10$	Ch <sup>F;A</sup>	$-1.42^{+2.20}_{-2.53}$	$-2.06^{+1.67}_{-1.70}$	$25.6 \pm 9.4$	Hygiea/Aemilia

Table 4 — continued

Object	$D_{eff}$	$p_V$	$\Gamma^a$	Source	Tax/Color	$P_{rot}$	$T_{surf}$ (K)	Model Comp.	$d_{g\phi}^{G\&B}$	$d_{g\phi}^{Sak}$	$l_s$ (mm)	Family
(167) Urda	$40.1 \pm 0.6$	$0.240^{+0.011}_{-0.011}$	$80^{+40}_{-40}$	[T9][T13]	Sk <sup>2</sup>	$13.0613^{\dagger}$	$217 \pm 4$	$S^{F;A}$	$-1.39^{+2.00}_{-2.57}$	$-1.66^{+1.37}_{-1.57}$	$18.2 \pm 5.1$	Koronis
(183) Istria	$31.43 \pm 3.06$	$0.288^{+0.030}_{-0.034}$	$21^{+13}_{-11}$	[T13]	V <sup>2</sup>	11.77	$192 \pm 2$	$V^S$	$0.41^{+2.13}_{-2.43}$	$1.14^{+0.47}_{-0.80}$	$10.2 \pm 2.9$	
(188) Menippe	$35.6 \pm 1.0$	$0.275^{+0.054}_{-0.054}$	$17^{+17}_{-11}$	[T9]	S <sup>2</sup>	12.0	$209 \pm 3$	$S^S$	$1.71^{+1.27}_{-1.50}$	$1.08^{+0.63}_{-0.63}$	$9.1 \pm 3.3$	
(193) Ambrosia	$30.5 \pm 1.0$	$0.225^{+0.031}_{-0.031}$	$49^{+20}_{-14}$	[T9]	S <sup>2</sup>	$6.5817^{\dagger}$	$197 \pm 34$	$S^S$	$-0.26^{+1.40}_{-1.30}$	$-1.09^{+1.47}_{-1.97}$	$11.2 \pm 2.9$	
(195) Eurykleia	$87 \pm 10$	$0.060^{+0.020}_{-0.020}$	$15^{+55}_{-15}$	[T11]	Ch <sup>2</sup>	$16.5218^{\dagger}$	$231 \pm 3$	$C^S$	$-0.49^{+2.23}_{-2.60}$	$-0.99^{+1.37}_{-1.67}$	$14.6 \pm 6.4$	
(208) Lacrimosa	$40.4 \pm 0.7$	$0.253^{+0.009}_{-0.012}$	$77^{+23}_{-18}$	[T13]	Sk <sup>2</sup>	14.085	$212 \pm 4$	$S^{S;F}$	$-0.76^{+1.90}_{-2.87}$	$-0.82^{+1.07}_{-1.33}$	$19.2 \pm 3.9$	Koronis
(220) Stephania	$29.8 \pm 0.6$	$0.066^{+0.023}_{-0.023}$	$4^{+6}_{-4}$	[T9]	Xk <sup>3</sup>	18.2087	$230 \pm 2$	$K^S$	$1.18^{+2.27}_{-2.40}$	$6.64^{+0.00}_{-0.00}$	$5.7 \pm 2.2$	
(226) Weringia	$28.7 \pm 0.2$	$0.230^{+0.022}_{-0.022}$	$30^{+10}_{-10}$	[T9]	S <sup>2</sup>	$11.1485^{\dagger}$	$213 \pm 2$	$S^S$	$1.84^{+1.03}_{-1.27}$	$1.68^{+0.47}_{-0.47}$	$10.4 \pm 2.3$	
(227) Philosophia	$101 \pm 5$	$0.041^{+0.005}_{-0.005}$	$125^{+90}_{-90}$	[T12]	X <sup>3</sup>	26.468	$225 \pm 10$	$P^S$	$-2.82^{+2.03}_{-1.43}$	$-3.29^{+2.03}_{-1.90}$	$38.5 \pm 13.5$	
(263) Dresda	$23.87 \pm 0.85$	$0.230^{+0.039}_{-0.039}$	$26^{+24}_{-26}$	[T9]	S <sup>2</sup>	$16.8139^{\dagger}$	$210 \pm 3$	$S^{S;F}$	$0.88^{+1.43}_{-1.27}$	$0.41^{+0.83}_{-0.97}$	$12.1 \pm 5.0$	Koronis
(271) Penthesilea	$65.05 \pm 2.30$	$0.054^{+0.003}_{-0.003}$	$16^{+33}_{-16}$	[T10]	C <sup>3</sup>	18.787	$210 \pm 1$	$C^S$	$0.01^{+2.10}_{-2.57}$	$-0.09^{+1.00}_{-1.20}$	$13.6 \pm 5.6$	
(272) Antonia	$30.5 \pm 1.1$	$0.104^{+0.025}_{-0.025}$	$75^{+10}_{-10}$	[T9]	X <sup>2</sup>	3.8548	$209 \pm 3$	$C^{F;A}$	$-0.66^{+1.97}_{-2.63}$	$0.38^{+0.60}_{-0.60}$	$9.6 \pm 1.7$	Hoffmeister
(274) Philagoria	$28.45 \pm 0.85$	$0.238^{+0.025}_{-0.025}$	$93^{+8}_{-13}$	[T9]	L <sup>3</sup>	$17.9410^{\dagger}$	$227 \pm 1$	$S^S$	$-0.66^{+0.53}_{-0.50}$	$0.04^{+0.63}_{-0.53}$	$21.9 \pm 4.0$	
(277) Elvira	$38 \pm 2$	$0.152^{+0.006}_{-0.005}$	$190^{+210}_{-90}$	[T6]	S <sup>4b</sup>	$29.6922^{\dagger}$	$230 \pm 10$	$S^{F;C}$	$-4.19^{+2.33}_{-2.60}$	$-4.76^{+1.93}_{-1.87}$	$49.0 \pm 16.2$	Koronis
(281) Lucretia	$11.19 \pm 0.15$	$0.247^{+0.030}_{-0.030}$	$48^{+12}_{-13}$	[T9]	S <sup>2</sup>	$4.3497^{\dagger}$	$226 \pm 3$	$S^{S;F}$	$1.18^{+0.97}_{-1.00}$	$1.41^{+0.57}_{-0.57}$	$7.9 \pm 1.6$	Flora
(283) Emma	$135 \pm 15$	$0.040^{+0.002}_{-0.002}$	$110^{+105}_{-105}$	[T6]	X <sup>3</sup>	$6.8952^{\dagger}$	$237 \pm 10$	$C^{F;C;A}$	$-2.36^{+2.20}_{-2.57}$	$-3.02^{+1.73}_{-1.70}$	$15.9 \pm 5.8$	Emma
(290) Bruna	$9.8 \pm 0.2$	$0.259^{+0.032}_{-0.032}$	$21^{+39}_{-21}$	[T9]	S <sup>1</sup>	$13.8055^{\dagger}$	$237 \pm 18$	$S^{S;F}$	$0.74^{+1.67}_{-1.40}$	$-0.66^{+1.20}_{-1.50}$	$11.5 \pm 5.3$	Phocaea
(295) Theresia	$30.5 \pm 1.2$	$0.220^{+0.013}_{-0.013}$	$24^{+38}_{-17}$	[T10]	S <sup>2</sup>	10.73	$211 \pm 3$	$S^S$	$0.24^{+1.73}_{-1.40}$	$-0.19^{+1.20}_{-1.50}$	$11.5 \pm 4.6$	
(301) Bavaria	$55 \pm 2$	$0.047^{+0.004}_{-0.003}$	$45^{+60}_{-30}$	[T11]	C <sup>2</sup>	12.2409	$240 \pm 2$	$C^A$	$-0.89^{+2.13}_{-2.50}$	$-1.36^{+1.43}_{-1.63}$	$15.1 \pm 5.6$	
(306) Unitas	$56 \pm 1$	$0.178^{+0.007}_{-0.009}$	$200^{+60}_{-100}$	[T6]	S <sup>2</sup>	$8.7387^{\dagger}$	$248 \pm 10$	$S^S$	$-2.49^{+2.00}_{-2.47}$	$-2.49^{+2.00}_{-2.47}$	$20.1 \pm 5.1$	
(311) Claudia	$26.2 \pm 0.7$	$0.252^{+0.027}_{-0.027}$	$17^{+13}_{-17}$	[T9]	Sk <sup>3</sup>	$7.5314^{\dagger}$	$211 \pm 4$	$S^{F;A}$	$0.88^{+2.13}_{-2.47}$	$1.51^{+0.00}_{-0.67}$	$6.7 \pm 2.3$	Koronis
(322) Phaeo	$59.7 \pm 1.3$	$0.126^{+0.004}_{-0.007}$	$12^{+11}_{-7}$	[T10]	X <sup>2</sup>	17.5845	$210 \pm 6$	$P^{S;A}$	$2.71^{+1.30}_{-1.27}$	$2.28^{+0.90}_{-1.00}$	$11.1 \pm 3.7$	Phaeo
(329) Svea	$78 \pm 4$	$0.055^{+0.015}_{-0.015}$	$75^{+50}_{-50}$	[T12]	C <sup>3</sup>	22.777	$234 \pm 10$	$C^{S;F}$	$-1.12^{+2.10}_{-2.53}$	$-1.52^{+1.40}_{-1.60}$	$22.7 \pm 7.2$	Svea
(340) Eduarda	$27.2 \pm 0.4$	$0.241^{+0.032}_{-0.032}$	$25^{+19}_{-25}$	[T9]	S <sup>8</sup>	$8.0061^{\dagger}$	$216 \pm 1$	$S^{C;A}$	$1.48^{+1.30}_{-1.37}$	$0.98^{+0.67}_{-0.73}$	$7.7 \pm 3.1$	
(343) Ostara	$19.6 \pm 1.4$	$0.113^{+0.009}_{-0.010}$	$139^{+117}_{-63}$	[T10]	CSGU <sup>4b</sup>	109.87	$226 \pm 7$	$C^{C;A}$	$-3.06^{+2.17}_{-2.53}$	$-3.62^{+1.73}_{-1.70}$	$75.7 \pm 22.7$	
(349) Dembowska	$155.8 \pm 7.1$	$0.309^{+0.026}_{-0.038}$	$20^{+12}_{-7}$	[T14]	Sr <sup>2</sup>	4.701	$211 \pm 5$	$S^S$	$1.98^{+1.27}_{-1.67}$	$1.64^{+0.33}_{-0.57}$	$5.7 \pm 1.5$	
(351) Yrsa	$42.49 \pm 1.25$	$0.230^{+0.030}_{-0.030}$	$50^{+19}_{-20}$	[T9]	S <sup>4b</sup>	$13.3120^{\dagger}$	$207 \pm 4$	$S^{C;A}$	$0.21^{+1.33}_{-1.00}$	$0.24^{+0.83}_{-0.90}$	$14.8 \pm 3.6$	
(352) Gisela	$24.5 \pm 0.5$	$0.227^{+0.027}_{-0.027}$	$10^{+24}_{-10}$	[T9]	S <sup>2</sup>	$7.4801^{\dagger}$	$243 \pm 4$	$S^{F;C}$	$2.01^{+1.63}_{-1.53}$	$1.31^{+0.70}_{-0.77}$	$6.4 \pm 3.0$	Flora
(355) Gabriella	$24.49 \pm 0.8$	$0.230^{+0.031}_{-0.031}$	$35^{+5}_{-5}$	[T9]	S <sup>2</sup>	$4.8290^{\dagger}$	$239 \pm 7$	$S^{S;F}$	$2.54^{+1.10}_{-1.33}$	—	$6.9 \pm 1.3$	Astraea
(378) Holmia	$28.8 \pm 0.7$	$0.241^{+0.023}_{-0.023}$	$13^{+12}_{-12}$	[T9]	S <sup>2</sup>	$4.4404^{\dagger}$	$217 \pm 2$	$S^S$	$2.21^{+1.53}_{-2.10}$	$1.84^{+0.47}_{-0.57}$	$4.4 \pm 1.8$	
(380) Fiducia	$72 \pm 8$	$0.057^{+0.009}_{-0.012}$	$10^{+140}_{-10}$	[T11]	C <sup>4b</sup>	$13.7172^{\dagger}$	$242 \pm 3$	$C^{C;A}$	$-2.09^{+2.30}_{-2.53}$	$-2.79^{+1.80}_{-1.77}$	$19.4 \pm 9.0$	
(382) Dodona	$75 \pm 1$	$0.111^{+0.004}_{-0.005}$	$60^{+90}_{-45}$	[T6]	X <sup>9</sup>	$4.1132^{\dagger}$	$232 \pm 10$	$Met^{C;A}$	$-1.69^{+1.67}_{-1.37}$	$-2.12^{+1.37}_{-1.63}$	$7.8 \pm 3.1$	
(390) Alma	$24.9 \pm 0.5$	$0.234^{+0.034}_{-0.034}$	$37^{+13}_{-29}$	[T9]	S <sup>3</sup>	$3.7412^{\dagger}$	$235 \pm 5$	$S^S$	$1.84^{+1.33}_{-1.27}$	$1.71^{+0.50}_{-0.57}$	$5.5 \pm 1.8$	Eunomia
(394) Arduina	$30.9 \pm 0.9$	$0.234^{+0.025}_{-0.025}$	$83^{+17}_{-28}$	[T9]	S <sup>2</sup>	$16.6217^{\dagger}$	$218 \pm 2$	$S^S$	$-0.56^{+1.10}_{-0.83}$	$-0.39^{+0.90}_{-1.03}$	$19.9 \pm 4.2$	
(400) Ducrosa	$34.6 \pm 0.8$	$0.093^{+0.025}_{-0.025}$	$38^{+16}_{-13}$	[T9]	B <sup>3</sup>	$6.8679^{\dagger}$	$198 \pm 3$	$B^S$	$0.18^{+1.97}_{-2.53}$	$0.21^{+1.13}_{-1.37}$	$11.1 \pm 2.6$	
(413) Edburga	$33.8 \pm 0.6$	$0.158^{+0.018}_{-0.020}$	$100^{+60}_{-60}$	[T9][T13]	X <sup>2</sup>	$15.7715^{\dagger}$	$211 \pm 10$	$Met^{S;A}$	$-2.02^{+1.47}_{-1.17}$	$-2.06^{+1.20}_{-1.53}$	$16.6 \pm 5.2$	
(423) Diotima	$200 \pm 4$	$0.053^{+0.004}_{-0.004}$	$40^{+30}_{-20}$	[T1]	C <sup>2</sup>	4.775	$208 \pm 15$	$K^{S;F}$	$-0.52^{+2.13}_{-2.53}$	$-0.56^{+1.10}_{-1.40}$	$8.6 \pm 2.6$	Eos
(430) Hybris	$33.2 \pm 0.7$	$0.069^{+0.031}_{-0.031}$	$55^{+9}_{-5}$	[T9]	C <sup>1</sup>	$7.2166^{\dagger}$	$197 \pm 2$	$C^S$	$-0.52^{+2.07}_{-2.53}$	$0.88^{+0.53}_{-0.53}$	$11.9 \pm 2.1$	
(433) Eros	$17.8 \pm 0.5$	$0.315^{+0.024}_{-0.034}$	$150^{+50}_{-50}$	[T6]	S <sup>4</sup>	5.27	$278 \pm 10$	$S^S$	$-1.29^{+1.93}_{-2.47}$	$-1.76^{+1.33}_{-1.53}$	$14.0 \pm 3.1$	
(444) Gyptis	$162 \pm 23$	$0.049^{+0.007}_{-0.008}$	$74^{+74}_{-74}$	[T10]	C <sup>2</sup>	6.214	$253 \pm 25$	$C^S$	$-1.29^{+2.20}_{-2.57}$	$-1.89^{+1.63}_{-1.73}$	$12.1 \pm 4.5$	

Table 4 — continued

Object	$D_{eff}$	$p_V$	$\Gamma^a$	Source	Tax/Color	$P_{rot}$	$T_{surf}$ (K)	Model Comp.	$d_{g\phi}^{G\&B}$	$d_{g\phi}^{Sak}$	$l_s$ (mm)	Family
(463) Lola	$20.3 \pm 1.5$	$0.115^{+0.009}_{-0.010}$	$68^{+30}_{-28}$	[T10]	X <sup>4b</sup>	6.206	$221 \pm 4$	M <sup>C;A</sup>	$-0.72^{+2.00}_{-2.57}$	$-0.52^{+0.97}_{-1.17}$	$11.1 \pm 2.8$	Themis
(464) Megaira	$69.56 \pm 6.38$	$0.053^{+0.006}_{-0.006}$	$117^{+117}_{-117}$	[T10]	C <sup>2</sup>	12.726	$209 \pm 2$	C <sup>S</sup>	$-3.19^{+2.23}_{-2.57}$	$-3.82^{+1.77}_{-1.73}$	$24.1 \pm 8.7$	
(468) Lina	$69 \pm 10$	$0.052^{+0.006}_{-0.014}$	$20^{+280}_{-20}$	[T11]	B <sup>3</sup>	$16.4784^\dagger$	$239 \pm 3$	B <sup>F;A</sup>	$-3.69^{+2.80}_{-2.93}$	$-4.36^{+2.43}_{-2.27}$	$34.3 \pm 16.3$	
(478) Tergeste	$87 \pm 6$	$0.150^{+0.020}_{-0.020}$	$75^{+45}_{-45}$	[T12]	L <sup>2</sup>	16.105	$201 \pm 10$	S <sup>S</sup>	$-1.56^{+1.60}_{-1.23}$	$-2.19^{+1.47}_{-1.63}$	$20.5 \pm 6.5$	
(482) Petrina	$44.2 \pm 0.8$	$0.185^{+0.019}_{-0.019}$	$4^{+20}_{-4}$	[T9]	S <sup>4b</sup>	$11.7921^\dagger$	$209 \pm 2$	S <sup>C;A</sup>	$1.78^{+1.53}_{-1.77}$	$1.04^{+0.60}_{-0.73}$	$7.6 \pm 3.6$	
(484) Pittsburghia	$29.2 \pm 0.7$	$0.202^{+0.025}_{-0.020}$	$6^{+5}_{-5}$	[T9]	S <sup>2</sup>	$10.6498^\dagger$	$218 \pm 3$	S <sup>S</sup>	$1.88^{+2.10}_{-2.20}$	—	$4.5 \pm 1.7$	
(487) Venetia	$70 \pm 4$	$0.210^{+0.025}_{-0.020}$	$100^{+75}_{-75}$	[T12]	S <sup>3</sup>	13.342	$214 \pm 10$	S <sup>S</sup>	$-2.29^{+1.80}_{-1.33}$	$-2.92^{+1.63}_{-1.67}$	$20.9 \pm 7.6$	
(493) Griseldis	$40.86 \pm 1.13$	$0.054^{+0.003}_{-0.004}$	$56^{+25}_{-32}$	[T10]	X <sup>3</sup>	51.94	$203 \pm 2$	P <sup>S;A</sup>	$-0.69^{+1.53}_{-1.17}$	$-1.19^{+1.53}_{-1.57}$	$36.4 \pm 10.4$	
(497) Iva	$37.39 \pm 0.65$	$0.139^{+0.026}_{-0.026}$	$70^{+19}_{-25}$	[T9]	M <sup>4b</sup>	$4.6209^\dagger$	$191 \pm 2$	M <sup>C;A</sup>	$-1.22^{+2.07}_{-2.57}$	$-0.59^{+0.83}_{-0.87}$	$10.1 \pm 2.2$	
(500) Selinur	$41.15 \pm 0.37$	$0.196^{+0.004}_{-0.017}$	$16^{+7}_{-8}$	[T10]	S <sup>3</sup>	8.0111	$218 \pm 7$	S <sup>S</sup>	$2.31^{+1.60}_{-2.43}$	—	$6.2 \pm 1.7$	
(509) Iolanda	$55.1 \pm 1.8$	$0.222^{+0.020}_{-0.026}$	$9.0^{+12.0}_{-9.0}$	[T9][T13]	S <sup>2</sup>	$12.2909^\dagger$	$204 \pm 3$	S <sup>S</sup>	$2.08^{+1.50}_{-2.20}$	$2.08^{+0.03}_{-0.33}$	$6.9 \pm 3.0$	Meliboea
(511) Davida	$307 \pm 6$	$0.065^{+0.003}_{-0.003}$	$35^{+15}_{-17}$	[T1]	C <sup>2</sup>	5.1297	$200 \pm 15$	C <sup>S</sup>	$0.01^{+2.13}_{-2.47}$	$0.48^{+0.77}_{-0.77}$	$7.7 \pm 2.1$	
(512) Taurinensis	$18 \pm 0.7$	$0.234^{+0.020}_{-0.020}$	$4^{+4}_{-4}$	[T9]	S <sup>2</sup>	$5.5820^\dagger$	$241 \pm 6$	S <sup>S</sup>	$2.18^{+2.00}_{-2.30}$	$-13.39^{+0.00}_{-0.00}$	$2.6 \pm 1.1$	
(520) Franziska	$27.8 \pm 1$	$0.141^{+0.014}_{-0.014}$	$30^{+40}_{-30}$	[T9][T10]	CGU <sup>4b</sup>	$16.5045^\dagger$	$205 \pm 3$	K <sup>F;C;A</sup>	$-1.12^{+2.03}_{-2.83}$	$-0.99^{+1.23}_{-1.53}$	$14.3 \pm 6.2$	Eos
(532) Herculina	$207 \pm 12$	$0.172^{+0.012}_{-0.024}$	$15^{+10}_{-10}$	[T6]	S <sup>2</sup>	9.4049	$221 \pm 10$	S <sup>S</sup>	$2.31^{+1.60}_{-2.33}$	—	$6.3 \pm 2.1$	Hygeia
(537) Pauly	$41.92 \pm 0.95$	$0.276^{+0.027}_{-0.027}$	$7^{+9}_{-7}$	[T9]	S <sup>3</sup>	$16.2961^\dagger$	$200 \pm 2$	S <sup>S</sup>	$1.84^{+1.90}_{-2.40}$	—	$7.0 \pm 3.0$	
(538) Friederike	$71.0 \pm 4.5$	$0.068^{+0.008}_{-0.008}$	$30^{+17}_{-30}$	[T11][T10]	—	46.728	$207 \pm 3$	C <sup>F;A</sup>	$0.24^{+2.20}_{-2.43}$	$0.98^{+0.47}_{-0.97}$	$20.5 \pm 6.8$	
(544) Jetta	$26.94 \pm 1.25$	$0.210^{+0.027}_{-0.027}$	$28^{+16}_{-18}$	[T9]	S <sup>2</sup>	$7.7453^\dagger$	$212 \pm 3$	S <sup>S</sup>	$1.44^{+1.23}_{-1.27}$	$1.11^{+0.60}_{-0.63}$	$8.2 \pm 2.6$	
(550) Senta	$37.8 \pm 0.9$	$0.223^{+0.024}_{-0.024}$	$26^{+34}_{-26}$	[T9]	S <sup>1</sup>	$20.5726^\dagger$	$211 \pm 3$	S <sup>S</sup>	$0.34^{+1.47}_{-1.30}$	$-0.39^{+1.10}_{-1.40}$	$14.8 \pm 6.5$	Vesta
(556) Phyllis	$35.6 \pm 0.9$	$0.209^{+0.010}_{-0.010}$	$30^{+12}_{-11}$	[T7]	S <sup>2</sup>	4.923	$235 \pm 7$	S <sup>S;A;O</sup>	$2.18^{+1.27}_{-1.40}$	$1.91^{+0.47}_{-0.63}$	$6.6 \pm 1.6$	
(558) Carmen	$59.7 \pm 3.2$	$0.117^{+0.007}_{-0.011}$	$7.7^{+26.9}_{-7.7}$	[T10]	X <sup>9</sup>	11.387	$222 \pm 3$	P <sup>S;A</sup>	$1.48^{+1.70}_{-1.43}$	$0.54^{+1.47}_{-1.70}$	$10.2 \pm 4.8$	
(562) Salome	$34.7 \pm 0.9$	$0.147^{+0.010}_{-0.010}$	$20^{+15}_{-20}$	[T9][T10]	S <sup>4b</sup>	6.351	$206 \pm 5$	K <sup>S;F</sup>	$0.58^{+2.13}_{-2.47}$	$1.44^{+0.67}_{-0.70}$	$6.6 \pm 2.3$	Eos
(567) Eleutheria	$87.45 \pm 7.81$	$0.056^{+0.005}_{-0.007}$	$19^{+30}_{-11}$	[T10]	CFB: <sup>4b</sup>	7.717	$234 \pm 4$	C <sup>C;A</sup>	$0.48^{+2.13}_{-2.53}$	$0.58^{+0.90}_{-0.90}$	$8.4 \pm 3.1$	Eos
(573) Recha	$40.1 \pm 1.1$	$0.172^{+0.023}_{-0.023}$	$45^{+15}_{-15}$	[T9]	K <sup>3</sup>	$7.1659^\dagger$	$225 \pm 4$	K <sup>S;F</sup>	$0.31^{+2.10}_{-2.50}$	$1.18^{+0.57}_{-0.67}$	$9.8 \pm 2.2$	
(583) Klotilde	$80.78 \pm 6.25$	$0.067^{+0.006}_{-0.006}$	$30^{+12}_{-19}$	[T10]	C <sup>4b</sup>	9.2116	$224 \pm 11$	Cb <sup>C</sup>	$0.71^{+2.13}_{-2.47}$	$1.18^{+0.70}_{-0.13}$	$8.6 \pm 2.4$	
(590) Tomyris	$32.1 \pm 1.2$	$0.154^{+0.029}_{-0.029}$	$18^{+26}_{-18}$	[T9]	—	$5.5525^\dagger$	$209 \pm 2$	K <sup>F;A</sup>	$0.24^{+2.17}_{-2.50}$	$0.38^{+0.80}_{-0.97}$	$6.9 \pm 2.7$	Eos
(617) Patroclus	$106 \pm 11$	$0.103^{+0.007}_{-0.004}$	$20^{+15}_{-15}$	[T6]	X <sup>4b</sup>	103.02	$155 \pm 10$	P <sup>C;A</sup>	$0.14^{+1.63}_{-1.30}$	$-0.59^{+1.50}_{-1.63}$	$37.8 \pm 13.7$	
(624) Hektor	$186 \pm 20$	$0.058^{+0.017}_{-0.007}$	$6^{+4}_{-6}$	[T15]	D <sup>11</sup>	$6.9205^\dagger$	$167 \pm 3$	P <sup>S</sup>	$3.34^{+1.23}_{-1.90}$	$2.74^{+0.77}_{-0.07}$	$4.8 \pm 1.8$	
(644) Cosima	$19.40 \pm 0.45$	$0.205^{+0.030}_{-0.030}$	$46^{+24}_{-21}$	[T9]	S <sup>4b</sup>	$7.5571^\dagger$	$208 \pm 3$	S <sup>C;A</sup>	$0.21^{+1.33}_{-1.13}$	$-0.09^{+0.97}_{-1.10}$	$11.0 \pm 3.0$	
(651) Antikleia	$34.07 \pm 1.92$	$0.159^{+0.010}_{-0.014}$	$37^{+16}_{-26}$	[T10]	K <sup>13</sup>	20.299	$206 \pm 2$	K <sup>S;F</sup>	$0.14^{+2.13}_{-2.47}$	$0.88^{+0.60}_{-0.63}$	$14.8 \pm 4.3$	Eos
(653) Berenike	$46 \pm 3$	$0.180^{+0.020}_{-0.030}$	$40^{+120}_{-40}$	[T11]	K <sup>2</sup>	$12.4836^\dagger$	$217 \pm 1$	K <sup>S;F</sup>	$-2.69^{+2.20}_{-2.50}$	$-3.16^{+1.77}_{-1.77}$	$18.9 \pm 8.9$	Eos
(656) Beagle	$55.14 \pm 3.02$	$0.068^{+0.005}_{-0.004}$	$32^{+14}_{-14}$	[T10]	—	7.035	$210 \pm 0$	B <sup>F;A</sup>	$1.41^{+1.30}_{-1.27}$	$1.01^{+0.57}_{-0.63}$	$8.5 \pm 2.2$	Themis/Beagle
(662) Newtonia	$24.04 \pm 1.41$	$0.211^{+0.014}_{-0.022}$	$35^{+23}_{-25}$	[T10]	S <sup>3</sup>	16.46	$235 \pm 11$	S <sup>S</sup>	$1.31^{+1.17}_{-1.30}$	$0.81^{+0.83}_{-0.90}$	$12.8 \pm 4.4$	
(668) Dora	$23.18 \pm 0.48$	$0.062^{+0.004}_{-0.003}$	$52^{+8}_{-8}$	[T10]	Ch <sup>2</sup>	22.914	$216 \pm 7$	Ch <sup>S;F</sup>	$0.41^{+1.90}_{-2.63}$	$0.84^{+0.80}_{-1.03}$	$21.9 \pm 4.0$	Dora
(669) Kypria	$30.4 \pm 1.1$	$0.195^{+0.034}_{-0.034}$	$33^{+22}_{-30}$	[T9]	—	$14.2789^\dagger$	$206 \pm 2$	K <sup>F;A</sup>	$0.08^{+2.10}_{-2.53}$	$0.48^{+0.77}_{-0.83}$	$11.7 \pm 4.4$	Eos
(670) Ottegebe	$35.08 \pm 0.76$	$0.258^{+0.009}_{-0.018}$	$44^{+14}_{-18}$	[T10]	S <sup>2</sup>	10.045	$203 \pm 2$	S <sup>S</sup>	$0.01^{+2.10}_{-2.53}$	$0.81^{+0.67}_{-0.67}$	$11.9 \pm 2.8$	
(673) Edda	$38 \pm 5$	$0.130^{+0.030}_{-0.050}$	$3^{+33}_{-3}$	[T11]	S <sup>2</sup>	$22.3341^\dagger$	$225 \pm 2$	S <sup>S</sup>	$1.24^{+1.53}_{-1.43}$	$0.38^{+0.93}_{-1.10}$	$12.6 \pm 6.0$	
(687) Tinette	$21.8 \pm 0.6$	$0.087^{+0.025}_{-0.025}$	$50^{+15}_{-15}$	[T9]	X <sup>2</sup>	7.3971	$204 \pm 2$	P <sup>S;A</sup>	$-0.22^{+1.07}_{-0.90}$	$-0.49^{+1.27}_{-1.50}$	$13.5 \pm 2.8$	
(688) Melanie	$38.4 \pm 2.5$	$0.070^{+0.006}_{-0.007}$	$41^{+44}_{-19}$	[T10]	C <sup>2</sup>	18.87	$230 \pm 6$	C <sup>S</sup>	$-0.56^{+2.10}_{-2.53}$	$-0.79^{+1.23}_{-1.60}$	$17.8 \pm 5.8$	
(694) Ekard	$109.5 \pm 1.5$	$0.038^{+0.002}_{-0.002}$	$120^{+20}_{-20}$	[T6]	CP: <sup>4b</sup>	$5.9220^\dagger$	$166 \pm 10$	C <sup>C;A</sup>	$-3.16^{+1.80}_{-2.50}$	$-3.66^{+1.07}_{-1.40}$	$17.3 \pm 3.2$	

Table 4 — continued

Object	$D_{eff}$	$p_V$	$\Gamma^a$	Source	Tax/Color	$P_{rot}$	$T_{surf}$ (K)	Model Comp.	$d_{g\phi}^{G\&B}$	$d_{g\phi}^{Sak}$	$l_s$ (mm)	Family
(720) Bohlina	41 ± 1	0.160 <sup>+0.005</sup> <sub>-0.004</sub>	100 <sup>+100</sup> <sub>-30</sub>	[T6]	Sq <sup>2</sup>	8.9186 <sup>†</sup>	217 ± 10	S <sup>S;F</sup>	-2.66 <sup>+1.60</sup> <sub>-1.37</sub>	-3.19 <sup>+1.70</sup> <sub>-1.73</sub>	19.4 ± 5.6	Koronis
(731) Sorga	37.16 ± 1.35	0.161 <sup>+0.020</sup> <sub>-0.020</sub>	76 <sup>+44</sup> <sub>-36</sub>	[T9]	Xe <sup>2</sup>	8.1863 <sup>†</sup>	198 ± 2	M <sup>S;A</sup>	-1.79 <sup>+2.03</sup> <sub>-2.53</sub>	-2.12 <sup>+1.33</sup> <sub>-1.57</sub>	14.8 ± 4.1	
(734) Benda	66.3 ± 2.8	0.045 <sup>+0.002</sup> <sub>-0.003</sub>	13 <sup>+8</sup> <sub>-13</sub>	[T10]	X <sup>3</sup>	7.11	211 ± 2	P <sup>S</sup>	1.74 <sup>+2.20</sup> <sub>-2.47</sub>	2.98 <sup>+0.80</sup> <sub>-1.30</sub>	6.1 ± 2.3	
(735) Marghanna	65.1 ± 3.9	0.063 <sup>+0.004</sup> <sub>-0.005</sub>	17 <sup>+88</sup> <sub>-17</sub>	[T10]	Ch <sup>2</sup>	15.95	214 ± 24	Ch <sup>S</sup>	-1.76 <sup>+2.43</sup> <sub>-2.63</sub>	-2.42 <sup>+1.97</sup> <sub>-1.90</sub>	21.2 ± 9.7	
(749) Malzovia	13.53 ± 0.45	0.207 <sup>+0.028</sup> <sub>-0.028</sub>	63 <sup>+37</sup> <sub>-28</sub>	[T9]	S <sup>2</sup>	5.9275 <sup>†</sup>	237 ± 5	S <sup>S</sup>	-0.16 <sup>+1.40</sup> <sub>-1.17</sub>	-0.66 <sup>+1.23</sup> <sub>-1.53</sub>	10.9 ± 3.0	
(756) Lilliana	60.98 ± 1.25	0.059 <sup>+0.030</sup> <sub>-0.025</sub>	9 <sup>+7</sup> <sub>-9</sub>	[T9]	C <sup>3</sup>	7.8325	206 ± 2	Cb <sup>S</sup>	3.38 <sup>+1.97</sup> <sub>-2.73</sub>	3.48 <sup>+1.23</sup> <sub>-1.37</sub>	5.3 ± 2.1	
(757) Portlandia	32.9 ± 0.5	0.158 <sup>+0.025</sup> <sub>-0.025</sub>	56 <sup>+8</sup> <sub>-11</sub>	[T9]	Xk <sup>2</sup>	6.5811 <sup>†</sup>	237 ± 6	M <sup>S;A</sup>	0.98 <sup>+1.00</sup> <sub>-1.83</sub>	1.78 <sup>+0.27</sup> <sub>-0.43</sub>	7.5 ± 1.4	
(771) Libera	30.3 ± 2.8	0.154 <sup>+0.022</sup> <sub>-0.024</sub>	65 <sup>+85</sup> <sub>-35</sub>	[T15][T13]	X <sup>4b</sup>	5.8904 <sup>†</sup>	206 ± 8	M <sup>C;A</sup>	-2.39 <sup>+2.17</sup> <sub>-2.53</sub>	-2.99 <sup>+1.60</sup> <sub>-1.70</sub>	13.5 ± 4.7	
(784) Pickeringia	78.35 ± 1.65	0.054 <sup>+0.026</sup> <sub>-0.026</sub>	41 <sup>+23</sup> <sub>-21</sub>	[T9]	C <sup>2</sup>	13.1700 <sup>†</sup>	197 ± 1	C <sup>S</sup>	-0.49 <sup>+2.10</sup> <sub>-2.53</sub>	-0.16 <sup>+0.87</sup> <sub>-1.00</sub>	14.0 ± 3.9	
(787) Moskva	30.50 ± 0.45	0.213 <sup>+0.018</sup> <sub>-0.018</sub>	21 <sup>+23</sup> <sub>-19</sub>	[T9]	S <sup>1</sup>	6.0558 <sup>†</sup>	220 ± 3	S <sup>S;F</sup>	1.34 <sup>+1.47</sup> <sub>-1.30</sub>	0.81 <sup>+0.77</sup> <sub>-0.83</sub>	6.8 ± 2.8	Maria
(789) Lena	21.5 ± 0.8	0.116 <sup>+0.025</sup> <sub>-0.025</sub>	33 <sup>+21</sup> <sub>-33</sub>	[T9]	Xk <sup>1</sup>	5.8423 <sup>†</sup>	216 ± 3	P <sup>S;A</sup>	0.78 <sup>+1.60</sup> <sub>-1.23</sub>	0.14 <sup>+1.43</sup> <sub>-1.60</sub>	8.7 ± 3.4	
(793) Arizona	26.9 ± 1.3	0.237 <sup>+0.013</sup> <sub>-0.020</sub>	32 <sup>+16</sup> <sub>-13</sub>	[T10]	S <sup>2</sup>	7.399	215 ± 4	S <sup>S</sup>	1.41 <sup>+1.20</sup> <sub>-1.17</sub>	1.18 <sup>+0.60</sup> <sub>-0.63</sub>	8.5 ± 2.2	
(802) Epyaxa	7.2 ± 0.5	0.268 <sup>+0.040</sup> <sub>-0.040</sub>	62 <sup>+7</sup> <sub>-7</sub>	[T9]	—	4.3901 <sup>†</sup>	225 ± 11	S <sup>F;A</sup>	0.48 <sup>+0.57</sup> <sub>-0.57</sub>	1.38 <sup>+0.57</sup> <sub>-0.57</sub>	9.1 ± 1.6	Flora
(808) Merxia	28.9 ± 0.5	0.229 <sup>+0.021</sup> <sub>-0.021</sub>	112 <sup>+28</sup> <sub>-22</sub>	[T9]	Sq <sup>2</sup>	30.6297	219 ± 4	S <sup>S;F</sup>	-1.82 <sup>+0.83</sup> <sub>-0.73</sub>	-1.92 <sup>+1.10</sup> <sub>-1.47</sub>	33.5 ± 6.5	Merxia
(810) Atossa	8.05 ± 0.25	0.242 <sup>+0.051</sup> <sub>-0.051</sub>	68 <sup>+27</sup> <sub>-33</sub>	[T9]	—	4.3855 <sup>†</sup>	223 ± 7	S <sup>A</sup>	-0.22 <sup>+1.33</sup> <sub>-1.07</sub>	-0.52 <sup>+1.13</sup> <sub>-1.37</sub>	9.3 ± 2.5	
(816) Juliana	48.75 ± 0.65	0.054 <sup>+0.028</sup> <sub>-0.028</sub>	13 <sup>+27</sup> <sub>-13</sub>	[T9]	C <sup>3</sup>	10.5627 <sup>†</sup>	229 ± 3	C <sup>S</sup>	0.71 <sup>+2.17</sup> <sub>-2.53</sub>	0.78 <sup>+0.80</sup> <sub>-0.80</sub>	8.8 ± 3.6	Juliana
(826) Henrika	23.11 ± 0.97	0.096 <sup>+0.006</sup> <sub>-0.005</sub>	45 <sup>+16</sup> <sub>-21</sub>	[T10]	C <sup>2</sup>	5.9846	237 ± 8	C <sup>S</sup>	0.48 <sup>+2.17</sup> <sub>-2.50</sub>	1.18 <sup>+0.60</sup> <sub>-0.63</sub>	8.4 ± 2.1	
(829) Academia	37.2 ± 1.5	0.063 <sup>+0.003</sup> <sub>-0.004</sub>	15 <sup>+7</sup> <sub>-15</sub>	[T10]	Ch <sup>3</sup>	7.891	228 ± 0	Ch <sup>S</sup>	2.04 <sup>+2.23</sup> <sub>-2.43</sub>	3.24 <sup>+0.90</sup> <sub>-1.20</sub>	6.3 ± 2.0	
(832) Karin	17 ± 2	0.230 <sup>+0.050</sup> <sub>-0.060</sub>	65 <sup>+215</sup> <sub>-65</sub>	[T15]	S <sup>4</sup>	18.3512	212 ± 3	S <sup>S;F</sup>	-3.86 <sup>+2.33</sup> <sub>-1.77</sub>	-4.52 <sup>+2.10</sup> <sub>-1.93</sub>	31.4 ± 14.9	Koronis
(834) Burnhamia	67 ± 7	0.074 <sup>+0.014</sup> <sub>-0.016</sub>	22 <sup>+30</sup> <sub>-20</sub>	[T11]	C <sup>3</sup>	13.8759 <sup>†</sup>	217 ± 3	C <sup>S</sup>	0.14 <sup>+2.13</sup> <sub>-2.57</sub>	0.18 <sup>+0.90</sup> <sub>-1.07</sub>	11.7 ± 4.5	
(852) Wladilena	26.57 ± 0.25	0.205 <sup>+0.023</sup> <sub>-0.023</sub>	53 <sup>+26</sup> <sub>-23</sub>	[T9]	—	4.6133	225 ± 1	C <sup>F;A</sup>	-0.26 <sup>+2.07</sup> <sub>-2.50</sub>	0.08 <sup>+0.93</sup> <sub>-1.03</sub>	8.7 ± 2.3	Phocaea
(857) Glasenappia	12.2 ± 0.5	0.297 <sup>+0.022</sup> <sub>-0.024</sub>	45 <sup>+42</sup> <sub>-50</sub>	[T9][T13]	MU <sup>3</sup>	8.2076 <sup>†</sup>	244 ± 8	S <sup>S</sup>	-0.56 <sup>+2.07</sup> <sub>-2.77</sub>	-0.49 <sup>+1.27</sup> <sub>-1.53</sub>	10.2 ± 4.3	
(867) Kovacia	24.49 ± 0.95	0.075 <sup>+0.026</sup> <sub>-0.026</sub>	17 <sup>+17</sup> <sub>-17</sub>	[T9]	—	8.6781 <sup>†</sup>	198 ± 3	C <sup>F;A</sup>	0.14 <sup>+2.73</sup> <sub>-2.47</sub>	0.31 <sup>+0.83</sup> <sub>-0.83</sub>	8.5 ± 3.3	Hygiea
(873) Mechthild	31.8 ± 0.5	0.053 <sup>+0.026</sup> <sub>-0.026</sub>	46 <sup>+53</sup> <sub>-46</sub>	[T9]	—	11.0064 <sup>†</sup>	234 ± 1	C <sup>A</sup>	-0.76 <sup>+2.10</sup> <sub>-2.53</sub>	-1.19 <sup>+1.33</sup> <sub>-1.63</sub>	13.7 ± 5.1	
(874) Rotraut	51.7 ± 0.7	0.066 <sup>+0.026</sup> <sub>-0.026</sub>	49 <sup>+10</sup> <sub>-14</sub>	[T9]	—	14.3006 <sup>†</sup>	210 ± 2	C <sup>A</sup>	-0.02 <sup>+2.10</sup> <sub>-2.47</sub>	1.31 <sup>+0.37</sup> <sub>-0.63</sub>	14.5 ± 2.9	
(883) Matterania	7.60 ± 0.81	0.304 <sup>+0.034</sup> <sub>-0.038</sub>	36 <sup>+37</sup> <sub>-24</sub>	[T10]	S <sup>13</sup>	5.64	232 ± 6	S <sup>S;F</sup>	-0.02 <sup>+2.07</sup> <sub>-2.60</sub>	-0.26 <sup>+1.13</sup> <sub>-1.47</sub>	8.6 ± 3.2	Baptistina/Matterania
(890) Waltraut	29.2 ± 1.1	0.125 <sup>+0.032</sup> <sub>-0.032</sub>	94 <sup>+26</sup> <sub>-34</sub>	[T9]	CTGU <sup>4b</sup>	12.5831 <sup>†</sup>	211 ± 3	K <sup>F;C</sup>	-1.22 <sup>+1.90</sup> <sub>-2.70</sub>	-1.42 <sup>+1.13</sup> <sub>-1.43</sub>	18.8 ± 4.1	Eos
(900) Rosalinde	20.47 ± 0.65	0.099 <sup>+0.024</sup> <sub>-0.024</sub>	7 <sup>+7</sup> <sub>-7</sub>	[T9]	—	16.6868 <sup>†</sup>	221 ± 3	B <sup>*A</sup>	3.71 <sup>+1.87</sup> <sub>-2.33</sub>	4.01 <sup>+1.27</sup> <sub>-1.63</sub>	7.0 ± 2.9	
(906) Repsolda	71.08 ± 6.05	0.070 <sup>+0.007</sup> <sub>-0.007</sub>	47 <sup>+115</sup> <sub>-28</sub>	[T10]	—	15.368	225 ± 9	C <sup>A</sup>	-2.32 <sup>+2.27</sup> <sub>-2.53</sub>	-2.96 <sup>+1.77</sup> <sub>-1.73</sub>	22.1 ± 8.8	
(915) Cosette	12.35 ± 0.35	0.237 <sup>+0.031</sup> <sub>-0.031</sub>	36 <sup>+38</sup> <sub>-36</sub>	[T9]	S <sup>1</sup>	4.4697 <sup>†</sup>	225 ± 7	S <sup>S;F</sup>	0.31 <sup>+1.60</sup> <sub>-1.37</sub>	-0.52 <sup>+1.20</sup> <sub>-1.50</sub>	7.3 ± 3.1	Flora
(918) Itha	21.59 ± 0.37	0.222 <sup>+0.009</sup> <sub>-0.017</sub>	37 <sup>+10</sup> <sub>-10</sub>	[T10]	S <sup>1</sup>	3.4739 <sup>†</sup>	203 ± 7	S <sup>S</sup>	1.21 <sup>+1.20</sup> <sub>-1.00</sub>	1.24 <sup>+0.53</sup> <sub>-0.53</sub>	6.6 ± 1.4	Itha
(934) Thuringia	52.3 ± 1.0	0.061 <sup>+0.027</sup> <sub>-0.027</sub>	5 <sup>+5</sup> <sub>-5</sub>	[T9]	Ch <sup>2</sup>	8.1653 <sup>†</sup>	207 ± 3	Ch <sup>S</sup>	1.98 <sup>+2.20</sup> <sub>-2.50</sub>	4.68 <sup>+0.60</sup> <sub>-0.73</sub>	4.6 ± 1.7	
(956) Elisa	10.6 ± 0.8	0.228 <sup>+0.020</sup> <sub>-0.024</sub>	100 <sup>+50</sup> <sub>-70</sub>	[T6]	V <sup>3</sup>	16.494	270 ± 10	V <sup>S</sup>	-0.59 <sup>+1.53</sup> <sub>-1.20</sub>	-1.19 <sup>+1.40</sup> <sub>-1.60</sub>	19.8 ± 6.4	Flora
(958) Asplinda	46.05 ± 0.85	0.054 <sup>+0.019</sup> <sub>-0.019</sub>	1 <sup>+3</sup> <sub>-1</sub>	[T9]	—	25.305	200 ± 2	B <sup>*A</sup>	1.91 <sup>+2.17</sup> <sub>-2.53</sub>	4.84 <sup>+0.00</sup> <sub>-0.00</sub>	5.3 ± 2.3	
(972) Cohnia	73.11 ± 0.79	0.055 <sup>+0.002</sup> <sub>-0.003</sub>	19 <sup>+38</sup> <sub>-13</sub>	[T10]	C <sup>3</sup>	18.472	206 ± 3	C <sup>S;A</sup>	-0.42 <sup>+2.17</sup> <sub>-2.57</sub>	-0.69 <sup>+1.20</sup> <sub>-1.40</sub>	14.9 ± 5.9	
(977) Philippa	76.9 ± 6.3	0.040 <sup>+0.004</sup> <sub>-0.004</sub>	27 <sup>+84</sup> <sub>-21</sub>	[T10]	C <sup>4b</sup>	15.405	211 ± 3	C <sup>C;A</sup>	-2.16 <sup>+2.13</sup> <sub>-2.50</sub>	-2.16 <sup>+2.13</sup> <sub>-2.50</sub>	18.4 ± 8.1	
(984) Gretia	33.9 ± 0.9	0.223 <sup>+0.017</sup> <sub>-0.019</sub>	21 <sup>+16</sup> <sub>-15</sub>	[T9][T13]	Sr <sup>2</sup>	5.7780 <sup>†</sup>	202 ± 3	S <sup>S</sup>	1.41 <sup>+1.50</sup> <sub>-1.33</sub>	1.01 <sup>+0.57</sup> <sub>-0.63</sub>	6.6 ± 2.3	
(987) Wallia	43.1 ± 1.9	0.161 <sup>+0.009</sup> <sub>-0.012</sub>	46 <sup>+64</sup> <sub>-46</sub>	[T10]	—	10.0813	211 ± 13	S <sup>A</sup>	-1.22 <sup>+1.83</sup> <sub>-1.50</sub>	-2.19 <sup>+1.60</sup> <sub>-1.67</sub>	14.0 ± 6.2	
(998) Bodea	29.9 ± 0.7	0.052 <sup>+0.018</sup> <sub>-0.018</sub>	20 <sup>+16</sup> <sub>-8</sub>	[T9][T10]	—	8.5741 <sup>†</sup>	198 ± 3	C <sup>A</sup>	-1.76 <sup>+3.73</sup> <sub>-2.27</sub>	0.28 <sup>+1.87</sup> <sub>-4.37</sub>	8.6 ± 2.5	
(1013) Tombecka	33.73 ± 0.75	0.132 <sup>+0.023</sup> <sub>-0.023</sub>	52 <sup>+18</sup> <sub>-12</sub>	[T9]	XSC <sup>3</sup>	6.0502 <sup>†</sup>	209 ± 3	C <sup>F;C;A</sup>	-0.36 <sup>+2.03</sup> <sub>-2.53</sub>	0.38 <sup>+0.77</sup> <sub>-0.80</sub>	10.5 ± 2.2	Mitidika

Table 4 — continued

Object	$D_{eff}$	$p_V$	$\Gamma^a$	Source	Tax/Color	$P_{rot}$	$T_{surf}$ (K)	Model Comp.	$d_{g\phi}^{G\&B}$	$d_{g\phi}^{Sak}$	$l_s$ (mm)	Family
(1017) Jacqueline	$37.8 \pm 1.3$	$0.046^{+0.028}_{-0.028}$	$38^{+31}_{-38}$	[T9]	—	$7.8715^\dagger$	$223 \pm 2$	$C^A$	$-0.02^{+2.03}_{-2.57}$	$-0.06^{+0.97}_{-1.07}$	$9.2 \pm 3.7$	
(1018) Arnolda	$16.3 \pm 1.7$	$0.260^{+0.029}_{-0.037}$	$43^{+47}_{-43}$	[T10]	$X^{12}$	14.617	$221 \pm 10$	$M^{S;A}$	$-0.82^{+2.13}_{-2.60}$	$-1.19^{+1.30}_{-1.57}$	$15.2 \pm 5.6$	
(1036) Ganymed	$36 \pm 1$	$0.230^{+0.100}_{-0.100}$	$47^{+30}_{-20}$	[T13][T15][T16]	$S^4$	$10.3128^\dagger$	$204 \pm 10$	$S^S$	$-0.69^{+2.07}_{-2.57}$	$-0.76^{+1.17}_{-1.47}$	$13.8 \pm 3.9$	
(1047) Geisha	$10.5 \pm 0.4$	$0.283^{+0.015}_{-0.024}$	$35^{+58}_{-14}$	[T10]	$S^{4b}$	25.62	$225 \pm 1$	$S^{C;F}$	$-0.56^{+1.80}_{-1.43}$	$-1.49^{+1.47}_{-1.67}$	$22.5 \pm 7.9$	Flora
(1051) Merope	$53.5 \pm 1.8$	$0.066^{+0.004}_{-0.006}$	$48^{+81}_{-25}$	[T10]	$C^3$	27.2	$210 \pm 2$	$C^{F;A}$	$-2.26^{+2.13}_{-2.50}$	$-2.26^{+2.13}_{-2.50}$	$27.2 \pm 10.1$	Alauda
(1056) Azalea	$11.5 \pm 0.3$	$0.272^{+0.029}_{-0.004}$	$4^{+4}_{-4}$	[T9]	$S^2$	15.0276	$230 \pm 4$	$S^{F;A}$	$1.94^{+2.20}_{-2.27}$	—	$4.4 \pm 1.8$	Flora
(1076) Viola	$22.2 \pm 1.5$	$0.054^{+0.020}_{-0.005}$	$24^{+44}_{-24}$	[T10]	$C^2$	7.336	$235 \pm 4$	$C^S$	$-0.09^{+2.13}_{-2.57}$	$-0.42^{+1.20}_{-1.47}$	$8.8 \pm 4.0$	
(1077) Campanula	$10.1 \pm 0.8$	$0.230^{+0.022}_{-0.024}$	$56^{+40}_{-34}$	[T10]	$S^{13}$	$3.8509^\dagger$	$209 \pm 3$	$S^S$	$-1.29^{+2.07}_{-2.63}$	$-1.39^{+1.33}_{-1.60}$	$8.8 \pm 2.9$	
(1083) Salvia	$11.2 \pm 1.1$	$0.209^{+0.024}_{-0.029}$	$54^{+17}_{-30}$	[T10]	—	4.23	$240 \pm 8$	$S^A$	$1.01^{+1.27}_{-1.03}$	$1.11^{+0.70}_{-0.77}$	$7.4 \pm 2.0$	
(1087) Arabis	$34.4 \pm 0.5$	$0.174^{+0.023}_{-0.023}$	$1^{+1}_{-1}$	[T9]	—	5.795	$205 \pm 3$	$K^{F;A}$	$0.88^{+2.23}_{-2.50}$	—	$1.5 \pm 0.5$	Eos
(1095) Tulipa	$31.1 \pm 1.4$	$0.143^{+0.008}_{-0.010}$	$23^{+13}_{-13}$	[T10]	—	$2.7872^\dagger$	$211 \pm 3$	$K^{F;A}$	$-3.62^{+0.23}_{-0.07}$	$1.41^{+0.43}_{-0.60}$	$4.5 \pm 1.3$	Eos
(1102) Pepita	$35.5 \pm 0.5$	$0.246^{+0.023}_{-0.023}$	$9^{+11}_{-9}$	[T9]	$S^2$	$5.1053^\dagger$	$204 \pm 3$	$S^S$	$2.04^{+1.60}_{-2.33}$	—	$4.3 \pm 1.9$	
(1109) Tata	$64.1 \pm 2.6$	$0.049^{+0.003}_{-0.002}$	$10^{+46}_{-10}$	[T10]	$FC^{4b}$	8.277	$229 \pm 4$	$C^{F;C}$	$-0.06^{+2.17}_{-2.57}$	$-0.46^{+1.20}_{-1.53}$	$9.0 \pm 4.3$	Hygeia
(1119) Euboea	$30.2 \pm 0.55$	$0.054^{+0.022}_{-0.022}$	$9^{+6}_{-6}$	[T9]	—	$11.3981^\dagger$	$241 \pm 2$	$B^*A$	$2.24^{+2.20}_{-2.43}$	$4.91^{+1.17}_{-1.57}$	$6.3 \pm 2.0$	
(1123) Shapleya	$11.97 \pm 0.55$	$0.304^{+0.019}_{-0.027}$	$14^{+33}_{-14}$	[T10]	$S^3$	52.92	$230 \pm 3$	$S^{S;F}$	$1.14^{+1.67}_{-1.40}$	$0.34^{+0.97}_{-1.17}$	$20.5 \pm 9.6$	Flora
(1125) China	$26.9 \pm 1.1$	$0.060^{+0.004}_{-0.004}$	$34^{+8}_{-7}$	[T10]	—	5.367	$201 \pm 4$	$B^*A$	$0.74^{+2.03}_{-2.57}$	$1.54^{+0.77}_{-1.00}$	$9.0 \pm 1.7$	
(1127) Mimi	$46.9 \pm 0.8$	$0.045^{+0.025}_{-0.025}$	$8^{+2}_{-2}$	[T9]	$X^3$	$12.7455^\dagger$	$213 \pm 4$	$P^{S;A}$	$1.94^{+2.23}_{-2.47}$	$5.51^{+1.07}_{-2.77}$	$6.9 \pm 1.4$	
(1130) Skuld	$9.75 \pm 0.25$	$0.301^{+0.023}_{-0.023}$	$3^{+3}_{-3}$	[T9]	—	$4.8076^\dagger$	$242 \pm 4$	$S^A$	$2.08^{+2.20}_{-2.27}$	—	$2.1 \pm 0.9$	
(1136) Mercedes	$24.7 \pm 1.8$	$0.123^{+0.010}_{-0.012}$	$54^{+81}_{-34}$	[T10]	—	24.64	$226 \pm 12$	$S^A$	$-1.46^{+1.90}_{-1.50}$	$-2.36^{+1.67}_{-1.70}$	$25.3 \pm 9.7$	
(1140) Crimea	$29.6 \pm 0.9$	$0.259^{+0.022}_{-0.024}$	$23^{+15}_{-23}$	[T9][T13]	$S^2$	$9.7869^\dagger$	$211 \pm 2$	$S^S$	$0.74^{+2.13}_{-2.50}$	$1.14^{+0.60}_{-0.77}$	$8.0 \pm 3.1$	
(1142) Aetolia	$23.9 \pm 1.3$	$0.260^{+0.018}_{-0.022}$	$8.0^{+29.7}_{-8.0}$	[T10]	$S^{13}$	10.73	$216 \pm 2$	$S^S$	$1.18^{+1.37}_{-1.47}$	$0.38^{+0.90}_{-1.07}$	$8.8 \pm 4.2$	
(1152) Pawona	$17.5 \pm 0.9$	$0.203^{+0.012}_{-0.017}$	$26^{+35}_{-14}$	[T10]	$S^2$	3.4154	$233 \pm 0$	$S^S$	$0.88^{+1.57}_{-1.33}$	$0.14^{+1.03}_{-1.27}$	$6.2 \pm 2.2$	
(1162) Larissa	$41.1 \pm 2.3$	$0.152^{+0.011}_{-0.014}$	$19^{+14}_{-19}$	[T10]	$X^{11}$	6.516	$201 \pm 1$	$P^{S;A}$	$1.58^{+1.50}_{-1.20}$	$1.01^{+1.23}_{-1.53}$	$7.6 \pm 3.0$	
(1173) Anchises	$136 \pm 18$	$0.033^{+0.003}_{-0.002}$	$50^{+50}_{-25}$	[T6]	$P^{4b}$	11.6095	$171 \pm 10$	$P^{C;A}$	$-2.29^{+1.83}_{-1.47}$	$-2.79^{+1.87}_{-1.77}$	$21.7 \pm 7.1$	
(1188) Gothlandia	$13.20 \pm 0.05$	$0.237^{+0.020}_{-0.021}$	$45^{+25}_{-25}$	[T9][T13]	$S^2$	$3.4918^\dagger$	$222 \pm 7$	$S^{S;F}$	$-0.02^{+2.13}_{-2.57}$	$0.21^{+0.93}_{-1.10}$	$7.0 \pm 2.1$	Flora
(1210) Morosovia	$34.7 \pm 1.0$	$0.153^{+0.027}_{-0.027}$	$65^{+25}_{-35}$	[T9]	$S^9$	$15.2609^\dagger$	$219 \pm 4$	$K^{S;F}$	$-0.49^{+2.00}_{-2.57}$	$-0.29^{+0.97}_{-1.17}$	$16.5 \pm 4.5$	Eos
(1224) Fantasia	$13.65 \pm 0.22$	$0.252^{+0.013}_{-0.022}$	$58^{+16}_{-12}$	[T10]	$S^{4b}$	4.995	$222 \pm 4$	$S^S$	$0.34^{+0.97}_{-0.87}$	$0.71^{+0.73}_{-0.77}$	$9.7 \pm 1.9$	
(1241) Dysona	$76.78 \pm 2.25$	$0.043^{+0.023}_{-0.023}$	$23^{+22}_{-23}$	[T9]	$PDC^{4b}$	$8.6074^\dagger$	$205 \pm 3$	$C^{C;A}$	$0.18^{+2.17}_{-2.47}$	$0.51^{+0.73}_{-0.83}$	$8.2 \pm 3.4$	
(1258) Sicilia	$44.0 \pm 2.6$	$0.060^{+0.004}_{-0.004}$	$61^{+76}_{-31}$	[T10]	—	13.5	$209 \pm 0$	$C^A$	$-2.26^{+2.10}_{-2.50}$	$-2.29^{+2.13}_{-2.47}$	$19.9 \pm 6.9$	
(1276) Uccia	$35.97 \pm 0.85$	$0.068^{+0.032}_{-0.032}$	$63^{+17}_{-18}$	[T9]	—	$4.9075^\dagger$	$206 \pm 3$	$C^{F;A}$	$-0.62^{+2.03}_{-2.53}$	$0.08^{+0.80}_{-0.83}$	$10.0 \pm 2.1$	Alauda
(1281) Jeanne	$24.38 \pm 0.94$	$0.079^{+0.004}_{-0.004}$	$90^{+44}_{-25}$	[T10]	$X^3$	15.2	$242 \pm 5$	$P^{S;A}$	$-1.46^{+1.17}_{-1.07}$	$-1.82^{+1.43}_{-1.57}$	$25.4 \pm 5.8$	
(1288) Santa	$30.7 \pm 1.3$	$0.060^{+0.004}_{-0.003}$	$15^{+23}_{-5}$	[T10]	—	8.28	$220 \pm 3$	$C^A$	$0.58^{+2.13}_{-2.50}$	$0.74^{+0.63}_{-0.63}$	$8.3 \pm 2.8$	
(1291) Phryne	$26.7 \pm 1.3$	$0.168^{+0.020}_{-0.007}$	$20^{+18}_{-20}$	[T9][T13]	$S^{13}$	$5.5841^\dagger$	$206 \pm 4$	$K^{S;F}$	$0.51^{+2.10}_{-2.53}$	$0.78^{+0.80}_{-0.60}$	$6.5 \pm 2.3$	Eos
(1296) Andree	$23.3 \pm 2.1$	$0.074^{+0.007}_{-0.008}$	$40^{+74}_{-12}$	[T10]	—	$5.1837^\dagger$	$238 \pm 12$	$C^A$	$-1.52^{+2.10}_{-2.53}$	$-1.56^{+2.13}_{-2.50}$	$10.9 \pm 3.8$	
(1299) Mertona	$15.2 \pm 1.2$	$0.194^{+0.017}_{-0.024}$	$15^{+29}_{-8}$	[T10]	$S^{13}$	4.977	$207 \pm 7$	$S^S$	$0.81^{+1.63}_{-1.37}$	$0.08^{+0.93}_{-1.17}$	$7.0 \pm 2.7$	
(1301) Yvonne	$21.2 \pm 0.9$	$0.111^{+0.025}_{-0.025}$	$1^{+1}_{-1}$	[T9]	$Cb^3$	$7.3197^\dagger$	$209 \pm 4$	$Cb^S$	$2.04^{+2.20}_{-2.50}$	—	$1.9 \pm 0.7$	
(1310) Villigera	$14.6 \pm 1.3$	$0.209^{+0.021}_{-0.026}$	$40^{+23}_{-30}$	[T10]	$S^{13}$	7.83	$224 \pm 26$	$S^S$	$0.14^{+2.17}_{-2.57}$	$0.11^{+1.07}_{-1.37}$	$9.3 \pm 3.3$	
(1316) Kasan	$6.54 \pm 0.50$	$0.277^{+0.033}_{-0.041}$	$10^{+34}_{-10}$	[T10]	$S^2$	5.82	$221 \pm 5$	$S^S$	$0.88^{+1.70}_{-1.33}$	$0.11^{+1.00}_{-1.27}$	$6.9 \pm 3.3$	
(1325) Inanda	$11.4 \pm 1.6$	$0.189^{+0.027}_{-0.030}$	$76^{+50}_{-36}$	[T10]	—	20.52	$214 \pm 3$	$S^A$	$-1.42^{+2.10}_{-1.20}$	$-2.02^{+1.47}_{-1.60}$	$23.8 \pm 6.9$	
(1335) Demoulina	$7.65 \pm 0.78$	$0.241^{+0.027}_{-0.031}$	$126^{+94}_{-98}$	[T10]	$S^3$	74.86	$227 \pm 3$	$S^{S;F}$	$-2.46^{+1.87}_{-1.37}$	$-3.09^{+1.67}_{-1.67}$	$50.4 \pm 18.3$	Koronis



Table 4 — continued

Object	$D_{eff}$	$p_V$	$\Gamma^a$	Source	Tax/Color	$P_{rot}$	$T_{surf}$ (K)	Model Comp.	$d_{g\phi}^{G\&B}$	$d_{g\phi}^{Sak}$	$l_s$ (mm)	Family
(1339) Desagneauxa	$25.4 \pm 1.1$	$0.122^{+0.025}_{-0.025}$	$63^{+17}_{-23}$	[T9]	S <sup>4b</sup>	9.3751	$207 \pm 9$	K <sup>F;C</sup>	$-0.56^{+2.03}_{-2.60}$	$0.08^{+0.80}_{-0.87}$	$13.4 \pm 3.0$	Eos
(1352) Wawel	$21.7 \pm 1.68$	$0.139^{+0.012}_{-0.012}$	$97^{+28}_{-71}$	[T10]	X <sup>2</sup>	16.97	$209 \pm 2$	M <sup>S</sup>	$-1.32^{+1.97}_{-2.60}$	$-1.49^{+1.10}_{-1.37}$	$20.0 \pm 5.5$	
(1360) Tarka	$29.4 \pm 0.4$	$0.059^{+0.030}_{-0.030}$	$40^{+5}_{-5}$	[T9]	Cb <sup>2</sup>	$8.8661^{\dagger}$	$217 \pm 3$	Cb <sup>S</sup>	$0.94^{+2.03}_{-2.57}$	$1.98^{+0.67}_{-0.80}$	$11.9 \pm 2.1$	
(1375) Alfreda	$14.46 \pm 0.55$	$0.222^{+0.012}_{-0.022}$	$30^{+48}_{-18}$	[T10]	S <sup>1</sup>	19.14	$224 \pm 2$	S <sup>S</sup>	$-0.09^{+1.70}_{-1.40}$	$-1.02^{+1.37}_{-1.63}$	$17.1 \pm 6.5$	
(1386) Storeria	$10.06 \pm 0.65$	$0.069^{+0.024}_{-0.024}$	$52^{+12}_{-51}$	[T9]	Ch <sup>2</sup>	$8.6780^{\dagger}$	$217 \pm 3$	Ch <sup>S;F</sup>	$0.51^{+1.97}_{-2.60}$	$0.54^{+0.97}_{-1.23}$	$9.4 \pm 3.3$	Chaldaea
(1388) Aphrodite	$21.1 \pm 0.5$	$0.182^{+0.025}_{-0.032}$	$69^{+21}_{-58}$	[T9]	—	11.9439	$206 \pm 2$	K <sup>F;A</sup>	$-0.79^{+2.00}_{-1.80}$	$-0.46^{+0.97}_{-1.07}$	$16.1 \pm 3.5$	Eos
(1401) Lavonne	$9.3 \pm 0.4$	$0.304^{+0.032}_{-0.032}$	$52^{+52}_{-52}$	[T9]	S <sup>4b</sup>	$3.9326^{\dagger}$	$226 \pm 4$	S <sup>C;A</sup>	$-0.76^{+1.80}_{-1.43}$	$-1.69^{+1.50}_{-1.63}$	$8.4 \pm 3.6$	
(1412) Lagrula	$9.13 \pm 0.50$	$0.267^{+0.019}_{-0.027}$	$37^{+23}_{-9}$	[T10]	S <sup>13</sup>	5.9176	$234 \pm 2$	S <sup>S</sup>	$0.34^{+2.13}_{-2.50}$	$0.81^{+0.80}_{-0.90}$	$9.0 \pm 2.2$	Flora
(1419) Danzig	$14.22 \pm 0.55$	$0.239^{+0.025}_{-0.025}$	$54^{+31}_{-42}$	[T9]	—	$8.1196^{\dagger}$	$253 \pm 7$	S <sup>F;A</sup>	$0.24^{+2.10}_{-2.50}$	$0.28^{+1.03}_{-1.23}$	$10.3 \pm 3.6$	Flora
(1424) Sundmania	$61.6 \pm 2.9$	$0.047^{+0.026}_{-0.026}$	$14^{+17}_{-14}$	[T9]	S <sup>2</sup>	$94.5371^{\dagger}$	$221 \pm 2$	P <sup>S</sup>	$2.11^{+1.50}_{-1.27}$	$1.44^{+1.20}_{-1.50}$	$26.6 \pm 11.4$	
(1432) Ethiopia	$7.15 \pm 0.67$	$0.535^{+0.058}_{-0.070}$	$71^{+180}_{-65}$	[T13]	—	9.8458	$218 \pm 8$	E <sup>A</sup>	$-3.59^{+2.40}_{-2.60}$	$-4.22^{+1.93}_{-1.83}$	$23.0 \pm 9.6$	
(1436) Salonta	$55.9 \pm 0.9$	$0.047^{+0.025}_{-0.025}$	$2^{+2}_{-2}$	[T9]	X <sup>3</sup>	$8.8699^{\dagger}$	$209 \pm 3$	P <sup>S;A</sup>	$1.94^{+2.23}_{-2.43}$	$4.78^{+0.57}_{-0.93}$	$4.6 \pm 2.0$	
(1443) Ruppina	$16.68 \pm 1.03$	$0.259^{+0.018}_{-0.020}$	$40^{+18}_{-14}$	[T10]	S <sup>13</sup>	5.88	$205 \pm 1$	S <sup>S;F</sup>	$-0.06^{+2.07}_{-2.53}$	$0.54^{+0.70}_{-0.80}$	$9.2 \pm 2.2$	Koronis
(1452) Hunnia	$21.2 \pm 2.0$	$0.065^{+0.007}_{-0.008}$	$24^{+34}_{-20}$	[T10]	—	17.2	$216 \pm 12$	C <sup>F;A</sup>	$-0.09^{+2.10}_{-2.57}$	$-0.29^{+1.10}_{-1.20}$	$13.3 \pm 5.6$	Meliboea
(1472) Muonio	$9.1 \pm 1.3$	$0.230^{+0.090}_{-0.060}$	$25^{+65}_{-25}$	[T15]	—	$8.7054^{\dagger}$	$216 \pm 6$	S <sup>A</sup>	$-0.76^{+1.83}_{-1.57}$	$-1.82^{+1.53}_{-1.70}$	$12.0 \pm 5.6$	
(1495) Helsinki	$12.8 \pm 0.3$	$0.285^{+0.040}_{-0.040}$	$19^{+13}_{-13}$	[T9][T13]	—	$5.3312^{\dagger}$	$229 \pm 5$	S <sup>F;A</sup>	$2.21^{+1.33}_{-1.80}$	$1.84^{+0.10}_{-0.40}$	$5.5 \pm 1.9$	Eunomia
(1501) Baade	$11.48 \pm 0.88$	$0.240^{+0.020}_{-0.022}$	$34^{+48}_{-34}$	[T10]	V <sup>12</sup>	15.132	$205 \pm 5$	V <sup>S</sup>	$-1.09^{+2.10}_{-2.63}$	$-1.16^{+1.43}_{-1.70}$	$12.2 \pm 5.7$	
(1508) Kemi	$14.75 \pm 0.15$	$0.146^{+0.027}_{-0.027}$	$16^{+8}_{-6}$	[T9]	B <sup>2</sup>	$9.1918^{\dagger}$	$191 \pm 6$	B <sup>S</sup>	$1.24^{+2.17}_{-2.43}$	$2.11^{+1.00}_{-1.13}$	$8.6 \pm 2.2$	
(1517) Beograd	$34.21 \pm 2.25$	$0.061^{+0.004}_{-0.004}$	$19^{+55}_{-5}$	[T10]	X <sup>2</sup>	6.943	$231 \pm 3$	P <sup>S;A</sup>	$-0.19^{+1.97}_{-1.57}$	$-0.96^{+1.80}_{-1.73}$	$12.6 \pm 4.7$	
(1536) Pielinen	$8.53 \pm 0.19$	$0.225^{+0.013}_{-0.019}$	$74^{+23}_{-35}$	[T10]	S <sup>13</sup>	66.22	$227 \pm 5$	S <sup>S</sup>	$-0.12^{+1.10}_{-1.03}$	$-0.26^{+1.00}_{-1.23}$	$36.3 \pm 9.1$	
(1542) Schalen	$46.48 \pm 1.54$	$0.053^{+0.003}_{-0.004}$	$10^{+15}_{-10}$	[T10]	D <sup>2</sup>	7.516	$208 \pm 1$	P <sup>S;A</sup>	$2.24^{+1.47}_{-1.27}$	$1.58^{+1.13}_{-1.37}$	$7.0 \pm 3.1$	
(1545) Thernoe	$17.29 \pm 0.86$	$0.124^{+0.027}_{-0.026}$	$27^{+27}_{-24}$	[T9]	K <sup>2</sup>	17.203	$209 \pm 4$	K <sup>S</sup>	$0.01^{+2.20}_{-2.47}$	$0.04^{+0.87}_{-0.97}$	$12.6 \pm 5.2$	
(1565) Lemaitre	$8.44 \pm 0.96$	$0.204^{+0.026}_{-0.033}$	$24^{+53}_{-24}$	[T10]	S <sup>2</sup>	11.403	$227 \pm 14$	S <sup>S</sup>	$-0.09^{+1.70}_{-1.43}$	$-1.06^{+1.40}_{-1.67}$	$11.6 \pm 5.4$	
(1567) Alikoski	$71.15 \pm 4.24$	$0.053^{+0.004}_{-0.005}$	$7.2^{+73.4}_{-7.2}$	[T10]	C <sup>2</sup>	16.405	$228 \pm 3$	C <sup>S</sup>	$-1.49^{+2.13}_{-2.57}$	$-1.49^{+2.13}_{-2.57}$	$15.8 \pm 7.5$	Ursula
(1568) Aisleen	$11.80 \pm 0.04$	$0.268^{+0.030}_{-0.030}$	$51^{+30}_{-15}$	[T9][T13]	S <sup>3</sup>	6.68	$212 \pm 8$	S <sup>S;F</sup>	$-0.19^{+1.37}_{-1.13}$	$-0.62^{+1.17}_{-1.43}$	$11.6 \pm 2.9$	Phocaea
(1573) Vaisala	$10.31 \pm 0.64$	$0.213^{+0.022}_{-0.033}$	$132^{+123}_{-76}$	[T10]	S <sup>3</sup>	252	$223 \pm 8$	S <sup>S;F</sup>	$-3.16^{+1.80}_{-1.43}$	$-3.72^{+1.80}_{-1.73}$	$112.7 \pm 38.2$	Phocaea
(1577) Reiss	$5.72 \pm 0.57$	$0.468^{+0.052}_{-0.066}$	$25^{+36}_{-20}$	[T10]	S <sup>1</sup>	4.505	$217 \pm 4$	S <sup>S;F</sup>	$0.41^{+1.60}_{-1.33}$	$-0.39^{+1.13}_{-1.43}$	$7.1 \pm 2.9$	Flora
(1580) Betulia	$5.39 \pm 0.54$	$0.070^{+0.010}_{-0.010}$	$189^{+40}_{-40}$	[T6][T16]	C <sup>4b</sup>	$6.1384^{\dagger}$	$331 \pm 10$	C <sup>C;A</sup>	$-0.76^{+1.83}_{-2.47}$	$-0.76^{+1.83}_{-2.47}$	$15.4 \pm 2.9$	
(1607) Mavis	$13.7 \pm 0.7$	$0.265^{+0.032}_{-0.032}$	$60^{+50}_{-45}$	[T9][T13]	V <sup>1</sup>	$6.1478^{\dagger}$	$204 \pm 4$	V <sup>S</sup>	$-1.79^{+2.07}_{-2.53}$	$-2.09^{+1.50}_{-1.63}$	$11.9 \pm 4.4$	
(1618) Dawn	$16.30 \pm 0.57$	$0.186^{+0.020}_{-0.020}$	$5^{+5}_{-5}$	[T9]	S <sup>2</sup>	$43.2191^{\dagger}$	$214 \pm 4$	S <sup>S;F</sup>	$1.88^{+1.97}_{-2.30}$	—	$8.1 \pm 3.4$	Karin
(1620) Geographos	$2.46 \pm 0.03$	$0.344^{+0.060}_{-0.062}$	$340^{+140}_{-100}$	[T6]	S <sup>4</sup>	$5.2233^{\dagger}$	$332 \pm 10$	S <sup>S</sup>	$-2.96^{+1.97}_{-2.50}$	$-3.49^{+1.40}_{-1.60}$	$20.2 \pm 4.6$	
(1627) Ivar	$8.0 \pm 0.7$	$0.255^{+0.020}_{-0.014}$	$100^{+120}_{-40}$	[T15]	S <sup>2</sup>	$4.7952^{\dagger}$	$244 \pm 4$	S <sup>S</sup>	$-2.39^{+1.83}_{-1.43}$	$-2.99^{+1.77}_{-1.73}$	$14.4 \pm 4.7$	
(1628) Strobel	$53.7 \pm 1.2$	$0.060^{+0.003}_{-0.005}$	$47^{+12}_{-30}$	[T10]	X <sup>1</sup>	9.52	$219 \pm 3$	P <sup>S</sup>	$0.68^{+1.43}_{-0.92}$	$0.34^{+1.23}_{-1.47}$	$12.4 \pm 3.5$	
(1644) Rafita	$13.49 \pm 0.84$	$0.263^{+0.019}_{-0.031}$	$28^{+25}_{-14}$	[T10]	S <sup>12</sup>	6.8	$235 \pm 4$	S <sup>S</sup>	$1.34^{+1.37}_{-1.30}$	$0.84^{+0.80}_{-0.90}$	$8.4 \pm 2.7$	
(1651) Behrens	$10.09 \pm 0.46$	$0.242^{+0.015}_{-0.025}$	$59^{+29}_{-19}$	[T10]	S <sup>1</sup>	34.34	$250 \pm 9$	S <sup>S;F</sup>	$0.51^{+1.07}_{-1.10}$	$0.24^{+1.03}_{-1.23}$	$24.9 \pm 6.0$	Flora
(1655) Comas Sola	$35.09 \pm 1.30$	$0.059^{+0.003}_{-0.005}$	$40^{+37}_{-30}$	[T10]	B <sup>2</sup>	20.456	$215 \pm 7$	B <sup>S</sup>	$-0.36^{+2.13}_{-2.50}$	$-0.86^{+1.70}_{-1.67}$	$19.3 \pm 7.2$	
(1672) Gezelle	$25.0 \pm 0.9$	$0.064^{+0.024}_{-0.024}$	$10^{+10}_{-10}$	[T9]	—	$40.6825^{\dagger}$	$205 \pm 2$	B <sup>*A</sup>	$1.64^{+2.17}_{-2.40}$	$2.64^{+1.00}_{-1.20}$	$14.5 \pm 5.3$	
(1691) Oort	$36.19 \pm 1.66$	$0.054^{+0.025}_{-0.025}$	$32^{+17}_{-32}$	[T9]	B <sup>3</sup>	$10.2684^{\dagger}$	$197 \pm 3$	B <sup>S;F</sup>	$0.41^{+2.03}_{-2.57}$	$0.14^{+1.40}_{-1.57}$	$10.9 \pm 4.1$	Themis
(1701) Okavango	$20.07 \pm 1.17$	$0.241^{+0.027}_{-0.027}$	$35^{+35}_{-35}$	[T9]	—	$13.1918^{\dagger}$	$231 \pm 3$	S <sup>A</sup>	$0.51^{+1.60}_{-1.30}$	$-0.12^{+1.10}_{-1.40}$	$12.1 \pm 5.0$	
(1702) Kalahari	$34.16 \pm 1.23$	$0.065^{+0.003}_{-0.006}$	$28^{+40}_{-9}$	[T10]	L <sup>2</sup>	21.153	$217 \pm 6$	C <sup>S</sup>	$-0.46^{+2.10}_{-2.57}$	$-0.66^{+1.20}_{-1.47}$	$17.9 \pm 5.8$	



Table 4 — continued

Object	$D_{eff}$	$p_V$	$\Gamma^a$	Source	Tax/Color	$P_{rot}$	$T_{surf}$ (K)	Model Comp.	$d_{g\phi}^{G\&B}$	$d_{g\phi}^{Sak}$	$l_s$ (mm)	Family
(1704) Wachmann	$6.6 \pm 0.14$	$0.235^{+0.023}_{-0.023}$	$110^{+50}_{-50}$	[T9]	—	$3.3139^\dagger$	$240 \pm 7$	$S^A$	$-1.42^{+1.43}_{-1.13}$	$-1.92^{+1.43}_{-1.57}$	$10.2 \pm 2.7$	
(1723) Klemola	$32.7 \pm 0.9$	$0.150^{+0.020}_{-0.020}$	$34^{+15}_{-15}$	[T9][T10]	$S^{13}$	6.2561	$216 \pm 3$	$S^{S;F}$	$0.31^{+2.20}_{-2.37}$	$1.14^{+0.70}_{-0.73}$	$8.1 \pm 2.1$	Eos
(1734) Zhongolovich	$25.33 \pm 0.71$	$0.069^{+0.004}_{-0.004}$	$35^{+31}_{-10}$	[T10]	$Ch^2$	7.171	$210 \pm 9$	$C^{S;F}$	$-0.46^{+2.07}_{-2.53}$	$-0.36^{+1.03}_{-1.30}$	$10.7 \pm 3.0$	Dora
(1738) Oosterhoff	$7.97 \pm 0.22$	$0.261^{+0.065}_{-0.065}$	$60^{+49}_{-20}$	[T9]	$S^2$	$4.4490^\dagger$	$230 \pm 10$	$S^{S;F}$	$-0.72^{+1.53}_{-1.30}$	$-1.39^{+1.43}_{-1.63}$	$10.3 \pm 2.9$	Flora
(1741) Giclas	$13.17 \pm 0.56$	$0.266^{+0.093}_{-0.015}$	$33^{+20}_{-10}$	[T10][T17]	$S^{13}$	2.943	$207 \pm 8$	$S^{S;F}$	$0.04^{+2.07}_{-2.47}$	$0.51^{+0.80}_{-0.97}$	$6.3 \pm 1.6$	Koronis
(1742) Schaifers	$15.25 \pm 0.58$	$0.229^{+0.056}_{-0.029}$	$91^{+18}_{-21}$	[T9]	—	$8.5327^\dagger$	$202 \pm 5$	$S^{F;A}$	$-1.12^{+1.87}_{-2.70}$	$-1.36^{+1.03}_{-1.33}$	$16.1 \pm 3.1$	Koronis
(1759) Kienle	$7.73 \pm 1.17$	$0.184^{+0.056}_{-0.030}$	$52^{+88}_{-52}$	[T10]	$S^3$	29.25	$208 \pm 0$	$S^S$	$-2.02^{+2.00}_{-1.50}$	$-2.86^{+1.70}_{-1.70}$	$27.3 \pm 12.4$	
(1768) Appenzella	$18.91 \pm 0.59$	$0.058^{+0.004}_{-0.003}$	$31^{+18}_{-12}$	[T10]	$C^2$	5.1839	$223 \pm 2$	$B^{S;F}$	$0.98^{+2.00}_{-2.63}$	$0.81^{+1.33}_{-1.57}$	$8.4 \pm 2.2$	Hertha/Nysa-Polana
(1789) Dobrovolsky	$8.63 \pm 0.22$	$0.284^{+0.035}_{-0.035}$	$15^{+5}_{-9}$	[T9]	—	4.8111	$233 \pm 7$	$S^A$	$2.28^{+1.80}_{-2.30}$	—	$4.2 \pm 1.2$	
(1807) Slovakia	$9.83 \pm 1.19$	$0.229^{+0.030}_{-0.033}$	$195^{+243}_{-45}$	[T10]	$S^2$	308	$231 \pm 4$	$S^{S;F}$	$-4.72^{+1.57}_{-1.43}$	$-5.16^{+1.80}_{-1.77}$	$174.3 \pm 52.0$	Flora
(1820) Lohmann	$6.08 \pm 0.32$	$0.234^{+0.041}_{-0.041}$	$118^{+22}_{-8}$	[T9]	—	$14.0449^\dagger$	$226 \pm 9$	$S^A$	$-1.89^{+0.53}_{-0.63}$	$-1.96^{+0.87}_{-1.37}$	$23.4 \pm 4.2$	
(1837) Osita	$6.9 \pm 0.3$	$0.264^{+0.025}_{-0.025}$	$111^{+19}_{-21}$	[T9]	—	3.8188	$244 \pm 7$	$S^A$	$-0.96^{+0.73}_{-0.67}$	$-1.72^{+1.73}_{-1.70}$	$10.8 \pm 2.0$	
(1862) Apollo	$1.55 \pm 0.07$	$0.316^{+0.031}_{-0.042}$	$140^{+140}_{-100}$	[T18]	$Q^4$	$3.0654^\dagger$	$352 \pm 10$	$S^S$	$-1.26^{+2.17}_{-2.50}$	$-1.76^{+1.73}_{-1.70}$	$10.2 \pm 3.8$	
(1865) Cerberus	$1.2 \pm 0.1$	$0.281^{+0.036}_{-0.034}$	$300^{+2200}_{-0}$	[T15]	$S^2$	$6.8033^\dagger$	$250 \pm 15$	$S^S$	$-8.19^{+2.13*}_{-1.27}$	$-8.75^{+2.40*}_{-2.27}$	$48.3 \pm 13.1$	
(1896) Beer	$5.07 \pm 0.96$	$0.229^{+0.045}_{-0.045}$	$80^{+335}_{-80}$	[T10]	—	3.3278	$201 \pm 5$	$S^{F;A}$	$-5.19^{+2.57*}_{-1.87}$	$-5.76^{+2.37*}_{-2.03}$	$17.0 \pm 8.1$	Hertha/Nysa-Polana
(1902) Shaposhnikov	$79.02 \pm 3.22$	$0.045^{+0.023}_{-0.023}$	$15^{+15}_{-15}$	[T9]	$P^{4b}$	$20.9958^\dagger$	$177 \pm 2$	$P^{C;A}$	$1.18^{+1.57}_{-1.30}$	$0.48^{+1.30}_{-1.60}$	$13.9 \pm 5.8$	
(1906) Neaf	$7.73 \pm 0.41$	$0.246^{+0.014}_{-0.024}$	$70^{+19}_{-19}$	[T7]	$V^1$	11.01	$230 \pm 6$	$V^{S;F}$	$-0.06^{+0.97}_{-0.87}$	$0.21^{+0.87}_{-1.00}$	$15.8 \pm 3.1$	Vesta
(1930) Lucifer	$30.73 \pm 1.34$	$0.081^{+0.022}_{-0.022}$	$60^{+50}_{-25}$	[T9]	$Cgh^2$	13.0536	$210 \pm 3$	$C^S$	$-1.62^{+2.03}_{-2.60}$	$-1.66^{+2.07}_{-2.57}$	$17.9 \pm 5.3$	
(1936) Lugano	$24.03 \pm 0.27$	$0.083^{+0.005}_{-0.007}$	$115^{+66}_{-77}$	[T10]	$Ch^2$	19.651	$249 \pm 2$	$Ch^{S;F}$	$-1.62^{+2.13}_{-2.53}$	$-2.22^{+1.67}_{-1.67}$	$23.8 \pm 7.8$	Adeona
(1979) Sakharov	$4.69 \pm 0.77$	$0.282^{+0.048}_{-0.062}$	$58^{+269}_{-27}$	[T10]	—	7.5209	$223 \pm 3$	$V^{F;A}$	$-4.12^{+2.37}_{-1.80}$	$-4.76^{+2.20}_{-1.97}$	$23.4 \pm 9.9$	Vesta
(1980) Tezcatlipoca	$5.6 \pm 0.7$	$0.210^{+0.080}_{-0.080}$	$200^{+400}_{-190}$	[T15][T13]	$S^2$	$7.2523^\dagger$	$227 \pm 8$	$S^S$	$-5.29^{+2.63*}_{-2.83}$	$-5.92^{+2.40*}_{-2.17}$	$27.3 \pm 12.4$	
(1987) Kaplan	$25.70 \pm 0.69$	$0.122^{+0.026}_{-0.026}$	$27^{+16}_{-19}$	[T9]	—	$12.5964^\dagger$	$216 \pm 3$	$S^{F;A}$	$0.68^{+2.13}_{-2.47}$	$1.18^{+0.67}_{-0.63}$	$10.1 \pm 3.4$	Phocaea
(2005) Hencke	$8.99 \pm 0.95$	$0.315^{+0.037}_{-0.046}$	$40^{+48}_{-34}$	[T10]	—	10.186	$204 \pm 1$	$S^{F;A}$	$-0.72^{+1.57}_{-1.40}$	$-1.66^{+1.43}_{-1.63}$	$13.1 \pm 5.4$	Eunomia
(2072) Kosmodemyanskaya	$4.74 \pm 1.44$	$0.657^{+0.201}_{-0.207}$	$19^{+129}_{-19}$	[T10]	—	4.4	$204 \pm 1$	$E^A$	$-2.92^{+2.30}_{-2.57}$	$-3.62^{+1.77}_{-1.77}$	$12.5 \pm 5.6$	
(2106) Hugo	$16.1 \pm 1.5$	$0.091^{+0.009}_{-0.010}$	$22^{+36}_{-9}$	[T10]	$C^2$	6.9297	$209 \pm 0$	$C^S$	$-0.36^{+2.10}_{-2.53}$	$-0.49^{+1.07}_{-1.40}$	$9.5 \pm 3.3$	
(2110) Moore-Sitterly	$6.2 \pm 1.1$	$0.160^{+0.065}_{-0.035}$	$120^{+80}_{-75}$	[T17]	—	$3.3447^\dagger$	$253 \pm 10$	$S^{A;P}$	$-1.92^{+2.10}_{-2.47}$	$-2.39^{+1.60}_{-1.63}$	$10.6 \pm 3.5$	
(2111) Tselina	$24.05 \pm 2.19$	$0.195^{+0.020}_{-0.026}$	$47^{+36}_{-24}$	[T10]	$S^3$	6.563	$201 \pm 2$	$K^{S;F}$	$-1.22^{+2.03}_{-2.80}$	$-1.16^{+1.23}_{-1.53}$	$11.0 \pm 3.4$	Eos
(2123) Vltava	$16.05 \pm 0.68$	$0.179^{+0.011}_{-0.010}$	$56^{+37}_{-22}$	[T10]	$S^{13}$	34	$210 \pm 2$	$S^{S;F}$	$-0.52^{+1.37}_{-1.23}$	$-1.09^{+1.27}_{-1.53}$	$25.8 \pm 7.0$	Koronis
(2140) Kemerovo	$33.56 \pm 2.05$	$0.050^{+0.004}_{-0.005}$	$20^{+39}_{-14}$	[T10]	$X^1$	9.2	$217 \pm 1$	$P^S$	$0.21^{+1.87}_{-1.50}$	$-0.59^{+1.67}_{-1.70}$	$12.4 \pm 5.1$	
(2144) Marietta	$17.26 \pm 0.45$	$0.203^{+0.009}_{-0.010}$	$53^{+10}_{-8}$	[T10]	$S^{13}$	5.489	$203 \pm 4$	$S^{S;F}$	$-0.26^{+2.10}_{-2.53}$	$0.94^{+0.60}_{-0.57}$	$10.1 \pm 1.9$	Koronis
(2156) Kate	$8.04 \pm 0.45$	$0.294^{+0.021}_{-0.025}$	$56^{+23}_{-23}$	[T13]	$S^{13}$	5.6228	$215 \pm 1$	$S^S$	$-0.36^{+2.03}_{-2.53}$	$-0.06^{+0.93}_{-1.13}$	$10.1 \pm 2.5$	
(2177) Oliver	$19.52 \pm 0.50$	$0.085^{+0.005}_{-0.003}$	$42^{+10}_{-10}$	[T10]	—	6.1065	$197 \pm 1$	$C^A$	$-3.16^{+5.53}_{-0.83}$	$-3.32^{+5.60}_{-0.67}$	$9.4 \pm 1.8$	
(2203) van Rhijn	$22.31 \pm 1.08$	$0.087^{+0.005}_{-0.005}$	$55^{+55}_{-27}$	[T10]	—	30.55	$194 \pm 4$	$B^{F;A}$	$-1.69^{+2.23}_{-2.57}$	$-2.26^{+1.83}_{-1.67}$	$32.1 \pm 10.4$	Themis
(2204) Lyyli	$25.05 \pm 0.95$	$0.047^{+0.003}_{-0.004}$	$90^{+36}_{-50}$	[T10]	$X^3$	11.063	$237 \pm 20$	$P^{S;A}$	$-1.12^{+1.63}_{-1.23}$	$-1.59^{+1.67}_{-1.67}$	$19.4 \pm 5.5$	
(2214) Carol	$26.28 \pm 1.60$	$0.061^{+0.005}_{-0.005}$	$21^{+15}_{-9}$	[T10]	—	4.987	$220 \pm 8$	$C^A$	$-3.29^{+5.57}_{-0.73}$	$-2.19^{+4.63}_{-1.50}$	$6.2 \pm 1.8$	
(2239) Paracelsus	$37.53 \pm 2.48$	$0.054^{+0.004}_{-0.006}$	$18^{+7}_{-18}$	[T10]	—	6.101	$201 \pm 1$	$B^{*A}$	$1.51^{+2.17}_{-2.47}$	$2.91^{+0.93}_{-1.50}$	$6.3 \pm 1.9$	
(2268) Szmytowna	$15.18 \pm 1.46$	$0.190^{+0.020}_{-0.019}$	$30^{+32}_{-32}$	[T10]	$S^2$	11.26	$207 \pm 0$	$S^{S;F}$	$0.38^{+1.53}_{-1.27}$	$-0.29^{+1.03}_{-1.33}$	$10.5 \pm 4.4$	Koronis
(2275) Cuitlahuac	$7.29 \pm 0.19$	$0.342^{+0.017}_{-0.028}$	$13^{+24}_{-13}$	[T10]	—	6.2891	$227 \pm 12$	$S^A$	$1.64^{+1.43}_{-1.50}$	$0.88^{+0.77}_{-0.87}$	$6.2 \pm 2.9$	
(2297) Daghestan	$25.06 \pm 0.89$	$0.086^{+0.005}_{-0.004}$	$58^{+23}_{-18}$	[T10]	—	7.75	$217 \pm 1$	$B^{F;A}$	$-0.22^{+1.97}_{-2.47}$	$-0.72^{+1.37}_{-1.53}$	$13.9 \pm 3.1$	Themis
(2306) Bauschinger	$19.24 \pm 0.97$	$0.072^{+0.005}_{-0.005}$	$18^{+14}_{-10}$	[T10]	$X^2$	21.64	$222 \pm 1$	$P^{S;F;A}$	$2.24^{+1.37}_{-1.20}$	$1.78^{+1.10}_{-1.33}$	$14.2 \pm 4.5$	Padua

Table 4 — continued

Object	$D_{eff}$	$p_V$	$\Gamma^a$	Source	Tax/Color	$P_{rot}$	$T_{surf}$ (K)	Model Comp.	$d_{g\phi}^{G\&B}$	$d_{g\phi}^{Sak}$	$l_s$ (mm)	Family
(2332) Kalm	$36.52 \pm 2.55$	$0.060^{+0.005}_{-0.005}$	$77^{+15}_{-48}$	[T10]	B <sup>3</sup>	22.8	$209 \pm 2$	B <sup>S;F</sup>	$-0.59^{+1.97}_{-2.47}$	$-1.12^{+1.43}_{-1.53}$	$23.1 \pm 6.2$	Themis
(2347) Vinata	$23.63 \pm 1.27$	$0.103^{+0.008}_{-0.008}$	$35^{+20}_{-14}$	[T10]	—	4.4835	$187 \pm 4$	C <sup>A</sup>	$-0.52^{+2.17}_{-2.53}$	$-0.02^{+0.80}_{-0.87}$	$8.0 \pm 2.1$	
(2365) Interkosmos	$16.62 \pm 1.41$	$0.195^{+0.018}_{-0.021}$	$41^{+10}_{-41}$	[T10]	S <sup>1</sup>	6.1548	$234 \pm 9$	S <sup>S;F</sup>	$1.84^{+1.27}_{-1.17}$	$1.78^{+0.50}_{-0.50}$	$6.9 \pm 2.4$	Astraea
(2375) Radek	$32.19 \pm 1.60$	$0.123^{+0.008}_{-0.010}$	$11^{+14}_{-11}$	[T10]	D <sup>4b</sup>	16.875	$241 \pm 2$	P <sup>C;A</sup>	$3.01^{+1.30}_{-1.27}$	$2.51^{+0.93}_{-1.07}$	$9.7 \pm 4.2$	
(2446) Lunacharsky	$12.43 \pm 0.31$	$0.078^{+0.003}_{-0.004}$	$33^{+12}_{-10}$	[T10]	B <sup>2</sup>	3.613	$244 \pm 13$	B <sup>S;F</sup>	$1.41^{+2.07}_{-2.50}$	$2.01^{+0.97}_{-1.13}$	$20.3 \pm 4.4$	Nysa-Polana
(2463) Sterpin	$11.93 \pm 0.69$	$0.221^{+0.016}_{-0.013}$	$17^{+43}_{-17}$	[T10]	S <sup>4</sup>	13.44	$217 \pm 7$	S <sup>S;F</sup>	$-0.86^{+2.07}_{-2.80}$	$-0.72^{+1.27}_{-1.60}$	$12.1 \pm 5.7$	Eunomia
(2500) Alascattalo	$7.99 \pm 0.27$	$0.278^{+0.023}_{-0.020}$	$41^{+18}_{-28}$	[T10]	—	2.754	$242 \pm 6$	S <sup>F;A</sup>	$1.48^{+1.40}_{-1.13}$	$1.31^{+0.67}_{-0.67}$	$5.2 \pm 1.7$	Flora
(2511) Patterson	$9.03 \pm 1.12$	$0.180^{+0.055}_{-0.034}$	$90^{+58}_{-43}$	[T7]	V <sup>2</sup>	4.141	$220 \pm 6$	V <sup>S;F</sup>	$-1.76^{+1.53}_{-1.23}$	$-2.36^{+1.53}_{-1.60}$	$11.7 \pm 3.4$	Vesta
(2556) Louise	$5.96 \pm 0.55$	$0.252^{+0.025}_{-0.031}$	$61^{+37}_{-33}$	[T10]	—	3.809	$238 \pm 3$	S <sup>A</sup>	$-0.09^{+1.40}_{-1.17}$	$-0.59^{+1.23}_{-1.53}$	$8.4 \pm 2.5$	
(2567) Elba	$18.40 \pm 1.27$	$0.110^{+0.008}_{-0.009}$	$50^{+11}_{-36}$	[T10]	Xc <sup>2</sup>	9.7785	$212 \pm 5$	C <sup>S</sup>	$-2.39^{+4.90}_{-1.50}$	$-2.86^{+5.30}_{-1.03}$	$10.3 \pm 3.1$	
(2606) Odessa	$17.0 \pm 2.5$	$0.130^{+0.040}_{-0.040}$	$90^{+80}_{-40}$	[T15]	Xk <sup>2</sup>	8.2444	$180 \pm 7$	Met <sup>S;A</sup>	$-3.12^{+1.57}_{-1.30}$	$-3.39^{+1.47}_{-1.63}$	$13.9 \pm 4.3$	
(2617) Jiangxi	$51.34 \pm 2.86$	$0.039^{+0.025}_{-0.025}$	$6^{+6}_{-6}$	[T9]	—	$11.7730^\dagger$	$230 \pm 3$	B <sup>*A</sup>	$2.18^{+2.27}_{-2.47}$	$4.31^{+1.17}_{-2.93}$	$5.7 \pm 2.1$	
(2659) Millis	$27.15 \pm 0.85$	$0.052^{+0.027}_{-0.027}$	$36^{+18}_{-20}$	[T9]	B <sup>2</sup>	$6.1246^\dagger$	$202 \pm 2$	B <sup>S;F</sup>	$0.34^{+2.03}_{-2.50}$	$0.04^{+1.40}_{-1.57}$	$9.6 \pm 2.8$	Themis
(2687) Tortali	$14.91 \pm 0.21$	$0.148^{+0.005}_{-0.011}$	$59^{+16}_{-10}$	[T10]	—	21.75	$226 \pm 10$	S <sup>A</sup>	$0.38^{+0.93}_{-0.83}$	$0.71^{+0.77}_{-0.80}$	$20.5 \pm 4.0$	
(2786) Grinevia	$11.07 \pm 0.98$	$0.237^{+0.023}_{-0.029}$	$12^{+19}_{-12}$	[T10]	—	2.911	$203 \pm 1$	S <sup>F;A</sup>	$1.48^{+1.50}_{-1.50}$	$0.94^{+0.60}_{-0.77}$	$4.1 \pm 1.8$	Eunomia
(2855) Bastian	$8.78 \pm 0.57$	$0.151^{+0.012}_{-0.012}$	$17^{+42}_{-7}$	[T10]	S <sup>2</sup>	3.516	$226 \pm 12$	S <sup>S</sup>	$0.44^{+1.70}_{-1.40}$	$-0.49^{+1.23}_{-1.57}$	$6.6 \pm 2.5$	
(2867) Steins	$5.3 \pm 0.4$	$0.450^{+0.037}_{-0.052}$	$210^{+30}_{-30}$	[T19]	—	$6.0468^\dagger$	$230 \pm 10$	E <sup>A</sup>	$-3.19^{+1.77}_{-2.40}$	$-3.72^{+1.00}_{-1.40}$	$20.0 \pm 3.6$	
(2870) Haupt	$15.51 \pm 2.28$	$0.057^{+0.009}_{-0.009}$	$125^{+184}_{-125}$	[T10]	—	274	$229 \pm 3$	C <sup>F;A</sup>	$-3.59^{+2.30}_{-2.60}$	$-3.59^{+2.30}_{-2.60}$	$115.4 \pm 51.3$	Nysa-Polana
(2947) Kippenhahn	$7.80 \pm 0.29$	$0.267^{+0.014}_{-0.017}$	$32^{+18}_{-11}$	[T10]	—	10.5	$236 \pm 12$	S <sup>A</sup>	$1.68^{+1.30}_{-1.23}$	$1.24^{+0.67}_{-0.73}$	$10.6 \pm 2.7$	
(2985) Shakespeare	$10.64 \pm 0.92$	$0.260^{+0.025}_{-0.024}$	$41^{+49}_{-13}$	[T10]	—	6.06	$211 \pm 0$	S <sup>F;A</sup>	$-1.39^{+2.07}_{-2.60}$	$-1.52^{+1.43}_{-1.63}$	$11.4 \pm 3.5$	Koronis
(3036) Krat	$41.41 \pm 1.28$	$0.090^{+0.006}_{-0.005}$	$15^{+57}_{-9}$	[T10]	B <sup>3</sup>	9.61	$204 \pm 2$	B <sup>S;F</sup>	$-0.92^{+2.27}_{-2.53}$	$-1.42^{+1.87}_{-1.80}$	$14.0 \pm 6.0$	Alauda
(3051) Nantong	$16.79 \pm 1.60$	$0.081^{+0.008}_{-0.009}$	$27^{+28}_{-14}$	[T10]	—	3.69	$203 \pm 3$	C <sup>A</sup>	$-0.26^{+2.13}_{-2.53}$	$-0.12^{+0.90}_{-1.10}$	$6.7 \pm 2.2$	
(3144) Brosche	$4.80 \pm 0.53$	$0.219^{+0.026}_{-0.027}$	$59^{+56}_{-45}$	[T10]	—	3.3	$226 \pm 2$	S <sup>F;A</sup>	$-0.86^{+1.60}_{-1.33}$	$-1.69^{+1.47}_{-1.63}$	$8.2 \pm 3.1$	Flora
(3162) Nostalgia	$28.88 \pm 1.48$	$0.064^{+0.005}_{-0.006}$	$29^{+51}_{-15}$	[T10]	B <sup>3</sup>	6.412	$199 \pm 6$	B <sup>S</sup>	$-1.16^{+2.20}_{-2.57}$	$-1.79^{+1.70}_{-1.73}$	$10.7 \pm 4.0$	
(3200) Phaethon	$5.1 \pm 0.2$	$0.122^{+0.008}_{-0.008}$	$600^{+200}_{-200}$	[T20]	B <sup>2</sup>	$3.6040^\dagger$	$311 \pm 10$	B <sup>S</sup>	$-5.09^{+2.13*}_{-3.23}$	$-5.76^{+1.63*}_{-2.10}$	$24.7 \pm 5.5$	
(3249) Musashino	$6.43 \pm 1.22$	$0.185^{+0.036}_{-0.036}$	$93^{+132}_{-73}$	[T10]	S <sup>2</sup>	$4.5527^\dagger$	$197 \pm 3$	S <sup>S;F</sup>	$-3.59^{+2.27}_{-2.53}$	$-4.12^{+1.87}_{-1.80}$	$14.6 \pm 6.0$	Nysa-Polana
(3267) Glo	$7.37 \pm 1.28$	$0.262^{+0.049}_{-0.053}$	$23^{+43}_{-13}$	[T10]	S <sup>3</sup>	6.8782	$225 \pm 6$	S <sup>S;F</sup>	$0.31^{+1.53}_{-1.40}$	$-0.62^{+1.27}_{-1.57}$	$9.5 \pm 3.7$	Phocaea
(3281) Maupertuis	$5.51 \pm 0.44$	$0.484^{+0.051}_{-0.074}$	$60^{+58}_{-31}$	[T7]	—	6.73	$232 \pm 12$	V <sup>A;F</sup>	$-0.89^{+1.70}_{-1.37}$	$-1.72^{+1.53}_{-1.63}$	$12.9 \pm 4.2$	Vesta
(3305) Ceadams	$10.37 \pm 0.12$	$0.218^{+0.007}_{-0.013}$	$21^{+6}_{-3}$	[T10]	—	2.729	$228 \pm 11$	S <sup>F;A</sup>	$2.64^{+1.17}_{-2.23}$	—	$4.4 \pm 0.8$	Eunomia
(3411) Debetencourt	$5.18 \pm 0.21$	$0.294^{+0.017}_{-0.020}$	$22^{+83}_{-12}$	[T10]	—	9.93	$244 \pm 10$	S <sup>F;A</sup>	$-0.72^{+1.90}_{-1.53}$	$-1.76^{+1.63}_{-1.70}$	$14.0 \pm 5.9$	Flora
(3428) Roberts	$17.25 \pm 0.63$	$0.086^{+0.025}_{-0.025}$	$66^{+14}_{-21}$	[T9]	—	$3.2784^\dagger$	$198 \pm 2$	C <sup>A</sup>	$-0.76^{+2.03}_{-2.60}$	$0.04^{+0.73}_{-0.73}$	$8.3 \pm 1.7$	
(3438) Inarradas	$25.18 \pm 0.68$	$0.058^{+0.003}_{-0.003}$	$54^{+15}_{-15}$	[T10]	—	24.82	$206 \pm 5$	C <sup>F;A</sup>	$-0.36^{+2.03}_{-2.50}$	$0.54^{+0.67}_{-0.67}$	$20.9 \pm 4.3$	Inarrados
(3483) Svetlov	$2.96 \pm 0.48$	$0.496^{+0.107}_{-0.114}$	$107^{+402}_{-34}$	[T10]	—	6.79	$222 \pm 11$	E <sup>F;A</sup>	$-5.26^{+2.67*}_{-2.70}$	$-5.86^{+2.33*}_{-2.03}$	$27.9 \pm 11.4$	Hungaria
(3509) Sanshui	$9.93 \pm 0.84$	$0.243^{+0.023}_{-0.028}$	$62^{+27}_{-34}$	[T10]	—	13.68	$212 \pm 1$	S <sup>A</sup>	$-0.32^{+1.23}_{-1.10}$	$-0.62^{+1.10}_{-1.37}$	$16.0 \pm 4.5$	
(3536) Schleicher	$3.67 \pm 1.14$	$0.375^{+0.118}_{-0.119}$	$32^{+182}_{-10}$	[T10]	S <sup>2,13</sup>	5.79	$230 \pm 8$	S <sup>S</sup>	$-2.89^{+2.23}_{-1.73}$	$-3.66^{+1.97}_{-1.87}$	$16.1 \pm 6.8$	
(3544) Borodino	$8.5 \pm 0.5$	$0.257^{+0.031}_{-0.032}$	$65^{+25}_{-40}$	[T9][T10]	—	5.442	$237 \pm 18$	S <sup>A</sup>	$0.21^{+1.50}_{-1.10}$	$-0.06^{+1.10}_{-1.30}$	$9.3 \pm 2.8$	
(3554) Amun	$2.71 \pm 0.02$	$0.140^{+0.027}_{-0.028}$	$1382^{+737}_{-205}$	[T10]	—	$2.5300^\dagger$	$274 \pm 6$	Met <sup>A,T</sup>	$-8.69^{+0.93*}_{-0.97}$	$-9.09^{+1.27*}_{-1.50}$	$33.5 \pm 7.2$	
(3560) Chenqian	$22.84 \pm 0.56$	$0.152^{+0.007}_{-0.011}$	$44^{+22}_{-10}$	[T10]	—	18.79	$206 \pm 3$	K <sup>F;A</sup>	$-0.39^{+2.07}_{-2.53}$	$0.11^{+0.83}_{-0.87}$	$17.9 \pm 4.0$	Eos
(3628) Boznemcova	$8.07 \pm 0.80$	$0.223^{+0.023}_{-0.024}$	$32^{+23}_{-32}$	[T10]	O <sup>2</sup>	$3.3354^\dagger$	$201 \pm 12$	S <sup>S</sup>	$0.61^{+1.50}_{-1.30}$	$0.01^{+0.97}_{-1.07}$	$5.8 \pm 2.3$	
(3678) Mongmanwai	$8.5 \pm 0.3$	$0.183^{+0.069}_{-0.069}$	$72^{+17}_{-17}$	[T9]	S <sup>2</sup>	$4.1830^\dagger$	$205 \pm 8$	S <sup>S</sup>	$-0.62^{+0.90}_{-0.83}$	$-0.42^{+0.93}_{-1.07}$	$10.1 \pm 2.0$	

Table 4 — continued

Object	$D_{eff}$	$p_V$	$\Gamma^a$	Source	Tax/Color	$P_{rot}$	$T_{surf}$ (K)	Model Comp.	$d_{g\phi}^{G\&B}$	$d_{g\phi}^{Sak}$	$l_s$ (mm)	Family
(3751) Kiang	$22.38 \pm 0.68$	$0.083^{+0.005}_{-0.007}$	$62^{+20}_{-16}$	[T10]	—	8.2421	$211 \pm 0$	$C^A$	$-0.56^{+2.00}_{-2.57}$	$0.01^{+0.87}_{-0.90}$	$13.0 \pm 2.7$	
(3823) Yorii	$13.66 \pm 1.47$	$0.064^{+0.007}_{-0.008}$	$49^{+22}_{-49}$	[T10]	—	6.669	$209 \pm 10$	$C^A$	$-0.22^{+2.07}_{-2.63}$	$0.04^{+0.93}_{-1.00}$	$8.9 \pm 3.3$	
(3907) Kilmartin	$8.16 \pm 1.12$	$0.530^{+0.076}_{-0.083}$	$26^{+47}_{-26}$	[T10]	—	3.841	$183 \pm 14$	$E^A$	$-1.59^{+2.17}_{-2.60}$	$-2.12^{+1.40}_{-1.70}$	$8.5 \pm 3.4$	
(3915) Fukushima	$22.18 \pm 0.39$	$0.059^{+0.004}_{-0.003}$	$22^{+13}_{-7}$	[T10]	$C^1$	9.418	$240 \pm 1$	$Cb^S$	$1.74^{+2.07}_{-2.57}$	$2.31^{+0.93}_{-1.10}$	$9.4 \pm 2.4$	
(3935) Toatenmongakkai	$12.02 \pm 0.82$	$0.219^{+0.017}_{-0.021}$	$121^{+88}_{-55}$	[T10]	$S^1$	106.3	$215 \pm 5$	$S^S$	$-2.79^{+1.57}_{-1.33}$	$-3.36^{+1.67}_{-1.67}$	$70.0 \pm 20.6$	
(3936) Elst	$5.00 \pm 0.68$	$0.490^{+0.069}_{-0.074}$	$22^{+56}_{-22}$	[T10]	—	6.6322	$235 \pm 3$	$V^{F;A}$	$-0.12^{+1.83}_{-1.40}$	$-1.09^{+1.43}_{-1.67}$	$9.6 \pm 4.5$	Vesta
(4003) Schumann	$31.92 \pm 0.41$	$0.063^{+0.003}_{-0.002}$	$32^{+35}_{-11}$	[T10]	—	5.7502	$208 \pm 3$	$C^A$	$-0.52^{+2.07}_{-2.60}$	$-0.62^{+1.13}_{-1.40}$	$9.5 \pm 2.9$	
(4006) Sandler	$16.89 \pm 0.64$	$0.059^{+0.003}_{-0.003}$	$36^{+7}_{-11}$	[T10]	$X^1$	3.4	$212 \pm 1$	$P^{S;A}$	$1.31^{+0.97}_{-0.77}$	$1.58^{+0.87}_{-1.00}$	$7.3 \pm 1.5$	
(4008) Corbin	$6.18 \pm 0.31$	$0.307^{+0.025}_{-0.035}$	$67^{+37}_{-25}$	[T10]	—	6.203	$240 \pm 16$	$S^A$	$-0.22^{+1.43}_{-1.20}$	$-0.76^{+1.30}_{-1.57}$	$11.6 \pm 3.0$	
(4029) Bridges	$7.87 \pm 0.62$	$0.246^{+0.021}_{-0.025}$	$32^{+26}_{-18}$	[T10]	—	3.5746	$240 \pm 3$	$S^A$	$1.21^{+1.47}_{-1.20}$	$0.81^{+0.83}_{-0.90}$	$6.2 \pm 2.0$	
(4077) Asuka	$19.27 \pm 0.45$	$0.189^{+0.032}_{-0.032}$	$10^{+2}_{-4}$	[T9]	—	7.9231	$202 \pm 3$	$K^{F;A}$	$0.81^{+2.23}_{-2.53}$	—	$4.8 \pm 1.0$	Eos
(4142) Dersu-Uzala	$6.31 \pm 0.52$	$0.236^{+0.048}_{-0.049}$	$109^{+140}_{-31}$	[T10]	$A^2$	140	$263 \pm 10$	$S^S$	$-2.36^{+1.70}_{-1.50}$	$-2.96^{+1.83}_{-1.73}$	$81.8 \pm 25.4$	
(4150) Starr	$6.93 \pm 0.39$	$0.304^{+0.021}_{-0.024}$	$29^{+16}_{-14}$	[T10]	—	4.5179	$231 \pm 6$	$S^A$	$1.81^{+1.23}_{-1.30}$	$1.44^{+0.57}_{-0.63}$	$6.4 \pm 1.8$	
(4255) Spacewatch	$15.71 \pm 0.45$	$0.042^{+0.003}_{-0.002}$	$24^{+22}_{-17}$	[T10]	—	20	$209 \pm 2$	$P^{F;A}$	$0.91^{+1.60}_{-1.30}$	$0.21^{+1.43}_{-1.63}$	$16.2 \pm 5.9$	Schubart
(4264) Karljosephine	$6.37 \pm 1.83$	$0.202^{+0.059}_{-0.059}$	$108^{+299}_{-108}$	[T10]	—	30.96	$206 \pm 2$	$S^A$	$-4.96^{+2.50}_{-1.77}$	$-5.49^{+2.27}_{-2.00}$	$49.4 \pm 23.3$	
(4265) Kani	$13.97 \pm 0.67$	$0.048^{+0.023}_{-0.023}$	$6^{+6}_{-6}$	[T9]	$C^2$	$5.7276^\dagger$	$218 \pm 4$	$Cb^S$	$2.01^{+2.20}_{-2.43}$	$4.74^{+1.77}_{-3.00}$	$4.1 \pm 1.5$	
(4294) Horatius	$8.07 \pm 0.66$	$0.242^{+0.023}_{-0.023}$	$12^{+77}_{-12}$	[T10]	—	12.499	$225 \pm 2$	$S^A$	$-0.79^{+1.87}_{-1.60}$	$-1.89^{+1.60}_{-1.70}$	$14.6 \pm 7.0$	
(4352) Kyoto	$11.33 \pm 1.30$	$0.308^{+0.038}_{-0.041}$	$47^{+64}_{-32}$	[T10]	$S^{2,13}$	21.9352	$204 \pm 2$	$S^S$	$-1.42^{+1.83}_{-1.43}$	$-2.32^{+1.57}_{-1.67}$	$22.6 \pm 8.7$	
(4359) Berlage	$4.98 \pm 0.69$	$0.289^{+0.042}_{-0.042}$	$40^{+71}_{-26}$	[T10]	—	7.413	$228 \pm 1$	$S^A$	$-0.92^{+1.80}_{-1.47}$	$-1.89^{+1.57}_{-1.67}$	$12.5 \pm 5.0$	
(4363) Sergej	$5.48 \pm 0.48$	$0.282^{+0.026}_{-0.031}$	$27^{+94}_{-27}$	[T10]	—	13.04	$218 \pm 5$	$S^A$	$-1.59^{+2.00}_{-1.60}$	$-2.56^{+1.70}_{-1.73}$	$17.2 \pm 8.1$	
(4383) Suruga	$6.80 \pm 1.03$	$0.223^{+0.035}_{-0.040}$	$37^{+53}_{-17}$	[T10]	—	3.4069	$220 \pm 1$	$S^A$	$-0.49^{+1.70}_{-1.47}$	$-1.42^{+1.43}_{-1.67}$	$8.1 \pm 2.8$	
(4528) Berg	$10.45 \pm 0.96$	$0.247^{+0.024}_{-0.032}$	$26^{+20}_{-26}$	[T10]	—	3.5163	$231 \pm 6$	$S^A$	$1.64^{+1.20}_{-1.37}$	$1.18^{+0.67}_{-0.73}$	$5.0 \pm 2.0$	
(4565) Grossman	$7.57 \pm 0.37$	$0.240^{+0.017}_{-0.022}$	$51^{+36}_{-12}$	[T10]	—	4.7429	$233 \pm 3$	$S^{F;A}$	$0.01^{+1.27}_{-1.17}$	$-0.46^{+1.20}_{-1.47}$	$9.7 \pm 2.4$	Eunomia
(4569) Baerbel	$9.21 \pm 0.73$	$0.292^{+0.026}_{-0.028}$	$48^{+45}_{-9}$	[T10]	—	2.737	$225 \pm 5$	$S^{F;A}$	$-0.42^{+1.43}_{-1.27}$	$-1.12^{+1.37}_{-1.60}$	$7.8 \pm 2.1$	Maria
(4606) Saheki	$6.8 \pm 0.4$	$0.211^{+0.040}_{-0.040}$	$9^{+11}_{-9}$	[T9]	$S^1$	$4.9735^\dagger$	$225 \pm 13$	$S^S$	$2.28^{+1.67}_{-2.33}$	$6.64^{+0.00}_{-0.00}$	$4.0 \pm 1.8$	Nysa-Polana
(4611) Vulkaneifel	$12.1 \pm 1.1$	$0.216^{+0.023}_{-0.028}$	$32^{+23}_{-32}$	[T13]	$S^{2,13}$	3.756	$202 \pm 1$	$S^S$	$0.61^{+1.33}_{-1.27}$	$0.18^{+0.87}_{-1.00}$	$6.1 \pm 2.4$	Eunomia
(4613) Mamoru	$11.96 \pm 1.48$	$0.280^{+0.036}_{-0.037}$	$9.4^{+22.6}_{-9.4}$	[T10]	$S^3$	5.388	$194 \pm 3$	$S^{S*;A}$	$1.14^{+1.37}_{-1.50}$	$0.38^{+0.77}_{-0.83}$	$5.9 \pm 2.8$	
(4713) Steel	$6.58 \pm 0.18$	$0.196^{+0.025}_{-0.037}$	$40^{+28}_{-13}$	[T10]	$A^2$	5.199	$258 \pm 0$	$S^S$	$1.24^{+1.30}_{-1.17}$	$0.91^{+0.83}_{-1.00}$	$8.3 \pm 2.2$	
(4771) Hayashi	$13.32 \pm 0.96$	$0.101^{+0.008}_{-0.008}$	$61^{+37}_{-29}$	[T10]	—	9.801	$208 \pm 10$	$C^A$	$-1.32^{+2.03}_{-2.70}$	$-1.32^{+2.07}_{-2.70}$	$14.5 \pm 4.2$	
(4800) Veveri	$13.25 \pm 0.57$	$0.173^{+0.027}_{-0.027}$	$39^{+25}_{-29}$	[T9]	—	6.2157	$218 \pm 7$	$K^{F;A}$	$0.04^{+2.07}_{-2.57}$	$0.28^{+0.83}_{-0.97}$	$8.4 \pm 2.9$	Eos
(4898) Nishiizumi	$2.46 \pm 0.22$	$0.600^{+0.073}_{-0.103}$	$34^{+445}_{-34}$	[T10]	—	3.289	$243 \pm 13$	$E^A$	$-4.82^{+2.73*}_{-2.73}$	$-5.46^{+2.37*}_{-2.07}$	$17.8 \pm 8.3$	
(4899) Candace	$7.17 \pm 0.57$	$0.271^{+0.028}_{-0.039}$	$79^{+104}_{-60}$	[T10]	—	40.7	$255 \pm 8$	$S^A$	$-1.62^{+1.97}_{-1.47}$	$-2.39^{+1.70}_{-1.70}$	$34.4 \pm 13.7$	
(4905) Hiromi	$10 \pm 1$	$0.183^{+0.039}_{-0.031}$	$45^{+55}_{-45}$	[T17]	—	6.0428	$244 \pm 10$	$S^A$	$-0.96^{+2.07}_{-2.60}$	$-1.09^{+1.43}_{-1.67}$	$9.5 \pm 4.1$	
(4908) Ward	$4.91 \pm 0.71$	$0.262^{+0.040}_{-0.042}$	$12^{+68}_{-12}$	[T10]	—	10.96	$229 \pm 4$	$S^A$	$-0.46^{+1.87}_{-1.50}$	$-1.52^{+1.53}_{-1.70}$	$12.7 \pm 6.1$	
(5035) Swift	$10.22 \pm 1.06$	$0.211^{+0.023}_{-0.025}$	$26^{+35}_{-20}$	[T10]	—	9.4752	$223 \pm 7$	$S^{F;A}$	$0.61^{+1.60}_{-1.40}$	$-0.19^{+1.10}_{-1.37}$	$10.3 \pm 4.1$	Eunomia
(5052) Nancyruth	$4.66 \pm 0.78$	$0.167^{+0.029}_{-0.032}$	$10^{+72}_{-10}$	[T10]	—	17.204	$231 \pm 1$	$S^{F;A}$	$-0.52^{+1.93}_{-1.50}$	$-1.59^{+1.57}_{-1.70}$	$16.2 \pm 7.8$	Flora
(5080) Oja	$7.98 \pm 0.53$	$0.243^{+0.018}_{-0.026}$	$26^{+50}_{-17}$	[T10]	—	7.222	$235 \pm 7$	$S^{F;A}$	$0.11^{+1.70}_{-1.40}$	$-0.82^{+1.37}_{-1.63}$	$10.0 \pm 4.1$	Baptistina/Matterania
(5088) Tancredi	$16.17 \pm 1.02$	$0.066^{+0.005}_{-0.005}$	$40^{+12}_{-19}$	[T10]	—	5.0591	$197 \pm 4$	$B^{F;A}$	$0.54^{+1.90}_{-2.60}$	$0.24^{+1.23}_{-1.50}$	$9.0 \pm 2.2$	Themis
(5104) Skripnichenko	$9.49 \pm 0.48$	$0.329^{+0.021}_{-0.026}$	$41^{+31}_{-22}$	[T10]	—	$2.8271^\dagger$	$229 \pm 4$	$S^A$	$0.54^{+1.47}_{-1.27}$	$-0.02^{+1.07}_{-1.27}$	$6.3 \pm 2.0$	
(5111) Jacliff	$5.3 \pm 0.4$	$0.523^{+0.088}_{-0.044}$	$0^{+15}_{-0}$	[T7]	$V^2$	2.839	$225 \pm 7$	$V^{S;F}$	$1.28^{+2.20}_{-2.43}$	—	$2.6 \pm 0.8$	Vesta

Table 4 — continued

Object	$D_{eff}$	$p_V$	$\Gamma^a$	Source	Tax/Color	$P_{rot}$	$T_{surf}$ (K)	Model Comp.	$d_{g\phi}^{G\&B}$	$d_{g\phi}^{Sak}$	$l_s$ (mm)	Family
(5226) Pollack	$5.74 \pm 1.03$	$0.303^{+0.056}_{-0.062}$	$24^{+51}_{-18}$	[T10]	—	2.725	$221 \pm 3$	$S^A$	$-0.19^{+1.67}_{-1.40}$	$-1.16^{+1.40}_{-1.63}$	$6.2 \pm 2.6$	
(5333) Kanaya	$13.86 \pm 1.32$	$0.066^{+0.007}_{-0.007}$	$23^{+32}_{-7}$	[T10]	Ch <sup>2</sup>	3.8022	$249 \pm 12$	Ch <sup>S;F</sup>	$0.78^{+2.10}_{-2.57}$	$0.41^{+1.40}_{-1.63}$	$7.3 \pm 2.3$	Chaldaea
(5378) Ellyett	$2.77 \pm 0.25$	$0.776^{+0.095}_{-0.119}$	$75^{+455}_{-62}$	[T10]	—	47.32	$246 \pm 7$	$E^{F;A}$	$-4.89^{+2.70}_{-2.73}$	$-5.52^{+2.37}_{-2.03}$	$69.7 \pm 31.3$	Hungaria
(5427) Jensmartin	$3.13 \pm 0.14$	$0.622^{+0.055}_{-0.084}$	$19^{+76}_{-19}$	[T10]	—	5.81	$239 \pm 6$	$E^{F;A}$	$-1.12^{+2.20}_{-2.57}$	$-1.72^{+1.50}_{-1.67}$	$10.4 \pm 4.5$	Hungaria
(5489) Oberkochen	$14.57 \pm 0.45$	$0.191^{+0.027}_{-0.027}$	$18^{+16}_{-12}$	[T9]	—	5.6244	$214 \pm 3$	$S^{F;A}$	$1.84^{+1.40}_{-1.53}$	$1.28^{+0.60}_{-0.63}$	$6.1 \pm 2.2$	Eunomia
(5527) 1991 UQ <sub>3</sub>	$5.30 \pm 0.56$	$0.233^{+0.026}_{-0.029}$	$117^{+131}_{-80}$	[T10]	—	4.2554	$254 \pm 17$	$S^A$	$-2.42^{+1.93}_{-1.50}$	$-3.06^{+1.80}_{-1.77}$	$13.2 \pm 5.0$	
(5574) Seagrave	$9.72 \pm 1.05$	$0.225^{+0.027}_{-0.032}$	$34^{+34}_{-34}$	[T10]	—	4.6629	$225 \pm 3$	$S^{F;A}$	$0.44^{+1.73}_{-1.30}$	$-0.19^{+1.10}_{-1.37}$	$7.2 \pm 3.0$	Eunomia
(5592) Oshima	$23.91 \pm 1.16$	$0.065^{+0.004}_{-0.005}$	$34^{+23}_{-27}$	[T10]	C <sup>3</sup>	12.54	$206 \pm 4$	$C^{F;A}$	$-0.02^{+2.10}_{-2.57}$	$0.24^{+0.87}_{-0.87}$	$11.5 \pm 4.2$	Veritas
(5604) 1992 FE	$0.673 \pm 0.005$	$0.447^{+0.077}_{-0.086}$	$1058^{+2229}_{-575}$	[T10]	V <sup>4</sup>	5.3375	$281 \pm 0$	$V^S$	$-9.22^{+2.40}_{-1.80}$	$-9.55^{+2.47}_{-1.97}$	$54.7 \pm 21.3$	
(5625) Jamesferguson	$14.46 \pm 0.86$	$0.062^{+0.005}_{-0.006}$	$52^{+14}_{-15}$	[T13]	—	6.671	$204 \pm 1$	$C^{F;A}$	$-0.26^{+2.03}_{-2.57}$	$0.64^{+0.63}_{-0.67}$	$10.6 \pm 2.2$	Adeona
(5682) Beresford	$5.37 \pm 1.83$	$0.233^{+0.080}_{-0.082}$	$29^{+152}_{-29}$	[T10]	—	3.769	$212 \pm 10$	$S^A$	$-2.86^{+2.20}_{-1.70}$	$-3.66^{+1.93}_{-1.83}$	$11.7 \pm 5.6$	
(5712) Funke	$7.22 \pm 1.60$	$0.269^{+0.061}_{-0.062}$	$33^{+50}_{-33}$	[T10]	—	3.95	$202 \pm 7$	$S^{A;O}$	$-0.72^{+1.77}_{-1.73}$	$-1.72^{+1.47}_{-1.67}$	$7.8 \pm 3.5$	Gefion/Minerva
(6091) Mitsuru	$4.94 \pm 0.75$	$0.423^{+0.068}_{-0.070}$	$45^{+25}_{-13}$	[T10]	—	5.853	$253 \pm 11$	$S^A$	$1.18^{+1.30}_{-1.17}$	$0.88^{+0.87}_{-0.97}$	$9.2 \pm 2.2$	
(6121) Plachinda	$5.83 \pm 0.82$	$0.250^{+0.036}_{-0.038}$	$56^{+63}_{-34}$	[T10]	—	4.0863	$217 \pm 1$	$S^A$	$-1.22^{+1.70}_{-1.40}$	$-2.09^{+1.57}_{-1.63}$	$9.9 \pm 3.5$	
(6136) Gryphon	$15.33 \pm 0.54$	$0.160^{+0.023}_{-0.023}$	$38^{+17}_{-13}$	[T9]	—	16.4684 <sup>†</sup>	$213 \pm 4$	$K^{F;A}$	$0.98^{+2.23}_{-2.43}$	$1.24^{+0.80}_{-1.30}$	$14.5 \pm 3.4$	Eos
(6139) Naomi	$10.68 \pm 0.36$	$0.207^{+0.014}_{-0.025}$	$66^{+31}_{-36}$	[T10]	S <sup>3</sup>	21.35	$242 \pm 0$	$S^S$	$0.14^{+1.37}_{-1.13}$	$-0.22^{+1.10}_{-1.37}$	$19.5 \pm 5.6$	
(6159) Andreseloy	$5.65 \pm 1.37$	$0.246^{+0.061}_{-0.061}$	$61^{+177}_{-70}$	[T13]	—	10.639	$222 \pm 2$	$V^{F;A}$	$-3.22^{+2.23}_{-1.70}$	$-3.92^{+1.97}_{-1.87}$	$22.0 \pm 10.3$	Vesta
(6170) Levasseur	$5.57 \pm 0.63$	$0.238^{+0.031}_{-0.040}$	$76^{+161}_{-56}$	[T10]	—	2.6529	$239 \pm 16$	$S^{F;A}$	$-2.72^{+2.20}_{-1.67}$	$-3.46^{+1.93}_{-1.83}$	$10.5 \pm 4.5$	Phocaea
(6185) Mitsuma	$10.36 \pm 1.00$	$0.113^{+0.012}_{-0.013}$	$66^{+61}_{-45}$	[T10]	—	21.05	$240 \pm 11$	$C^A$	$-1.39^{+2.07}_{-2.53}$	$-1.39^{+2.10}_{-2.53}$	$21.1 \pm 7.6$	
(6261) Chione	$3.91 \pm 0.56$	$0.270^{+0.046}_{-0.052}$	$41^{+52}_{-41}$	[T10]	—	5.3334	$230 \pm 22$	$S^A$	$-0.36^{+1.70}_{-1.43}$	$-1.36^{+1.53}_{-1.70}$	$8.9 \pm 3.9$	
(6361) Koppel	$3.59 \pm 0.19$	$0.728^{+0.049}_{-0.062}$	$20^{+172}_{-20}$	[T10]	—	9.1122	$232 \pm 5$	$E^A$	$-2.92^{+2.37}_{-2.57}$	$-3.59^{+1.87}_{-1.80}$	$19.1 \pm 8.8$	
(6572) Carson	$8.56 \pm 1.21$	$0.262^{+0.038}_{-0.038}$	$21^{+33}_{-15}$	[T10]	—	2.8235	$218 \pm 11$	$S^A$	$0.64^{+1.70}_{-1.37}$	$-0.12^{+1.07}_{-1.33}$	$5.4 \pm 2.2$	
(6635) Zuber	$3.6 \pm 0.1$	$0.326^{+0.060}_{-0.060}$	$52^{+48}_{-49}$	[T9]	—	5.5356 <sup>†</sup>	$237 \pm 11$	$S^A$	$-0.22^{+1.73}_{-1.40}$	$-1.06^{+1.40}_{-1.63}$	$9.3 \pm 3.8$	
(6838) Okuda	$11.88 \pm 0.28$	$0.185^{+0.010}_{-0.014}$	$47^{+13}_{-10}$	[T10]	—	8.983	$230 \pm 20$	$S^A$	$1.18^{+1.00}_{-1.07}$	$1.04^{+0.73}_{-0.80}$	$11.5 \pm 2.4$	
(6870) 1991 OM <sub>1</sub>	$2.80 \pm 0.66$	$0.647^{+0.180}_{-0.193}$	$59^{+330}_{-59}$	[T10]	—	4.487	$226 \pm 0$	$E^{F;A}$	$-4.56^{+2.57}_{-2.70}$	$-5.19^{+2.17}_{-2.00}$	$19.2 \pm 8.6$	Hungaria
(6901) Roybishop	$5.05 \pm 0.44$	$0.337^{+0.054}_{-0.058}$	$59^{+83}_{-40}$	[T10]	—	4.682	$241 \pm 3$	$S^A$	$-1.26^{+1.83}_{-1.47}$	$-2.09^{+1.60}_{-1.70}$	$10.8 \pm 4.2$	
(6905) Miyazaki	$14.30 \pm 0.73$	$0.222^{+0.015}_{-0.019}$	$26^{+66}_{-26}$	[T10]	—	2.7418	$220 \pm 3$	$S^{F;A}$	$-0.79^{+1.80}_{-1.47}$	$-1.79^{+1.53}_{-1.67}$	$6.7 \pm 3.1$	Eunomia
(6911) Nancygreen	$2.90 \pm 0.32$	$0.515^{+0.068}_{-0.081}$	$208^{+1223}_{-150}$	[T10]	—	59.1	$230 \pm 38$	$E^A$	$-7.72^{+3.13}_{-2.80}$	$-8.35^{+2.90}_{-2.37}$	$133.5 \pm 61.7$	
(7001) Neother	$5.92 \pm 0.38$	$0.241^{+0.034}_{-0.013}$	$20^{+21}_{-20}$	[T7]	—	9.581	$235 \pm 7$	$V^{A;F}$	$1.78^{+1.50}_{-1.40}$	—	$8.0 \pm 3.4$	Vesta
(7476) Ogiltsbie	$18.41 \pm 1.21$	$0.146^{+0.013}_{-0.015}$	$70^{+30}_{-20}$	[T10]	—	3.92	$219 \pm 9$	$S^A$	$-0.66^{+1.23}_{-1.00}$	$-0.89^{+1.20}_{-1.50}$	$9.8 \pm 2.2$	
(7783) 1994 JD	$2.78 \pm 0.33$	$0.461^{+0.098}_{-0.104}$	$173^{+191}_{-109}$	[T10]	—	31.83	$237 \pm 4$	$E^{F;A}$	$-3.86^{+2.37}_{-2.53}$	$-4.42^{+1.90}_{-1.80}$	$48.1 \pm 16.4$	Hungaria
(7829) Jaroff	$2.55 \pm 0.50$	$0.430^{+0.117}_{-0.133}$	$32^{+176}_{-32}$	[T10]	—	4.398	$225 \pm 1$	$E^{F;A}$	$-3.16^{+2.37}_{-2.57}$	$-3.82^{+1.90}_{-1.80}$	$13.9 \pm 6.2$	Hungaria
(7832) 1993 FA <sub>27</sub>	$3.55 \pm 0.53$	$0.444^{+0.070}_{-0.073}$	$46^{+160}_{-46}$	[T10]	—	8.295	$245 \pm 2$	$S^F$	$-2.32^{+2.20}_{-1.70}$	$-3.16^{+1.90}_{-1.80}$	$16.8 \pm 8.0$	Flora
(7949) 1992 SU	$18.26 \pm 1.36$	$0.066^{+0.006}_{-0.006}$	$37^{+28}_{-27}$	[T10]	—	17.91	$209 \pm 7$	$C^A$	$-0.26^{+2.07}_{-2.53}$	$-0.16^{+0.90}_{-1.13}$	$14.8 \pm 5.3$	
(8213) 1995 FE	$4.80 \pm 1.02$	$0.287^{+0.063}_{-0.068}$	$36^{+167}_{-18}$	[T10]	—	2.911	$228 \pm 12$	$S^{F;A}$	$-2.76^{+2.23}_{-1.73}$	$-3.52^{+1.93}_{-1.87}$	$11.0 \pm 4.7$	Phocaea
(8359) 1989 WD	$8.1 \pm 0.5$	$0.116^{+0.031}_{-0.031}$	$86^{+64}_{-41}$	[T9]	—	2.9	$218 \pm 11$	$V^{F;A}$	$-1.89^{+1.60}_{-1.27}$	$-2.49^{+1.57}_{-1.67}$	$9.9 \pm 3.0$	Vesta
(8862) Takayukiota	$7.76 \pm 2.35$	$0.229^{+0.070}_{-0.070}$	$43^{+195}_{-40}$	[T10]	—	3.2549	$193 \pm 4$	$S^A$	$-3.99^{+2.33}_{-1.77}$	$-4.66^{+2.07}_{-1.93}$	$13.0 \pm 6.2$	Astraea
(8887) Scheeres	$7.56 \pm 0.81$	$0.275^{+0.032}_{-0.037}$	$21^{+52}_{-21}$	[T10]	—	2.9827	$220 \pm 6$	$S^{F;A}$	$-0.12^{+1.70}_{-1.50}$	$-1.19^{+1.40}_{-1.67}$	$6.2 \pm 2.9$	Maria
(9158) Plate	$4.11 \pm 0.14$	$0.379^{+0.026}_{-0.024}$	$10^{+19}_{-10}$	[T7]	—	5.165	$227 \pm 21$	$V^{A;F}$	$2.01^{+1.33}_{-1.73}$	—	$5.2 \pm 2.4$	Vesta
(9297) Marchuk	$9.55 \pm 0.57$	$0.260^{+0.019}_{-0.020}$	$22^{+120}_{-22}$	[T10]	—	18.09	$240 \pm 9$	$S^{F;A}$	$-1.62^{+2.00}_{-1.63}$	$-2.56^{+1.77}_{-1.77}$	$21.3 \pm 10.2$	Eunomia

Table 4 — continued

Object	$D_{eff}$	$p_V$	$\Gamma^a$	Source	Tax/Color	$P_{rot}$	$T_{surf}$ (K)	Model Comp.	$d_{g\phi}^{G\&B}$	$d_{g\phi}^{Sak}$	$l_s$ (mm)	Family
(10936) 1998 FN <sub>11</sub>	11.75 ± 0.50	0.127 <sup>+0.008</sup> <sub>-0.010</sub>	13 <sup>+22</sup> <sub>-13</sub>	[T10]	—	25.7	212 ± 2	S <sup>A</sup>	1.51 <sup>+1.53</sup> <sub>-1.47</sub>	0.81 <sup>+0.73</sup> <sub>-0.77</sub>	12.7 ± 5.7	
(11549) 1992 YY	10.30 ± 0.44	0.247 <sup>+0.017</sup> <sub>-0.030</sub>	30 <sup>+18</sup> <sub>-5</sub>	[T10]	—	2.671	236 ± 7	S <sup>A</sup>	1.71 <sup>+1.13</sup> <sub>-1.20</sub>	1.38 <sup>+0.60</sup> <sub>-0.70</sub>	5.5 ± 1.3	
(11780) Thunder Bay	7.82 ± 2.43	0.214 <sup>+0.067</sup> <sub>-0.067</sub>	126 <sup>+449</sup> <sub>-126</sub>	[T10]	—	295	212 ± 6	S <sup>A</sup>	-5.72 <sup>+2.63</sup> <sub>-1.90</sub>	-6.26 <sup>+2.50</sup> <sub>-2.10</sub>	180.9 ± 85.9	
(12088) Macalintal	4.11 ± 0.14	0.379 <sup>+0.026</sup> <sub>-0.024</sub>	70 <sup>+68</sup> <sub>-53</sub>	[T7]	—	3.342	210 ± 22	V <sup>A;F</sup>	-1.79 <sup>+1.83</sup> <sub>-1.53</sub>	—	9.7 ± 3.8	Vesta
(12376) Cochabamba	5.93 ± 0.97	0.245 <sup>+0.041</sup> <sub>-0.046</sub>	120 <sup>+61</sup> <sub>-110</sub>	[T10]	—	6.3207 <sup>†</sup>	240 ± 11	S <sup>A</sup>	-1.66 <sup>+1.73</sup> <sub>-1.27</sub>	-2.32 <sup>+1.57</sup> <sub>-1.60</sub>	13.2 ± 4.8	
(12753) Povenmire	8.00 ± 0.19	0.249 <sup>+0.015</sup> <sub>-0.027</sub>	17 <sup>+23</sup> <sub>-11</sub>	[T10]	—	12.854	238 ± 0	S <sup>A</sup>	1.84 <sup>+1.53</sup> <sub>-1.47</sub>	1.21 <sup>+0.70</sup> <sub>-0.73</sub>	9.6 ± 3.6	
(13474) V'yus	6.63 ± 1.41	0.146 <sup>+0.032</sup> <sub>-0.033</sub>	64 <sup>+123</sup> <sub>-44</sub>	[T10]	—	6.587	196 ± 8	S <sup>A</sup>	-3.12 <sup>+2.07</sup> <sub>-1.60</sub>	-3.86 <sup>+1.90</sup> <sub>-1.80</sub>	16.5 ± 6.8	
(13856) 1999 XZ <sub>105</sub>	14.79 ± 1.23	0.059 <sup>+0.005</sup> <sub>-0.006</sub>	20 <sup>+12</sup> <sub>-10</sub>	[T10]	—	4.4475	209 ± 1	B <sup>*F;A</sup>	1.31 <sup>+2.13</sup> <sub>-2.50</sub>	1.84 <sup>+0.87</sup> <sub>-1.00</sub>	6.4 ± 1.8	Adeona
(14342) Iglia	16.22 ± 1.11	0.079 <sup>+0.006</sup> <sub>-0.007</sub>	24 <sup>+8</sup> <sub>-14</sub>	[T10]	—	3.9867	202 ± 5	B <sup>*F;A</sup>	1.31 <sup>+2.13</sup> <sub>-2.47</sub>	2.14 <sup>+0.83</sup> <sub>-1.17</sub>	6.0 ± 1.6	Chloris
(14950) 1996 BE <sub>2</sub>	6.66 ± 1.01	0.145 <sup>+0.023</sup> <sub>-0.024</sub>	54 <sup>+49</sup> <sub>-34</sub>	[T10]	—	3.2792 <sup>†</sup>	246 ± 0	S <sup>F;A</sup>	-0.12 <sup>+1.67</sup> <sub>-1.33</sub>	-0.89 <sup>+1.37</sup> <sub>-1.63</sub>	7.6 ± 2.7	Flora
(15032) Alexlevin	2.83 ± 0.15	0.349 <sup>+0.024</sup> <sub>-0.035</sub>	20 <sup>+15</sup> <sub>-20</sub>	[T7]	—	4.405	229 ± 12	V <sup>A;F</sup>	1.94 <sup>+1.43</sup> <sub>-1.50</sub>	—	5.1 ± 2.0	Vesta
(15362) 1996 ED	4.95 ± 1.01	0.275 <sup>+0.058</sup> <sub>-0.058</sub>	112 <sup>+122</sup> <sub>-112</sub>	[T10]	—	31.4	226 ± 12	S <sup>A;F</sup>	-2.82 <sup>+2.00</sup> <sub>-1.50</sub>	-3.49 <sup>+1.83</sup> <sub>-1.77</sub>	34.5 ± 14.7	Flora
(15430) 1998 UR <sub>31</sub>	3.78 ± 0.43	0.297 <sup>+0.037</sup> <sub>-0.039</sub>	72 <sup>+127</sup> <sub>-63</sub>	[T10]	—	2.5274 <sup>†</sup>	249 ± 16	S <sup>A</sup>	-2.02 <sup>+2.03</sup> <sub>-1.60</sub>	-2.82 <sup>+1.83</sup> <sub>-1.77</sub>	8.9 ± 3.9	
(15499) Cloyd	9.67 ± 1.25	0.146 <sup>+0.020</sup> <sub>-0.020</sub>	33 <sup>+36</sup> <sub>-33</sub>	[T10]	—	6.878	203 ± 4	K <sup>F;A</sup>	-0.56 <sup>+2.03</sup> <sub>-2.67</sub>	-0.82 <sup>+1.17</sup> <sub>-1.47</sub>	9.2 ± 3.9	Eos
(15914) 1997 UM <sub>3</sub>	4.20 ± 0.95	0.234 <sup>+0.054</sup> <sub>-0.054</sub>	88 <sup>+188</sup> <sub>-72</sub>	[T10]	—	12.8	214 ± 7	S <sup>F;A</sup>	-3.69 <sup>+2.20</sup> <sub>-1.67</sub>	-4.32 <sup>+2.03</sup> <sub>-1.87</sub>	26.1 ± 11.4	Hertha/Nysa-Polana
(16681) 1994 EV <sub>7</sub>	3.94 ± 0.34	0.209 <sup>+0.037</sup> <sub>-0.038</sub>	63 <sup>+74</sup> <sub>-30</sub>	[T10]	—	5.3147	245 ± 2	S <sup>A</sup>	-0.99 <sup>+1.67</sup> <sub>-1.43</sub>	-1.86 <sup>+1.60</sup> <sub>-1.63</sub>	11.7 ± 3.9	
(16886) 1998 BC <sub>26</sub>	7.11 ± 0.78	0.211 <sup>+0.025</sup> <sub>-0.027</sub>	33 <sup>+49</sup> <sub>-15</sub>	[T10]	—	5.9908	220 ± 3	S <sup>A</sup>	-0.32 <sup>+1.77</sup> <sub>-1.27</sub>	-1.19 <sup>+1.37</sup> <sub>-1.67</sub>	10.0 ± 3.7	
(17681) Tweedledum	2.48 ± 0.31	0.441 <sup>+0.071</sup> <sub>-0.098</sub>	133 <sup>+317</sup> <sub>-113</sub>	[T10]	—	75.2	243 ± 7	E <sup>F;A</sup>	-4.36 <sup>+2.53</sup> <sub>-2.67</sub>	-4.99 <sup>+2.17</sup> <sub>-1.93</sub>	80.4 ± 32.7	Merxia
(17822) 1998 FM <sub>135</sub>	10.92 ± 1.43	0.058 <sup>+0.008</sup> <sub>-0.008</sub>	79 <sup>+53</sup> <sub>-52</sub>	[T10]	—	4.613	188 ± 1	C <sup>F;A</sup>	-2.42 <sup>+2.07</sup> <sub>-2.50</sub>	-2.42 <sup>+2.07</sup> <sub>-2.50</sub>	11.6 ± 3.8	Hygeia
(18487) 1996 AU <sub>3</sub>	7.78 ± 0.79	0.259 <sup>+0.030</sup> <sub>-0.035</sub>	46 <sup>+36</sup> <sub>-26</sub>	[T10]	—	6.512	216 ± 11	S <sup>F;A</sup>	-0.16 <sup>+1.57</sup> <sub>-1.27</sub>	-0.86 <sup>+1.27</sup> <sub>-1.53</sub>	10.5 ± 3.4	Eunomia
(19251) Totziens	6.24 ± 2.14	0.196 <sup>+0.068</sup> <sub>-0.069</sub>	32 <sup>+121</sup> <sub>-32</sub>	[T10]	—	18.446	209 ± 8	S <sup>A</sup>	-2.46 <sup>+2.10</sup> <sub>-1.63</sub>	-3.29 <sup>+1.83</sup> <sub>-1.80</sub>	23.6 ± 11.2	
(19848) Yeungchuchiu	11.05 ± 1.14	0.170 <sup>+0.078</sup> <sub>-0.078</sub>	18 <sup>+17</sup> <sub>-17</sub>	[T9]	—	3.4510 <sup>†</sup>	211 ± 5	K <sup>F;A</sup>	0.54 <sup>+2.23</sup> <sub>-2.37</sub>	1.51 <sup>+0.47</sup> <sub>-0.97</sub>	4.5 ± 1.8	Eos
(20378) 1998 KZ <sub>46</sub>	7.78 ± 0.80	0.212 <sup>+0.026</sup> <sub>-0.035</sub>	34 <sup>+23</sup> <sub>-14</sub>	[T10]	—	5.14	210 ± 5	S <sup>F;A</sup>	0.71 <sup>+1.40</sup> <sub>-1.20</sub>	0.31 <sup>+0.87</sup> <sub>-0.97</sub>	8.2 ± 2.3	Maria
(20932) 2258 T-1	5.76 ± 1.32	0.247 <sup>+0.057</sup> <sub>-0.058</sub>	41 <sup>+111</sup> <sub>-41</sub>	[T10]	—	4.3239	206 ± 6	S <sup>A</sup>	-2.39 <sup>+2.13</sup> <sub>-1.63</sub>	-3.26 <sup>+1.80</sup> <sub>-1.77</sub>	11.3 ± 5.3	
(21594) 1998 VP <sub>31</sub>	10.30 ± 0.26	0.097 <sup>+0.005</sup> <sub>-0.005</sub>	44 <sup>+16</sup> <sub>-12</sub>	[T10]	—	5.5865	246 ± 3	C <sup>F;A</sup>	0.58 <sup>+2.10</sup> <sub>-2.50</sub>	1.41 <sup>+0.60</sup> <sub>-0.57</sub>	8.4 ± 1.8	Chloris
(23200) 2000 SH <sub>3</sub>	7.20 ± 1.10	0.219 <sup>+0.035</sup> <sub>-0.037</sub>	17 <sup>+66</sup> <sub>-17</sub>	[T10]	—	16.22	220 ± 10	S <sup>F;A</sup>	-0.66 <sup>+1.93</sup> <sub>-1.50</sub>	-1.72 <sup>+1.57</sup> <sub>-1.70</sub>	15.9 ± 7.6	Phocaea
(23276) 2000 YT <sub>101</sub>	7.00 ± 0.96	0.071 <sup>+0.010</sup> <sub>-0.010</sub>	27 <sup>+30</sup> <sub>-27</sub>	[T10]	—	3.661	214 ± 6	C <sup>A</sup>	-0.02 <sup>+2.10</sup> <sub>-2.57</sub>	0.01 <sup>+1.00</sup> <sub>-1.17</sub>	5.9 ± 2.5	
(24101) Cassini	7.4 ± 1.4	0.224 <sup>+0.045</sup> <sub>-0.045</sub>	15 <sup>+38</sup> <sub>-15</sub>	[T10]	—	3.986	200 ± 4	S <sup>A</sup>	0.11 <sup>+1.70</sup> <sub>-1.40</sub>	-0.79 <sup>+1.20</sup> <sub>-1.53</sub>	6.5 ± 3.0	
(25143) Itokawa	0.32 ± 0.03	0.300 <sup>+0.040</sup> <sub>-0.037</sub>	700 <sup>+100</sup> <sub>-100</sub>	[T6]	S <sup>4</sup>	12.132	337 ± 10	S <sup>S</sup>	-4.82 <sup>+1.83</sup> <sub>-2.63</sub>	-5.39 <sup>+1.10</sup> <sub>-1.57</sub>	42.0 ± 7.7	
(27851) 1994 VG <sub>2</sub>	10.4 ± 1.0	0.057 <sup>+0.006</sup> <sub>-0.006</sub>	11 <sup>+14</sup> <sub>-11</sub>	[T10]	—	7.733	234 ± 7	B <sup>*A;O</sup>	1.84 <sup>+2.20</sup> <sub>-2.43</sub>	2.44 <sup>+1.20</sup> <sub>-1.20</sub>	6.6 ± 2.5	Phocaea
(28126) Nydegger	2.63 ± 0.76	0.226 <sup>+0.066</sup> <sub>-0.067</sub>	33 <sup>+205</sup> <sub>-33</sub>	[T10]	S <sup>13</sup>	3.783	229 ± 7	S <sup>S</sup>	-3.16 <sup>+2.30</sup> <sub>-1.77</sub>	-3.92 <sup>+2.03</sup> <sub>-1.90</sub>	13.0 ± 6.2	Flora
(29075) 1950 DA	1.30 ± 0.13	0.200 <sup>+0.026</sup> <sub>-0.031</sub>	24 <sup>+20</sup> <sub>-14</sub>	[T21]	X <sup>4</sup>	2.1216	280 ± 10	M <sup>S;A</sup>	1.28 <sup>+2.17</sup> <sub>-2.43</sub>	—	3.7 ± 1.2	
(30470) 2000 OR <sub>19</sub>	9.42 ± 0.28	0.057 <sup>+0.004</sup> <sub>-0.004</sub>	45 <sup>+43</sup> <sub>-22</sub>	[T10]	—	23.02	224 ± 13	C <sup>F;A</sup>	-1.06 <sup>+2.07</sup> <sub>-2.73</sub>	-1.06 <sup>+2.07</sup> <sub>-2.73</sub>	20.1 ± 6.5	Gefion
(32802) 1990 SK	4.27 ± 1.76	0.273 <sup>+0.114</sup> <sub>-0.116</sub>	20 <sup>+162</sup> <sub>-20</sub>	[T10]	—	2.427	219 ± 22	S <sup>A</sup>	-2.76 <sup>+2.30</sup> <sub>-1.80</sub>	-3.62 <sup>+1.97</sup> <sub>-1.90</sub>	9.4 ± 4.6	
(33342) 1998 WT <sub>24</sub>	0.35 ± 0.04	0.560 <sup>+0.200</sup> <sub>-0.200</sub>	200 <sup>+100</sup> <sub>-100</sub>	[T6]	X <sup>4</sup>	3.697	315 ± 10	E <sup>S;A</sup>	-1.79 <sup>+2.07</sup> <sub>-2.47</sub>	-2.36 <sup>+1.57</sup> <sub>-1.60</sub>	13.3 ± 3.6	
(33916) 2000 LF <sub>19</sub>	4.08 ± 0.41	0.185 <sup>+0.020</sup> <sub>-0.020</sub>	38 <sup>+51</sup> <sub>-38</sub>	[T10]	—	4.4099	240 ± 19	S <sup>A</sup>	-0.02 <sup>+1.73</sup> <sub>-1.43</sub>	-0.99 <sup>+1.43</sup> <sub>-1.70</sub>	7.8 ± 3.5	
(41044) 1999 VW <sub>6</sub>	5.79 ± 1.58	0.297 <sup>+0.082</sup> <sub>-0.083</sub>	14 <sup>+157</sup> <sub>-14</sub>	[T10]	—	2.734	209 ± 7	S <sup>A</sup>	-2.86 <sup>+2.27</sup> <sub>-1.77</sub>	-3.72 <sup>+1.93</sup> <sub>-1.83</sub>	10.0 ± 4.8	
(41223) 1999 XD <sub>16</sub>	11.61 ± 1.15	0.055 <sup>+0.006</sup> <sub>-0.006</sub>	23 <sup>+43</sup> <sub>-23</sub>	[T10]	—	32.52	201 ± 8	C <sup>A</sup>	-1.32 <sup>+2.07</sup> <sub>-2.73</sub>	-1.29 <sup>+2.03</sup> <sub>-2.77</sub>	20.0 ± 9.1	
(41288) 1999 XD <sub>107</sub>	4.22 ± 0.98	0.207 <sup>+0.050</sup> <sub>-0.051</sub>	41 <sup>+86</sup> <sub>-34</sub>	[T10]	—	4.36	234 ± 10	S <sup>A</sup>	-1.22 <sup>+1.87</sup> <sub>-1.53</sub>	-2.16 <sup>+1.63</sup> <sub>-1.73</sub>	9.8 ± 4.3	
(42265) 2001 QL <sub>69</sub>	7.07 ± 1.35	0.177 <sup>+0.035</sup> <sub>-0.036</sub>	25 <sup>+89</sup> <sub>-25</sub>	[T10]	—	8.6	210 ± 2	K <sup>F;A</sup>	-2.26 <sup>+2.13</sup> <sub>-2.50</sub>	-2.62 <sup>+1.67</sup> <sub>-1.73</sub>	13.6 ± 6.4	Eos



Table 4 — continued

Object	$D_{eff}$	$p_V$	$\Gamma^a$	Source	Tax/Color	$P_{rot}$	$T_{surf}$ (K)	Model Comp.	$d_{g\phi}^{G\&B}$	$d_{g\phi}^{Sak}$	$l_s$ (mm)	Family
(42946) 1999 TU <sub>95</sub>	$4.74 \pm 0.79$	$0.266^{+0.046}_{-0.047}$	$37^{+60}_{-37}$	[T10]	—	3.42	$227 \pm 5$	S <sup>A</sup>	$-0.59^{+1.77}_{-1.43}$	$-1.56^{+1.50}_{-1.67}$	$7.4 \pm 3.3$	Eunomia
(44892) 1999 VJ <sub>8</sub>	$7.80 \pm 1.66$	$0.213^{+0.046}_{-0.048}$	$32^{+93}_{-32}$	[T10]	—	5.872	$210 \pm 7$	S <sup>F;A</sup>	$-1.82^{+2.07}_{-1.60}$	$-2.76^{+1.70}_{-1.73}$	$11.8 \pm 5.6$	
(45436) 2000 AD <sub>176</sub>	$3.89 \pm 1.54$	$0.240^{+0.098}_{-0.099}$	$75^{+482}_{-75}$	[T10]	—	18.47	$231 \pm 9$	S <sup>A</sup>	$-5.29^{+2.70}_{-1.93}$	$-5.86^{+2.50}_{-2.10}$	$43.7 \pm 20.9$	
(54509) YORP	$0.092 \pm 0.010$	$0.086^{+0.185}_{-0.060}$	$700^{+500}_{-500}$	[T6]	S <sup>5</sup>	0.2029	$360 \pm 10$	S <sup>S</sup>	$-4.92^{+2.17*}_{-1.47}$	$-5.32^{+2.17*}_{-1.83}$	$5.3 \pm 1.9$	
(68216) 2001 CV <sub>26</sub>	$1.24 \pm 0.05$	$0.322^{+0.022}_{-0.030}$	$432^{+1211}_{-284}$	[T10]	Sq <sup>4</sup>	2.429	$278 \pm 22$	S <sup>S</sup>	$-6.95^{+2.97*}_{-3.23}$	$-7.79^{+2.90*}_{-2.83}$	$76.2 \pm 32.3$	
(69350) 1993 YP	$2.87 \pm 0.69$	$0.162^{+0.041}_{-0.044}$	$238^{+490}_{-146}$	[T10]	—	31.79	$235 \pm 13$	S <sup>A</sup>	$-5.82^{+2.37}_{-1.77}$	$-6.29^{+2.40}_{-2.03}$	$65.9 \pm 26.5$	Phocaea
(72675) 2001 FP <sub>54</sub>	$3.77 \pm 1.32$	$0.219^{+0.078}_{-0.078}$	$29^{+367}_{-29}$	[T10]	—	2.5	$223 \pm 6$	S <sup>A</sup>	$-4.69^{+2.57*}_{-1.90}$	$-5.29^{+2.37*}_{-2.07}$	$14.1 \pm 6.8$	
(90698) Kosciuszko	$3.55 \pm 0.25$	$0.298^{+0.028}_{-0.034}$	$16^{+49}_{-16}$	[T10]	—	5.014	$258 \pm 29$	S <sup>F;A</sup>	$0.78^{+1.67}_{-1.47}$	$-0.39^{+1.40}_{-1.73}$	$7.1 \pm 3.4$	
(99942) Apophis	$0.375 \pm 0.014$	$0.166^{+0.043}_{-0.035}$	$150^{+350}_{-100}$	[T6]	S <sup>4</sup>	30.56	$362 \pm 10$	S <sup>S</sup>	$-2.66^{+2.23}_{-1.70}$	$-3.22^{+2.13}_{-1.93}$	$43.8 \pm 18.2$	
(101955) Bennu	$0.484 \pm 0.01$	$0.063^{+0.005}_{-0.005}$	$310^{+70}_{-70}$	[T6]	B <sup>4</sup>	$4.2975^\dagger$	$338 \pm 10$	B <sup>S</sup>	$-2.62^{+1.87}_{-2.57}$	$-3.19^{+1.23}_{-1.60}$	$18.7 \pm 3.6$	
(155140) 2005 UD	$1.3 \pm 0.2$	$0.100^{+0.020}_{-0.020}$	$300^{+120}_{-110}$	[T22]	B <sup>7</sup>	5.235	$343 \pm 18$	B <sup>S</sup>	$-2.52^{+2.07}_{-2.67}$	$-3.12^{+1.57}_{-1.73}$	$20.5 \pm 4.8$	
(162173) Ryugu	$0.87 \pm 0.03$	$0.044^{+0.007}_{-0.006}$	$350^{+250}_{-250}$	[T6]	C <sup>4</sup>	7.63	$250 \pm 10$	B <sup>S</sup>	$-4.86^{+2.53*}_{-3.03}$	$-5.52^{+2.23*}_{-2.20}$	$30.6 \pm 10.7$	
(175706) 1996 FG <sub>3</sub>	$1.63 \pm 0.04$	$0.029^{+0.004}_{-0.004}$	$80^{+40}_{-40}$	[T6]	B <sup>4</sup>	3.5942	$328 \pm 15$	B <sup>S</sup>	$0.81^{+2.07}_{-2.50}$	$0.31^{+1.53}_{-1.63}$	$8.8 \pm 2.4$	
(276049) 2002 CE <sub>26</sub>	$3.5 \pm 0.4$	$0.070^{+0.020}_{-0.020}$	$102^{+104}_{-75}$	[T16]	C <sup>10</sup>	3.2931	$300 \pm 30$	C <sup>S</sup>	$-1.42^{+2.17}_{-2.53}$	$-1.46^{+2.20}_{-2.50}$	$9.5 \pm 3.6$	
(308635) 2005 YU <sub>55</sub>	$0.31 \pm 0.025$	$0.032^{+0.004}_{-0.005}$	$550^{+250}_{-200}$	[T6]	C <sup>4</sup>	19.31	$325 \pm 10$	C <sup>S</sup>	$-4.39^{+2.07}_{-2.67}$	$-4.39^{+2.07}_{-2.67}$	$48.5 \pm 11.8$	
(341843) 2008 EV <sub>5</sub>	$0.31 \pm 0.006$	$0.184^{+0.082}_{-0.057}$	$450^{+60}_{-60}$	[T6]	C <sup>6</sup>	3.725	$321 \pm 15$	C <sup>S</sup>	$-3.72^{+1.80}_{-2.47}$	$-3.72^{+1.80}_{-2.47}$	$18.7 \pm 3.4$	
2002 NY <sub>40</sub>	$0.28 \pm 0.03$	$0.340^{+0.060}_{-0.060}$	$100^{+50}_{-50}$	[T22]	Q <sup>4</sup>	19.98	$363 \pm 15$	S <sup>S</sup>	$0.51^{+2.00}_{-2.70}$	$0.44^{+1.27}_{-1.53}$	$19.9 \pm 5.6$	

**Notes & References.** <sup>1</sup>SMASS I; <sup>2</sup>SMASS II; <sup>3</sup>S3OS2 (Lazzaro et al., 2004); <sup>4</sup>MITHNEOS; <sup>4b</sup>Tholen (1984); <sup>5</sup>Gietzen and Lacy (2007); <sup>6</sup>Reddy et al. (2012); <sup>7</sup>Jewitt and Hsieh (2006)

<sup>8</sup>Chapman and Gaffey (1979); <sup>9</sup>Hardersen et al. (2011); <sup>10</sup>Shepard et al. (2006); <sup>11</sup>Vilas et al. (1998); <sup>12</sup>Fieber-Beyer (2015); <sup>13</sup>MacLennan et al., (in prep)

[T1]Alí-Lagoa et al. (2020); [T2]Capria et al. (2014); [T3]Marsset et al. (2017); [T4]Matter et al. (2013); [T5]Keihm et al. (2012); [T6]Delbo' et al. (2015); [T7]Jiang et al. (2020);

[T8]Müller and Blommaert (2004); [T9]Hanus' et al. (2018); [T10]MacLennan and Emery (2021); [T11]Marciniak et al. (2019); [T12]Marciniak et al. (2018); [T13]MacLennan and Emery (2019);

[T14]Yu et al. (2017); [T15]Hanus' et al. (2015); [T16]Rozitis et al. (2018); [T17]Pravec et al. (2019); [T18]Rozitis et al. (2013); [T19]Leyrat et al. (2011);

[T20]Hanus' et al. (2016); [T21]Rozitis et al. (2014); [T22]Devogèle et al. (2020); [T22]Müller, T. G. et al. (2004)

<sup>†</sup>Indicates that the reported  $P_{rot}$  value has been rounded to four decimal places.

\*t The reported grain size is larger than the estimated thermal skin depth.

<sup>a</sup>Thermal inertia values are in SI units ( $\text{J m}^{-2}\text{K}^{-1}\text{s}^{-1/2}$ ).

<sup>c</sup>Colors from (Tholen, 1984) are used.

<sup>e</sup>The mutual eclipse duration of 4 hr is used to compute thermal skin depth.

<sup>f</sup>Family association (Table 8) is used.

<sup>o</sup>Family outlier, with suspected family crossed out in last column. See text for details.

<sup>A</sup>Object albedo (Fig. 2) is used to infer meteorite connection.

<sup>S</sup>Reflectance spectrum is used. See above for sources.

<sup>T</sup>Large thermal inertia is used to infer a metal-rich surface.

<sup>U</sup>A uniform, rather than a Gaussian, distribution was used for the thermal inertia.

Table 5: Comparison of Multi-linear Regression Models

Model	$n$	$r_{adj}^2$	$BIC$
$M-1$	4	0.062	1687
$M-2$	6	0.141	1660
$M-3$	6	0.149	1656
$M-4$	8	0.217	1617
$M-5$	8	0.141	1670

Table 6: Linear Coefficients and Intercept for  $M-4$

Parameter	Estimate	$1\sigma$ Uncertainty	$p$ -value
intercept [ $d_{g\phi}$ ]	-9.85	$\pm 1.27$	$< .01$
$D^b$ [km]	10.1	+1.2/-1.1	$< .01$
$P^b$ [hr]	4.84	+0.35/-0.32	$< .01$
$D_{eff}^{slope} (< D^b)$	5.27	$\pm 0.89$	$< .01$
$D_{eff}^{slope} (> D^b)$	-0.42	$\pm 0.24$	.11
$P_{rot}^{slope} (< P^b)$	7.83	$\pm 1.70$	$< .01$
$P_{rot}^{slope} (> P^b)$	-2.04	$\pm 0.28$	$< .01$



Table 7: Residual grain size statistics and Welch's t-test results for different spectral groups

		Spectral Group									Assumed Group			
		S	V	C	B	K	E	M	Met	P	S	C	B	E
$\Delta d_{g\phi}$	mean	-0.24	-0.29	0.63	0.10	0.46	1.15	1.18	2.14	-0.94	-0.24	1.06	-1.00	1.40
	s.d.	1.37	2.17	1.12	1.10	1.03	1.42	1.20	0.92	1.65	1.40	1.16	2.01	1.40
	count	146	17	49	32	26	8	8	7	23	207	71	42	15
$p$ -value	vs. all	<.01	.49	<.01	.86	.06	.06	.03	<.01	<.01	<.01	<.01	.08	<.01
	S	—	.92	<.01	.14	<.01	.03	.01	<.01	.06	.75	<.01	.67	<.01
	V		—	.11	.50	.20	.06	.04	<.01	.31	.86	.06	.93	<.01
	C			—	.04	.51	.36	.26	<.01	<.01	<.01	.44	<.01	.02
	B				—	.20	.08	<.04	<.01	.01	.19	<.01	.13	<.01
	K					—	.24	.16	<.01	<.01	<.01	.18	<.01	<.01
	E						—	.96	.13	<.01	.03	.52	.01	.46
	M							—	.10	<.01	.01	.41	<.01	.44
	Met								—	<.01	<.01	<.01	<.01	.29
	P									—	.05	<.01	.14	<.01

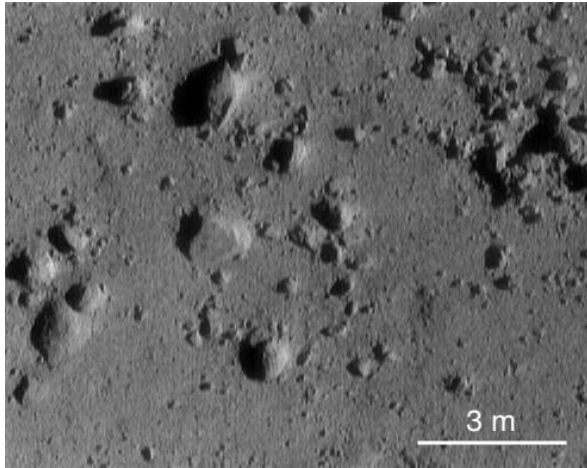
Table 8: Asteroid Family Properties

PDS Family ID	AstDyS Family ID	Num	Spec.	Collision Type <sup>1</sup> /Note	Count <sup>2</sup>
003 Hungaria	(434) Hungaria	2965	Xe/E	Fragmentation	6
<i>Inner Main Belt</i>					
401 Vesta	(4) Vesta	15252	V	Cratering	14 <sup>*</sup>
402 Flora	—	13786	S		25 <sup>*</sup>
403 Baptistina	(883) Matterania	2500	S	cluster within Flora	3 <sup>*</sup>
404 Massalia	(20) Massalia	6424	S	Cratering	1 <sup>*</sup>
405 Nysa-Polana high-pV)			S		8
405 Nysa-Polana (low-pV)			C		3
415 Chaldaea	—	1776	Ch		2
416 Svea	—	48	C/B		1 <sup>*</sup>
701 Phocaea	(25) Phocaea	1989	S		10
<i>Middle Main Belt</i>					
502 Eunomia	(15) Eunomia	5670	S	Cratering	14
505 Adeona	(145) Adeona	2236	C		3
506 Maria	(170) Maria	2940	S		4
507 Padua	(363) Padua/(110) Lydia	1087	X/P	Fragmentation	1
509 Chloris	(410) Chloris	424	C		2
512 Dora	(668) Dora	1259	C	Fragmentation	2 <sup>*</sup>
513 Merxia	(808) Merxia	1215	S	Fragmentation	2 <sup>*</sup>
516 Gefion	(93) Minerva	2547	S		2 <sup>*</sup>
519 Hoffmeister	(1726) Hoffmeister	1819	C	Fragmentation	1
531 Mitidika	—	653		—	2
—	(5) Astraea	6169	S?	Cratering	3
<i>Outer Main Belt</i>					
601 Hygiea	(10) Hygiea	4854	C	Cratering	7 <sup>*</sup>
602 Themis	(24) Themis	4782	C	Fragmentation	9 <sup>*</sup>
603 Sylvia	(87) Sylvia	255	X/P		1 <sup>*</sup>
604 Meliboea	—	444	C		2
605 Koronis	(158) Koronis	5949	S	Fragmentation	16
606 Eos	(221) Eos	9789	K	Fragmentation	23
607 Emma	(283) Emma	76	C	Cratering	1 <sup>*</sup>
609 Veritas	(490) Veritas	1294	C		1
610 Karin	—	541	S	cluster within Koronis	2
620 Beagle	(656) Beagle	148	C	cluster within Themis	1 <sup>*</sup>
631 Ursula	(375) Ursula	1466	C/X?		1
633 Itha	—	54	S		1 <sup>*</sup>
634 Inarradas	—	38			1 <sup>*</sup>
902 Alauda	—	1294	B?		3
<i>Hilda Group</i>					
002 Schubart	(1911) Schubart	352	P	Fragmentation	1

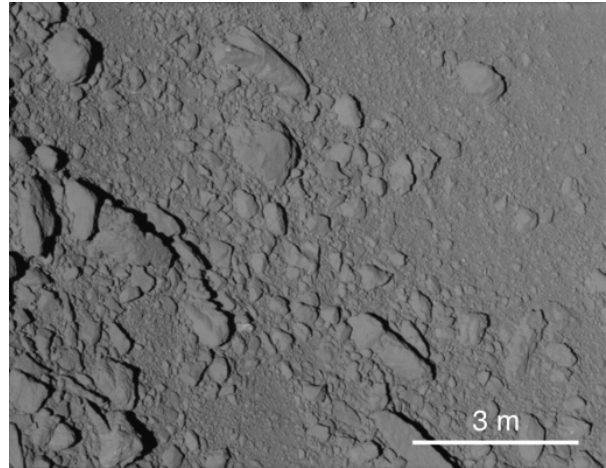
**Notes.**

\*Largest family member appears in this study.

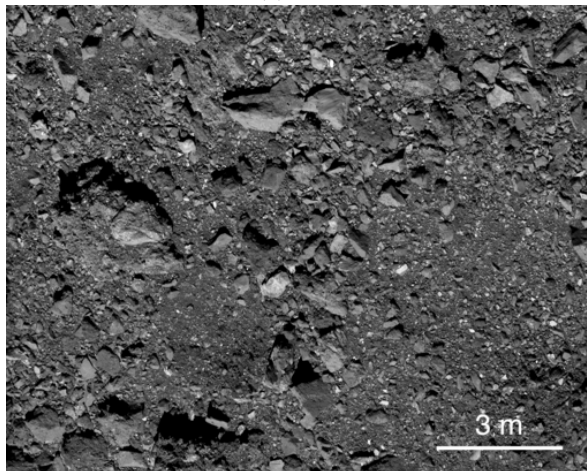
<sup>1</sup>Collisional type definitions from [Milani et al. \(2015\)](#).<sup>2</sup>Number of asteroid family members present in this study.



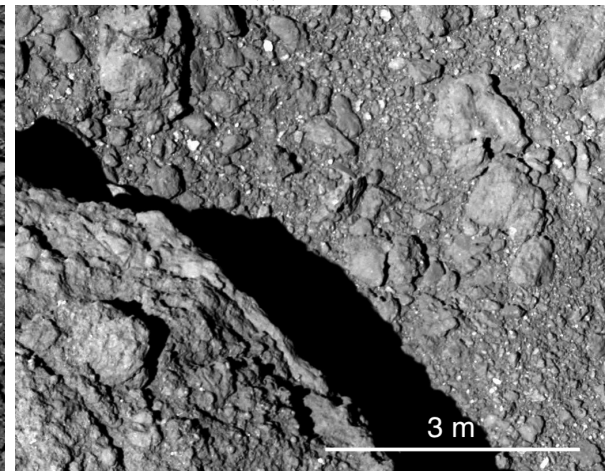
(a) Eros



(b) Itokawa



(c) Bennu



(d) Ryugu

Figure 1: Spacecraft images of the regolith on Eros, Itokawa, Bennu, and Ryugu acquired by the NEAR, Hayabusa, OSIRIS-REx, and Hayabusa 2 missions respectively.

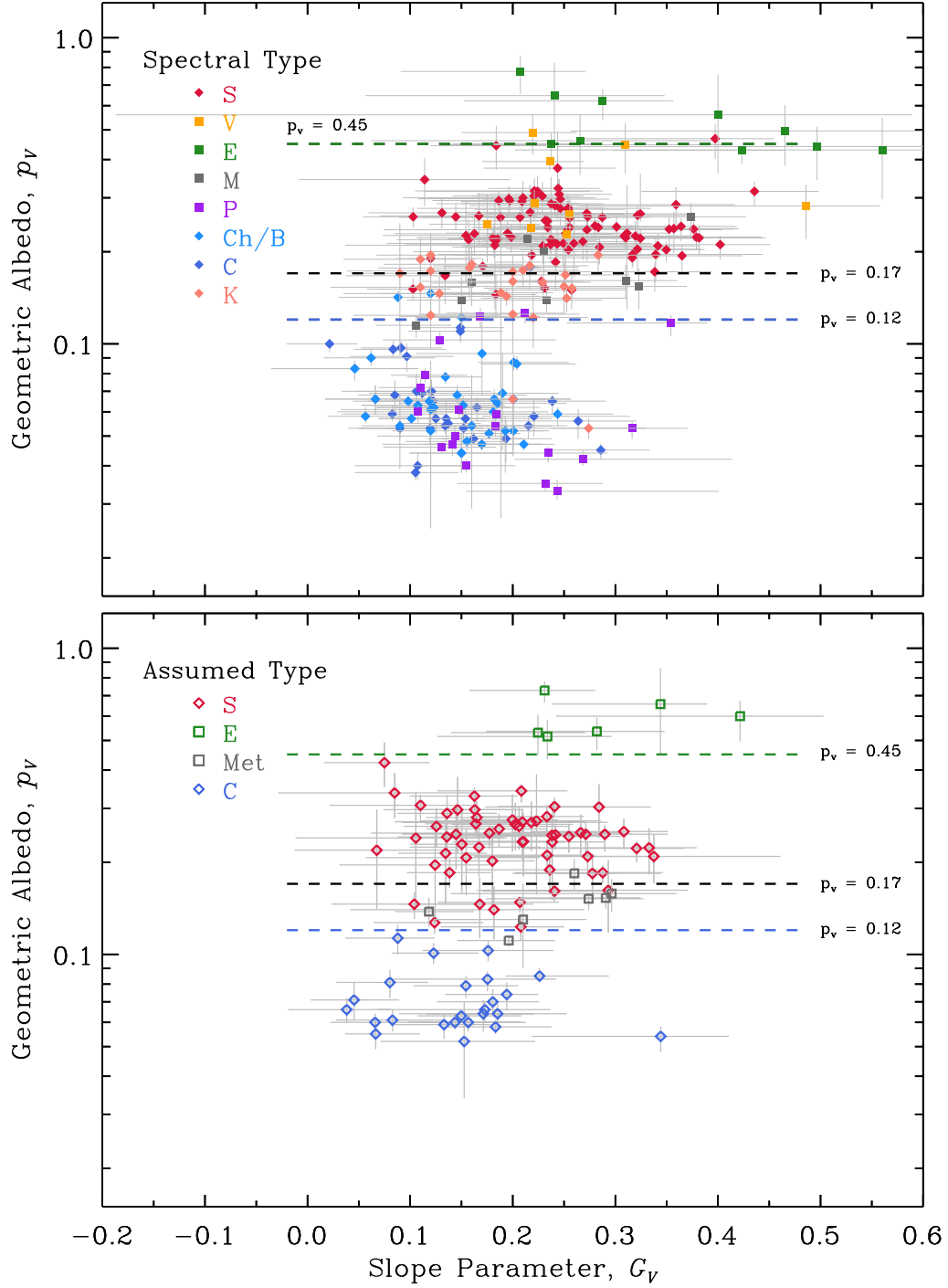


Figure 2: Geometric albedo ( $p_v$ ) versus slope parameter ( $G_v$ ) grouped by spectral type for all asteroids in this study. The top panel (filled symbols) shows the objects classified on the basis of spectral or color data and family membership, when applicable. The bottom panel (open symbols) are the objects classified only on the basis of albedo.

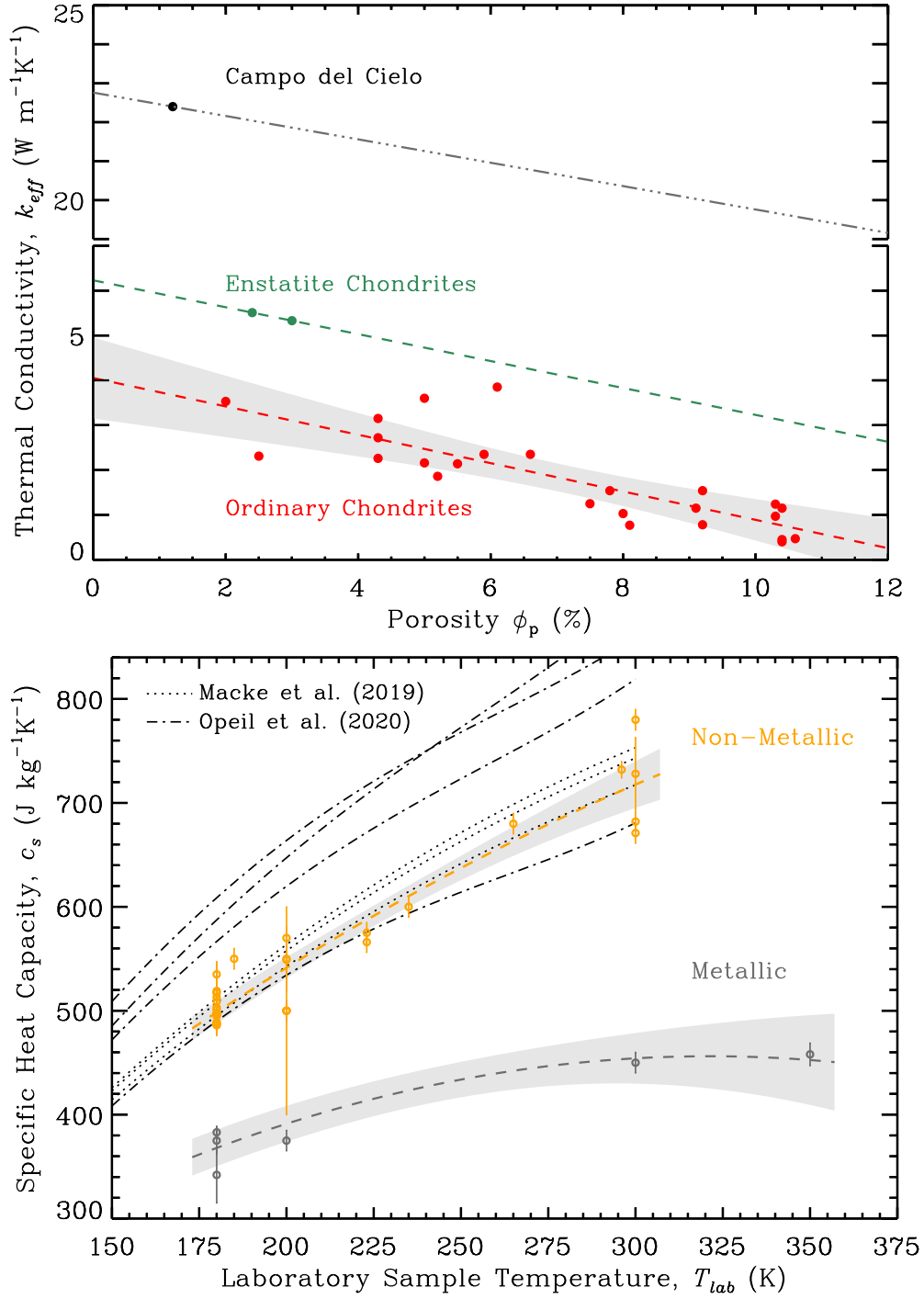


Figure 3: Meteorite thermal conductivity as a function of porosity (top) and specific heat capacity as a function of temperature (bottom). Dashed lines show linear fits in the top panel, and parabola fits through the origin in the bottom panel, with grey regions representing 95% confidence to the fits. The dashed-dotted line through the Campo del Cielo datum in the top panel assumes a slope of 0.3. Note the break in the y-axis in the top panel.

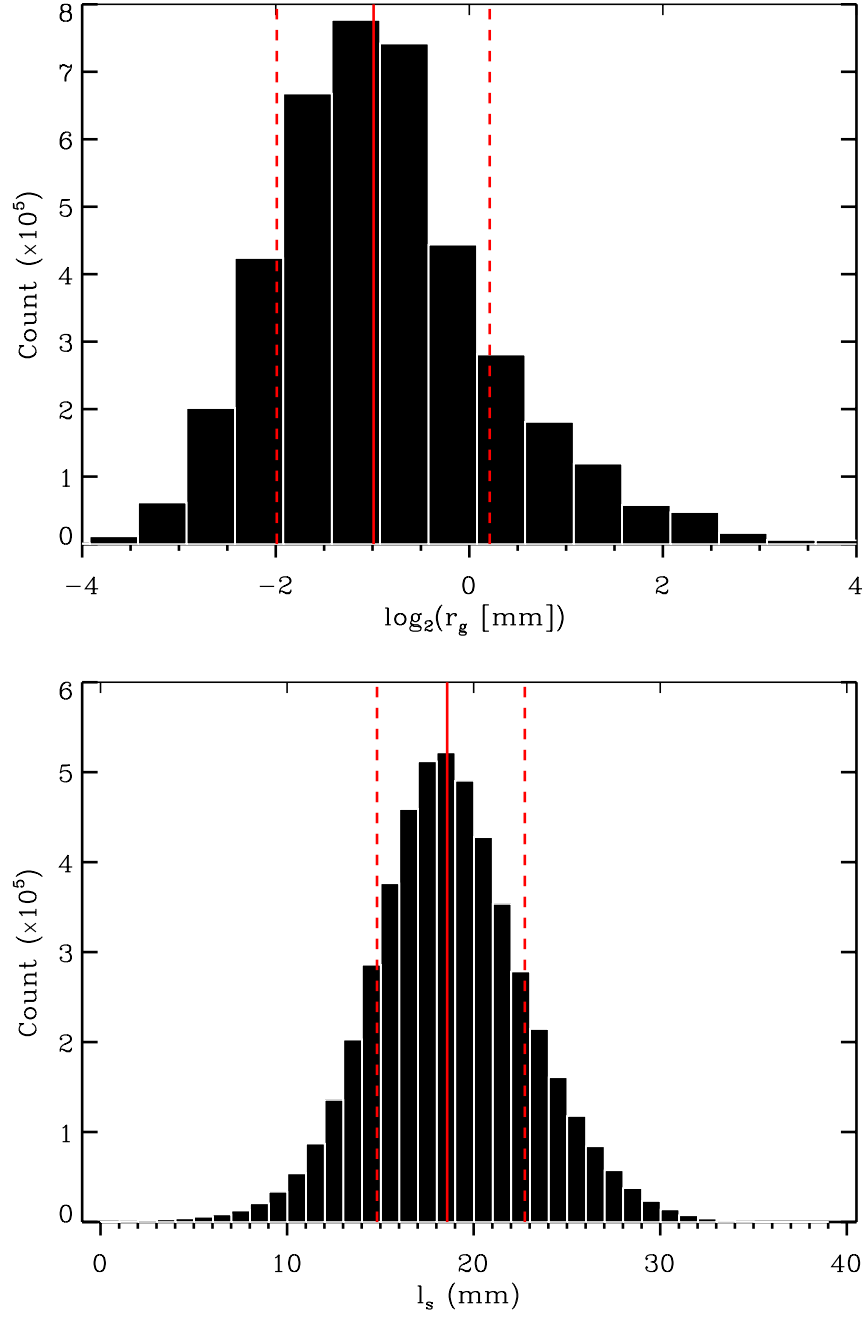


Figure 4: Example output grain size (top) and skin depth (bottom) from the thermal conductivity model. A hypothetical S-type asteroid with  $\Gamma = 150 \pm 50 J m^{-2} K^{-1} s^{-1/2}$ ,  $T_{surf} = 300 \pm 10 K$ , and  $P_{rot} = 10$  hr was used to generate these distributions. The red vertical lines show the mean (solid) and standard deviation (dashed) of each distribution.

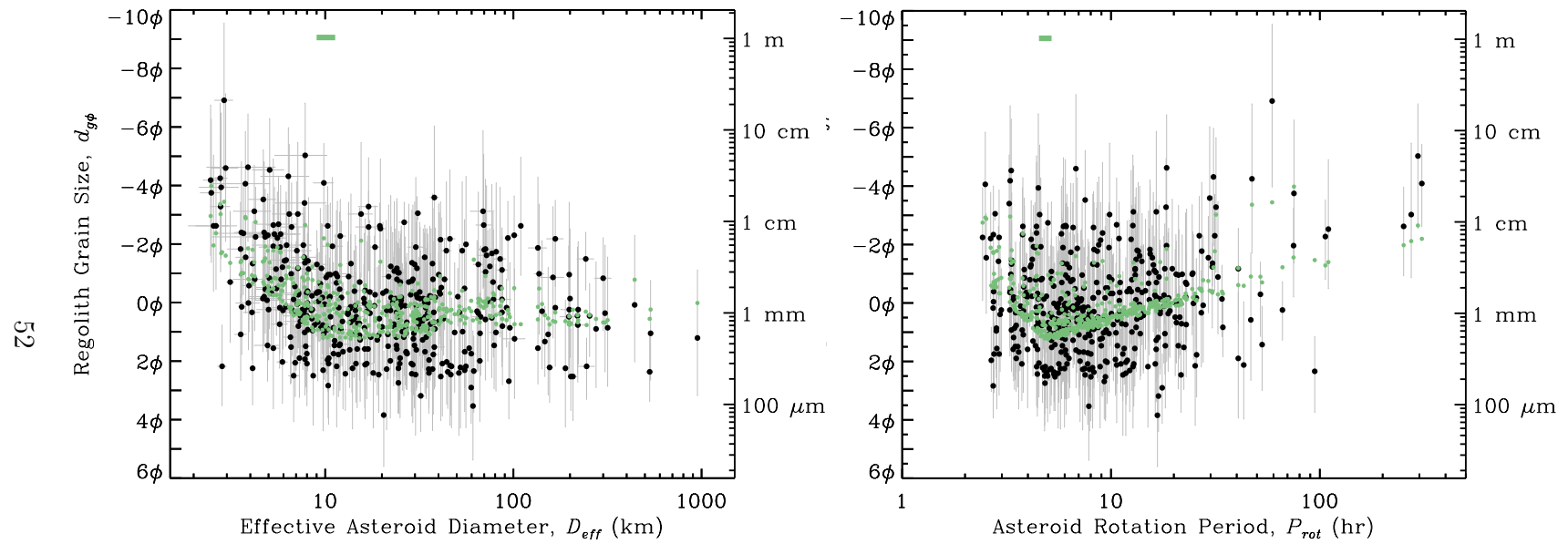


Figure 5: Multi-linear model fit  $M-4$ , shown by colored points, and the grain size dataset, shown by black dots, as a function of asteroid diameter (left) and rotation period (right). The colored bars at the top of each panel indicate the  $1\sigma$  range in uncertainty in the break-point between the two segments.



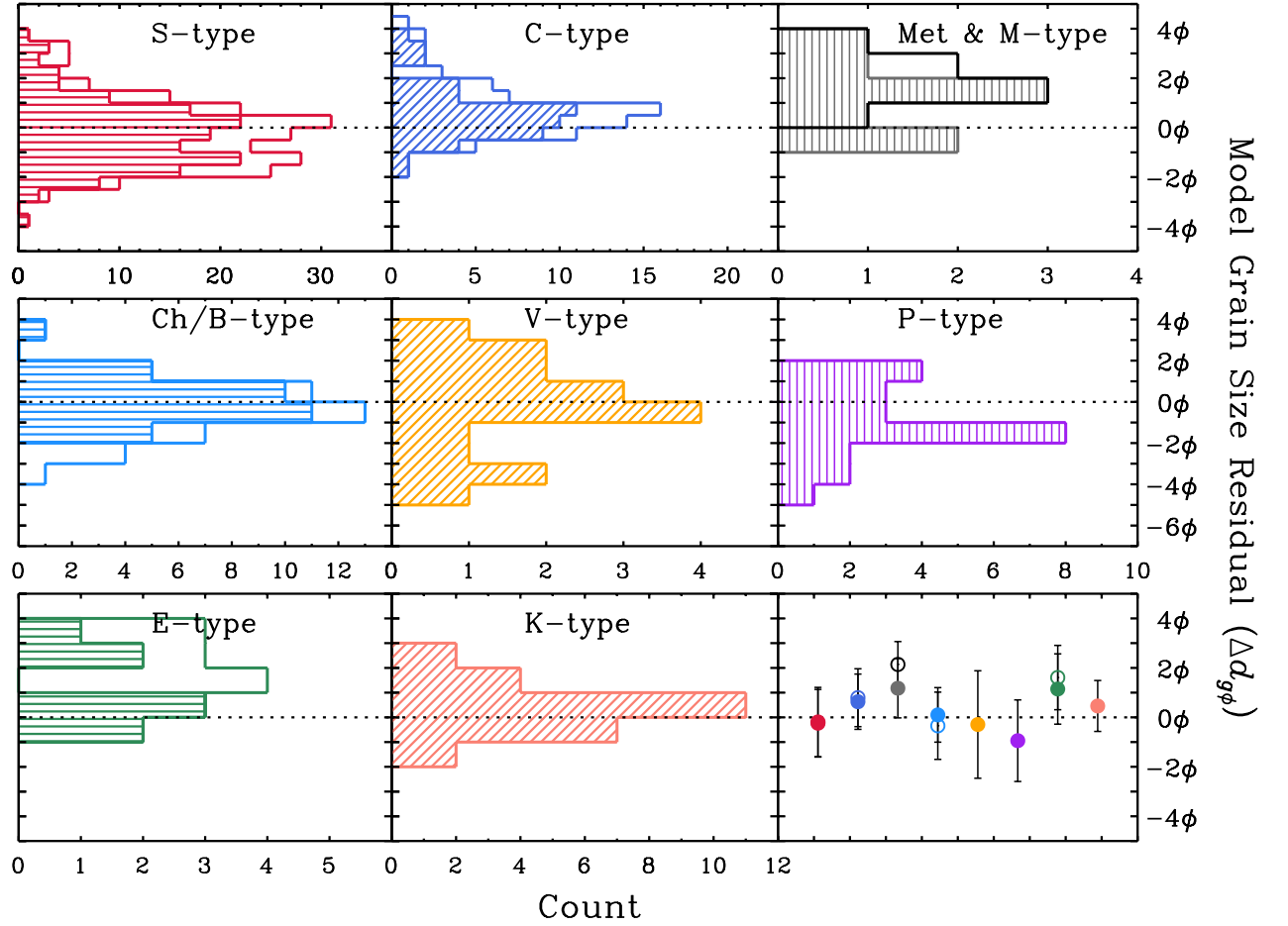


Figure 6: Grain size model residual distributions for different compositional groups and the group means and standard deviations (bottom right panel). Unfilled histograms and open circles in the bottom right panel indicate that objects with assumed spectral classification are included. The unfilled black histogram in the upper right panel is for metal-rich asteroids, as opposed to the filled-in histogram for M-types. The dotted horizontal line at  $0\phi$  in each panel is shown for comparison purposes. Note the change in the y-axis range for the middle three panels.

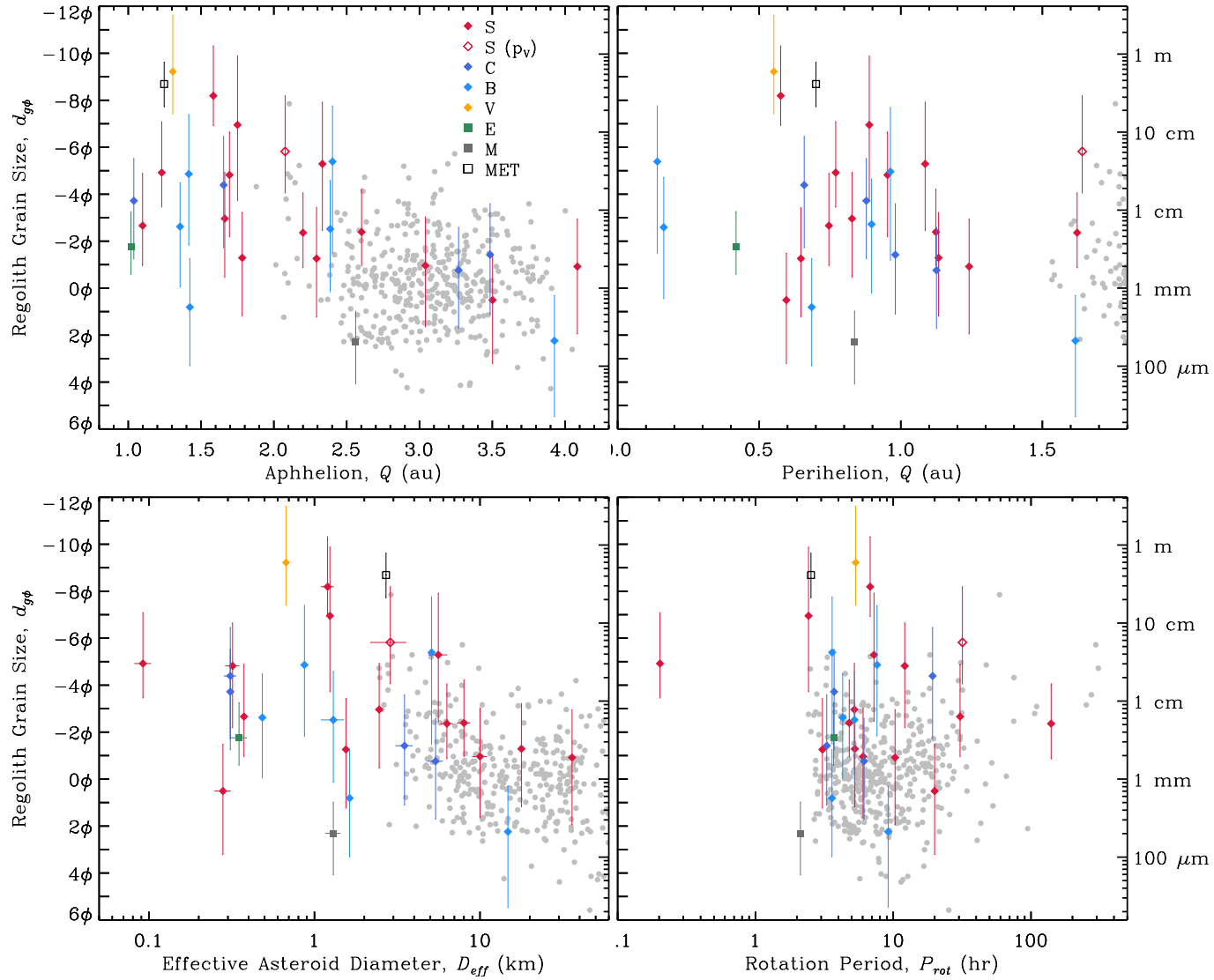


Figure 7: Regolith grain sizes of NEAs as a function of a) aphelion distance, b) perihelion distance, c) asteroid diameter, and d) rotation period. Symbol colors indicate spectral type as noted in the upper left panel, and are consistent with previous figures. The open symbols are objects with an inferred spectral type (see text) and grey dots are MBAs.